



Universität für Bodenkultur Wien



NANYANG
TECHNOLOGICAL
UNIVERSITY



**AUSTRIAN INSTITUTE
OF TECHNOLOGY**



A*STAR

Institute of
Medical Biology

Extracellular Vesicles and their Detection with Plasmonic Biosensors for the Diagnosis of Ovarian Cancer

Submitted by

Dipl.-Ing. Agnes Reiner

A thesis submitted for the degree of
Doctor of Philosophy (PhD)

International Graduate School in Bionanotechnology, IGS BioNanoTech
University of Natural Resources and Life Sciences, BOKU, Vienna
Nanyang Technological University, NTU, Singapore
Austrian Institute of Technology, AIT, Vienna
A*STAR, Institute of Medical Biology, Singapore

Supervisor:

Prof. Dr. Wolfgang Knoll, Institute for Biophysics, BOKU

Co-Supervisors:

Jakub Dostalek, PhD, BioSensor Technologies, AIT
Prof. Dr. Bo Liedberg, Centre for Biomimetic Sensor Science, NTU
Prof. Dr. Sai Kiang Lim, Institute for Medical Biology, A*STAR

Acknowledgements

First of all I want to thank Wolfgang Knoll and Bo Liedberg for the opportunity to study within the International Graduate School of Bionanotechnology at the University of Natural Resources and Life Sciences in Vienna and the Nanyang Technological University in Singapore. Within these three years I gained a lot of insight into the research field of extracellular vesicles and the biosensor development in combination with nanotechnologies, which broadened my horizon amazingly.

My deepest gratitude goes to Jakub Dostalek, who supported me and my project with greatest enthusiasm and effort. His willingness to step into biomedical topics made this interdisciplinary project possible and his physical point of view taught me to always consider the different aspects of science disciplines.

Furthermore, I want to especially thank Sai Kiang Lim and her team at the Institute of Medical Biology in Singapore. She not only supported my project financially, but more importantly gave me guidance through my work by sharing her knowledge in plenty of discussions.

Also Robert Zeillinger deserves acknowledgement for his support by providing the access to clinical samples and for the critical discussions of scientific results as well as future project plans.

Special thanks go to all my colleagues in Vienna and Singapore. We not only shared long hours at the lab, but also motivating and more than scientific discussions.

Finally I want to thank my family and friends for their backup and encouragements throughout years of studying. My parents deserve special credit for the extraordinary support they gave me.

Zusammenfassung

Durch die späte Diagnose und die erfolglose Therapie von Eierstockkrebs zählt dieser zu den tödlichsten Krebsarten. Eine frühere Diagnose würde die Erfolgschancen der Therapie und dadurch die Überlebensrate der Patientinnen enorm erhöhen. Eine solche frühere Diagnose könnte durch die Verwendung von extrazellulären Vesikeln (EV) als Biomarker erreicht werden, aber es mangelt den derzeit verfügbaren Methoden zur Isolierung und Analyse der Vesikel an Spezifität und Sensitivität. Daher war es das Ziel dieses Projektes durch die Verwendung von Lipid-bindenden Proteinen für die Isolierung der Vesikel neue EV-basierte Biomarker für eine verbesserte Diagnose von Eierstockkrebs zu identifizieren. Darüber hinaus sollen neue, hoch sensitive Methoden für deren Detektion entwickelt werden, die auf dem Prinzip der Oberflächenplasmonenresonanz basieren.

Wir haben unser Ziel erreicht, indem wir eine Gruppe von EV, die eine einzigartige Lipid- und Proteinzusammensetzung aufweist, als potentiellen Biomarker für Eierstockkrebs identifizieren konnten. Außerdem haben wir plasmonische Biosensoren entwickelt, die ermöglichen kleinste Konzentrationen von EV zu detektieren, indem magnetische Nanopartikel zur Signalverstärkung eingesetzt wurden.

Abstract

Ovarian cancer is the deadliest gynecological cancer, due to its late diagnosis resulting in unsuccessful treatment. An earlier diagnosis at a stage, when the disease is still treatable, would improve the chances of survival immensely. To achieve such an early diagnosis extracellular vesicles (EVs) have been proposed as a new class of biomarkers, but the currently used methods for their isolation and analysis lack in specificity and sensitivity. Hence this project aimed to identify new EV-based biomarkers for an improved diagnosis of ovarian cancer by usage of lipid-binding proteins for EV isolation and to develop new highly sensitive biosensors for EV detection based on surface plasmon resonance (SPR).

We achieved our aim by identifying a subpopulation of EVs that carries a distinct lipid and protein composition as candidate biomarker for ovarian cancer and will validate its value for clinical application in subsequent studies. Furthermore, we developed a plasmonic biosensor platform that was capable of detecting trace amounts of EVs by making use of magnetic nanoparticles for signal enhancement. The specific detection of cancer-derived EVs with this sensing platform will be studied in future.

Table of Contents

Acknowledgements	iii
Zusammenfassung	v
Abstract	vii
Table of Contents	ix
1 Introduction	1
1.1 Extracellular Vesicles	2
1.1.1 Types and Biogenesis	3
1.1.2 Composition and Function	5
1.1.3 Sources of EVs	9
1.1.4 Methods of Isolation	11
1.1.5 Methods of Analysis	15
1.1.6 EVs in Cancer	27
1.2 Plasmonic Biosensors	37
1.2.1 Principle of Surface Plasmon Resonance	38
1.2.2 Sensing Modalities and Instrumentation	39
1.2.3 Sensor Chip Architecture	43
1.2.4 Sensor Surface Architecture	46
1.2.5 Operation of Plasmonic Biosensors	49
1.2.6 Signal Enhancement with Nanoparticles	52
1.2.7 Surface Plasmon-Enhanced Fluorescence Spectroscopy	54
1.3 Plasmonic Biosensors for EV Analysis	57
2 Aim of the Project	65
3 Identification of EV-based Biomarkers for the Diagnosis of Ovarian Cancer	67
3.1 Material and Methods	68
3.1.1 Patient samples	68
3.1.2 EV isolation with lipid binding ligands	69
3.1.3 Western blot	69

3.1.4	Zymography and MMP9 ELISA	70
3.1.5	Cryo electron microscopy and AV gold labeling	70
3.1.6	Statistical analysis	71
3.2	Results and Discussion	71
3.2.1	Patient Cohort	71
3.2.2	Isolation method testing	72
3.2.3	Cancer marker search	73
3.2.4	MMP9 cargo of AV-binding EVs	75
3.3	Conclusions	82
4	Magnetic Nanoparticle-enhanced Grating Coupled SPR for EV Detection	85
4.1	Material and Methods	86
4.1.1	Materials	86
4.1.2	Biological samples and EV characterization	87
4.1.3	Preparation of GC-SPR sensor chips	88
4.1.4	Optical system	88
4.1.5	Functionalization of GC-SPR sensor chips	89
4.1.6	Detection assay	90
4.1.7	Observation of sensor chips	91
4.2	Results and Discussion	91
4.2.1	Modification of the sensor chip with ligands	92
4.2.2	GC-SPR readout of MNP-enhanced EV assay	93
4.2.3	Discrimination between AV- and CTB-binding EVs	97
4.3	Conclusions	98
5	Parallel Readout of Grating Coupled SPR and Plasmon-enhanced Epifluorescence	101
5.1	Material and Methods	102
5.1.1	Materials	102
5.1.2	Sensor chip preparation	103
5.1.3	Optical system	103

5.1.4	Functionalization of sensor chips	105
5.1.5	Direct detection bioassay	106
5.1.6	Magnetic nanoparticle-enhanced bioassay	106
5.2	Results and Discussion	107
5.2.1	Characterization of GC-SPR sensor chips	107
5.2.2	Observation of affinity binding of protein analyte	110
5.2.3	Magnetic nanoparticle-enhanced observation of affinity binding of extracellular vesicles	113
5.3	Conclusions	117
6	Concluding remarks	119
7	References	121
8	List of abbreviations	131
9	Curriculum Vitae	133

I Introduction

The work presented in this PhD thesis is based on and comprises of a book chapter and the following published, scientific studies:

- [1] **Reiner AT**, Tan S, Agreiter C, Auer K, Bachmayr-Heyda A, Aust S, Pecha N, Mandorfer M, Pils D, Brisson AR, Zeillinger R, Lim SK (2017). „EV-associated MMP9 in high grade serous ovarian cancer is preferentially localized to Annexin V-binding EVs”. Disease Markers 2017 May 18; vol. 2017, Article ID 9653194, 9 pp. (DOI: 10.1155/2017/9653194)
- [2] **Reiner AT**, Ferrer Sanchez NG, Venugopalan P, Lai RC, Lim SK, Dostalek J. „Magnetic nanoparticle-enhanced surface plasmon resonance biosensor for extracellular vesicle analysis“. Accepted with revisions at Analyst, Jun. 2017
- [3] **Reiner AT**, Fossati S, Dostalek J. „Biosensor platform for parallel surface plasmon-enhanced epifluorescence and surface plasmon resonance detection“. In review at Sensors and Actuators since Jun. 2017
- [4] **Reiner AT**, Koji T, Brisson AR, Pils D, Knoll W, Dostalek J (2016). „Plasmonics exosome biosensors for medical diagnostics“ In M. Olivo and U. S. Dinis (eds), Frontiers in Biophotonics for Translational Medicine, Progress in Optical Science and Photonics 3 (pp.249-272), Springer Science+Business Media Singapore 2016 (DOI: 10.1007/978-981-287-627-0_8)

An overview on the background of the different topics embraced in this work is given in section 1, which is partially based on the review published in [4]. Since extracellular vesicles are the core topic that connects all the presented studies, the introduction discusses the characteristics of extracellular vesicles in detail with a particular focus on their role in ovarian cancer and their potential in clinical applications. Also, currently used and emerging methods for isolation and analysis of extracellular vesicles are reviewed and their capabilities and limitations are discussed. Next, the principles and methodologies of surface plasmon resonance biosensors are introduced and the state of the art in regard to the use of plasmonic biosensors for the detection and analysis of extracellular vesicles is presented, because different plasmonic biosensors for this application were developed within this project.

Following the introduction, the aim of this project is outlined and the individual studies, listed above, are presented in the consecutive chapters. The first study, in which extracellular vesicle biomarkers for ovarian cancer were identified [1], is found in section 3. Next, a study on the

development of a grating coupled surface plasmon resonance biosensor for the detection of extracellular vesicles with signal enhancement by magnetic nanoparticles [2] is discussed in section 4. Finally, a plasmonic biosensing platform for the parallel detection of surface plasmon resonance and plasmonically enhanced fluorescence [3] is presented in section 5. The main conclusions of this project are drawn in the last section.

1.1 Extracellular Vesicles

About two decades after the discovery of exosomes in the 1980s, extracellular vesicles (EVs) are now expanding exponentially in many biomedical applications and scientific disciplines. Even though, we are just at the beginning of understanding the complexity of their biological functions, also their biogenesis and exact composition are to a great part still a mystery.

The group of Philip Stahl discovered a new pathway for the secretion of small vesicles by reticulocytes when examining the transferrin receptor life cycle [5]. The group found that the transmembrane protein is removed from the cell membrane by endocytosis, which was already known, but did not end up in lysosomes for degradation, which was a new discovery. Instead, it was incorporated into small lipid vesicles built by inward budding into the late endosome of the cell. They called these newly identified cell compartments multivesicular endosomes. The vesicles, produced in this way, were released to the extracellular space by fusion of the multivesicular endosome with the plasma membrane and called exosomes. Interestingly, the group of Rose M. Johnstone made the same discovery and published it just a few weeks later [6]. At such early stage, these vesicles were only seen as a waste disposal system and didn't receive much more attention. About 15 years later Raposo et al. discovered that such small lipid vesicles were also released by B lymphocytes and were capable of triggering a T cell response via antigen presentation with MHC class II proteins on their surface [7]. From this discovery onward EVs became the focus of attention in many studies and with time, a new field of research evolved around them.

As more and more people studied EVs, many different names were attributed to these vesicles, like microparticles, microvesicles, shedding vesicles, oncosomes, ectosomes, prostasomes, exosome-like vesicles and of course exosomes, to name just a few. At the current time, still no clear and defined characteristics for the different EV types are known. Hence the definitions vary and vesicle classification can be based on different criteria: biogenesis, size and density, cellular source, protein or lipid composition. Only some years ago the International Society of Extracellular Vesicles (ISEV) started working on standardization and unification of nomenclature, which defines extracellular vesicles as the umbrella term for mainly three different classes of vesicles: exosomes, microvesicles, and apoptotic bodies. ISEV is proposing the

biogenesis as most important criteria to differentiate these three types of EVs, which are described in section 1.1.1. The composition of EVs (see section 1.1.2), in particular their protein and nucleic acid components, are also often used to describe and define certain subgroups of vesicles, but it has to be borne in mind that so far no specific markers for exosomes or microvesicles have been identified.

Besides defining different EV groups and common markers, harmonization of methods used for production, isolation and analysis of EVs is missing. So far, no standardized protocols have been specified on how vesicles should be handled, because the currently available and used methods still suffer from many limitations. A detailed discussion on the different EV sources and the capabilities and restrictions of used methods is presented in sections 1.1.3, 1.1.4 and 1.1.5. Nevertheless, ISEV and its members are constantly working on defining common standards and publishing general recommendations on production, collection and analysis of EVs [8, 9] and detailed reviews that point out critical factors for consideration specified for different research areas [10-13].

Besides others, one of the key areas within current EV research deals with the diverse functions of EVs in cancer and their potential use in clinical applications. EVs have been shown to play critical roles in many processes related to cancer development and growth, modulation of the immune system, angiogenesis and metastasis. In this regard the vesicles serve as communication instruments that transfer information between adjacent or distant cells leading to a change in phenotype or function in the recipient cells. The major findings on EVs and their role in association to the hallmarks of cancer are explained in section 1.1.6. Also their potential for the clinical application as biomarker and in cancer therapy is discussed in this section.

1.1.1 Types and Biogenesis

All EVs are characterized by the lipid bilayer membrane that surrounds them and origins from the cellular plasma membrane. Even though the different types of vesicles share the property that their membranes resemble those of their cell of origin in composition and orientation, they are built and secreted by the cells via different pathways, according to which EVs are categorized as apoptotic bodies, microvesicles or exosomes.

A very well described cellular process is the programmed cell death or apoptosis. During this process the cell is decomposing itself by vesiculation of its constituents. In other words the cell is packaging all its molecules, nucleic acids, proteins, membranes and organelles into lipid vesicles that are destined to be taken up by other cells for clearing and recycling of the components. These vesicles are called apoptotic bodies and have a very broad size range from 50 to 4000 nm,

with the majority of vesicles being bigger than 500 nm [14]. The most important characteristic of this vesicle type is the exposure of phosphatidylserine on their surface [15]. In comparison to the other EV types and their usefulness in medical applications, apoptotic bodies don't seem to be very interesting and are excluded from most of the studies, because they originate from dying cells and have the function of controlled cell clearance, whereas the other types are actively secreted by viable cells.

Microvesicles (MVs), often referred to as microparticles, constitute another class of EVs that are formed by outward budding of the plasma membrane. This process takes place at locations on the cellular membrane, where certain lipid and protein composition allows higher curvature and bending of the bilayer, resulting in formation of lipid vesicles. These areas are often named microdomains or lipid rafts. To initiate the budding process the translocation of phospholipids, especially phosphatidylserine, from the inner leaflet of the plasma membrane to the outer leaflet plays an important role. For finalization of the vesiculation, cytoskeletal structures contract the membrane and complete the budding off of MVs from the cellular membrane to the extracellular space [14]. The characteristic size of MVs is often described as smaller than apoptotic bodies and larger than exosomes with a diameter ranging from 100 to 1000 nm [15], but there are many diverging results published on this topic due to the lack of standardized methods for isolation and analysis. Most likely there is a big overlap in size of different EVs and hence the size cannot be used as a differentiating criterion between different types of EVs.

Exosomes are the third group of EVs. Their biogenesis takes place during the maturation of early endosomes to late endosomes by inward budding of the endosomal membrane. In more detail, the different components of the endosomal sorting complex required for transport (ESCRT) and their associated proteins are responsible for this multi-step process: starting with sorting of transmembrane proteins in the endosome via ubiquitination, followed by endosomal membrane deformation with recruitment of soluble proteins into the vesicles, and finally scission of intraluminal vesicles from the membrane. These vesicle containing endosomes are then called multivesicular endosomes or multivesicular bodies (MVBs). The fate of most MVBs is to fuse with lysosomes and degrade their contents. However, there are MVBs that are destined to fuse with the cellular membrane and release the intraluminal vesicles into the extracellular space. Vesicles built and released through this ESCRT-dependent pathway are called exosomes [9, 16]. Furthermore, it was demonstrated that exosome biogenesis can also occur by ESCRT-independent mechanisms, in which intraluminal vesicle formation seems to require the presence of tetraspanin CD63 in the endosomal membrane for sorting of proteins to the intraluminal vesicles [16]. Another mechanism for vesicle formation in the endosomal membrane involves lipid-metabolism enzymes, like neutral sphingomyelinase, phospholipase D2, and diacyl glycerol

kinase [17, 18], that produce lipids with smaller headgroups, which changes the endosomal membrane curvature to induce inward budding of vesicles. However, little is known about the details of these ESCRT-independent pathways as well as the sorting of cargo molecules to the intraluminal vesicles [16]. Exosomes are reported to have a size ranging between 30 and 150 nm. As for MVs these numbers are again highly dependent on the isolation and analysis methods, but most publications attribute a mean diameter of 100 nm to exosomes [16].

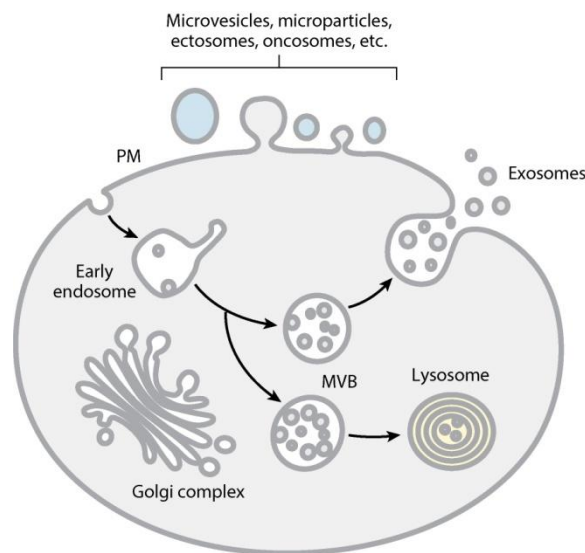


Figure 1 Schematic image of a cell and the different pathways for biogenesis of microvesicles and exosomes (PM – plasma membrane, MVB – multivesicular body). Figure reprinted from [16].

1.1.2 Composition and Function

EVs carry many different molecules within their interior, but also within or attached to the membrane. These cargo molecules make EVs unique in their composition and function and vary depending on the cell of origin and the influences acting on the vesicle-secreting cell, as for example the supply with nutrients. For example, soluble proteins and nucleic acids, including different kinds of ribonucleic acids (RNAs) and deoxyribonucleic acids (DNA), are found inside of EVs, whereas membrane associated proteins and different lipid types are localized within the vesicular membrane, as illustrated in Figure 2 [16]. However, the study of EV composition is a complex task, because results are highly influenced by the used EV isolation and analysis methods, the co-isolation of contaminating particles, or the inability to separate different EV populations, which makes data interpretation prone to false conclusions. Nevertheless, some molecules have been repeatedly identified in EV samples from different sources and using several methods, so they have potential to be used as marker for EVs, but it has to be kept in mind that these markers are not generally present in all EVs and it is unknown whether they are unique for a certain type of vesicles. Due to the specific sorting of cargo molecules to the EVs, proteins and molecules from some cellular compartments, namely the endoplasmic reticulum, the Golgi

apparatus, the nucleus, and mitochondria, are not contained in EVs and therefore can be used as negative control for characterization and determination of purity of EV isolations [16].

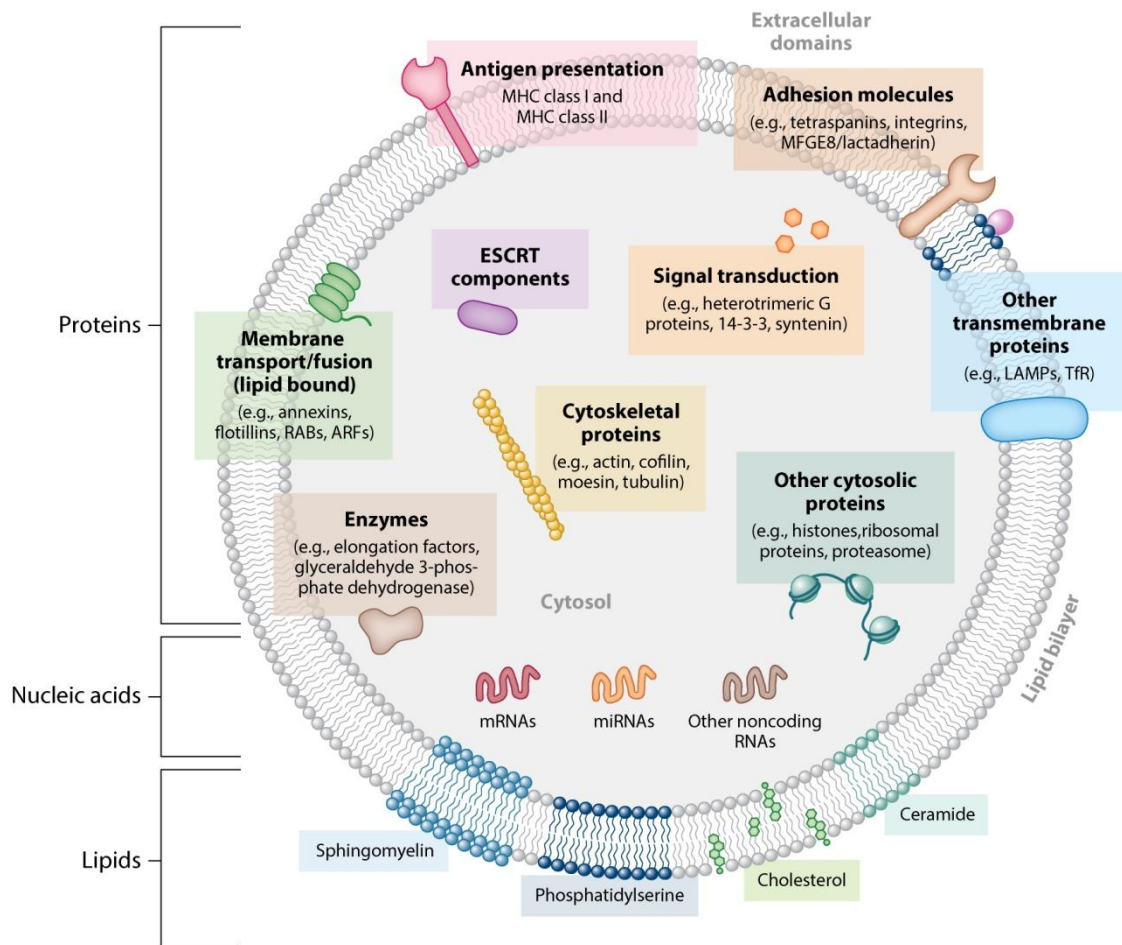


Figure 2 Overall composition of extracellular vesicles (EVs). Some of the listed components may only be present in certain types of EVs (ARF – ADP ribosylation factor, ESCRT – endosomal sorting complex required for transport, LAMP – lysosome-associated membrane protein, MHC – major histocompatibility complex, MFGE8 – milk fat globule-epidermal growth factor-factor VIII, RAB – Ras-related proteins in brain, TfR – transferrin receptor). Figure reprinted from [16].

The components of EVs are either related to their biogenesis and the sorting of cargo molecules to the vesicles or they are associated to their function and therefore more specific for their cell of origin. Examples of the first group are the proteins Alix and tsg101, which are two proteins interacting with the ESCRT for endosomal vesicle formation [19]. Even though ESCRT proteins are mainly involved in exosome biogenesis, a role in the formation of microvesicles also has been identified [16], illustrating how difficult it is to find EV type specific markers. Moreover, chaperones, like the heat shock cognate protein hsc70, are found in endosomal vesicles, i.e. exosomes, since they play a role in ESCRT-independent sorting of soluble proteins [16]. Rab proteins are key players in the regulation of intracellular vesicle transport and involved in vesicle budding, movement of vesicles within the cells, and their tethering to the target membrane to, for example, fuse with the plasma membrane. Some members of this protein family, Rab11, Rab35,

and Rab27, are also associated to the biogenesis of endosomal vesicles and therefore identified as their cargo [16]. Besides these soluble proteins, transmembrane proteins are also found in EVs and play a role in their biogenesis. Especially, the tetraspanins CD9, CD63 and CD81 are reported to be present in a broad range of EVs and play a role in vesicle formation at the endosomal membrane in an ESCRT-independent pathway, but also in shedding of vesicles from tetraspanin-enriched microdomains in the cellular membrane [20]. Other proteins that are often found in EVs are flotillins. These molecules are enriched in membrane subdomains, so called lipid rafts, which are found in the plasma membrane of cells but were also identified in EVs [21]. Lipid rafts are insoluble to detergents, contain high levels of cholesterol and glycosphingolipids, and through their special lipid composition influence membrane fluidity and vesicle transport [22]. Additionally to the already identified detergent resistant microdomains in EVs, vesicles of different cellular origins were found to be enriched in sphingomyelins, gangliosides, ceramides, and cholesterol compared to their parental cells [17]. Thus it is very likely that such lipid rafts are also involved in EV formation and protein sorting to vesicles. Besides these lipids, also phosphatidylserine is found in EVs. This phospholipid is only present on the inner leaflet of the plasma membrane of healthy cells, but through enzymatic activity can be shifted to the outer leaflet, thus changing the membrane curvature and inducing MV shedding [16]. Bis(Monoacylglycero)Phosphate (BMP) is a lipid that is only present in endosomal membranes and absent in the plasma membrane, hence it is exclusive to exosomes and not contained in MVs [18]. Even though these molecules, associated to EV biogenesis and processing, could theoretically serve as exosomal, MV, or general EV markers, experiments often showed that they are not unique to one type of EVs and thus more specific markers are still required. Since the pathways of EV formation are by far not fully understood yet, the elucidation of the involved molecules can yield new and more accurate markers. Also the further development of isolation and analysis techniques will help overcome these limitations of EV research.

The second group of cargo molecules are those associated to EV's functions and often specific to subgroups of EVs and their cell of origin. Due to the plethora of identified EV functions, only some examples of EV components and their particular function are highlighted in the following paragraphs. The transferrin receptor was the first protein identified in exosomes secreted from reticulocytes [5, 6]. During the cell's maturation to erythrocytes several proteins have to be removed from the cell for remodeling and thus exosomes serve as an alternative secretion pathway for disposal of unneeded and obsolete molecules. Furthermore, soluble proteins that don't carry a signal peptide for secretion can be externalized through this exosomal pathway too [19]. In addition to the simple removal of proteins from the cell, EVs serve as communication vehicles that transport information from one cell to another. To transfer such information to a

recipient cell, EVs were so far shown to use one of the two following mechanisms: the attachment of EVs to surface molecules on the target cells and triggering a certain signaling cascade within the cell through receptor-ligand binding or the internalization of EVs into the recipient cells and release of the intraluminal cargo of EVs. One example of the receptor-ligand interaction of EVs with cells works through the major histocompatibility complex class I and II (MHC I and MHC II). These transmembrane proteins are present on many cells and therefore also found on EVs from different cellular origins. They have the capability of antigen presentation, which enables them to induce an immune response in mammals [7]. In particular, EVs derived from dendritic cells carrying either MHC I or MHC II proteins including the antigen peptide and costimulatory factors have the potential to activate T cells and elicit a systemic immune response [23]. Another example showing that transmembrane proteins carried by EVs are functional is the cytotoxic effect of Fas ligand on EVs secreted from natural killer cells. This protein binds to Fas receptors on the target cells, which results in apoptosis of these cells [24]. Besides proteins, lipids on the surface of EVs also have physiological roles. For example, phosphatidylserine is found on platelet derived microvesicles and has an important function in the coagulation of blood, since it provides the negatively charged phospholipid surface that is required for binding and assembly of coagulation factors and activation of the coagulation process [25].

The uptake of EVs into recipient cells works primarily through endocytosis pathways. However, there is yet no consensus on whether EV uptake is mediated by specific endocytic mechanisms [26]. Nevertheless, the presence of EV specific uptake pathways is suggested, since factors influencing these uptake processes were presented already, including, for example, the glycosylation pattern of EVs. Hence, not only the protein and lipid components in EVs exert certain functions, but also their modifications with sugar molecules. Heparin sulfate proteoglycans, for instance, are known to be required for the uptake of EVs by recipient cells [26]. After uptake of EVs, the intraluminal components of EVs are released to interact with the cellular processes. For example, cytokines without a signal peptide for secretion are often found inside of vesicles to be transported to their target cells. TGF β was identified in thymus derived EVs and induced activation of regulatory T cells after internalization, to name just one example [24].

Another major class of biological molecules that are carried by EVs and exert their function after uptake by recipient cells are RNAs. Due to size limitation of vesicles mostly small RNA molecules are carried in EVs, including messenger RNAs or fragments thereof, micro RNAs, long non-coding RNAs and others. Ribosomal RNAs, which are abundant in the cellular cytosol,

are only present at very low or undetectable levels within EVs [16, 24]. A detailed study comparing the RNA content in the three EV types showed that ribosomal RNA is mainly present in apoptotic bodies, found only at low levels in some MVs and absent in exosomes, which only carry small RNA molecules [27]. The secretion of RNAs within EVs helps protecting the RNA from degradation by RNases that are ubiquitously present in extracellular body fluids [16, 24]. Therefore EV-RNAs unlike naked RNAs can travel through the extracellular space and deliver their signals to cells in close proximity or at distant sites. The successful transfer of messenger RNAs between mast cells via exosomes was first shown by Valadi et al. [28], introducing a new pathway for intercellular genetic exchange. This study showed that the RNA molecules were not only transferred, but were also biologically active and could be translated to proteins by the recipient cells, that were not able to express this protein before uptake of the EVs. Since then many studies examined the presence and function of exosomal RNAs with particular focus on micro RNAs. This is because the full length micro RNAs are small enough to fit into EVs and are capable of exerting gene regulatory functions in recipient cells [29]. Many of these studies show that RNAs can be delivered and induce certain changes in the gene expression of the recipient cells, but it is still unclear whether such changes are solely caused by RNAs or rather by the complex composition of EVs, and how RNAs are released within the cells to execute their function.

More biological roles and functions of EVs and their components in regard to cancer development are discussed in section 1.1.6.

1.1.3 Sources of EVs

EVs are secreted by all cell types that have been examined so far and were identified in all kinds of body fluids, including blood plasma and serum, urine, saliva, cerebrospinal fluid, breast milk, ascites, pleural fluid, semen, and others [16].

As described in an ISEV position paper on methodological standardization in EV research [8], besides the right choice of methods for EV isolation and analysis, also the source of EVs should be chosen depending on the aim of the conducted study. For instance, to examine cancer cell derived EVs and their functions, the isolation of EVs from conditioned medium of cultivated cell lines is useful, because all analyzed EVs originate from the same cell type and thus interpretation of results is easier. However, it has to be taken into consideration that even if a homogeneous cell population is cultivated, cells will secrete several types of EVs, e.g. microvesicles and exosomes, that harbor different functions and are difficult to separate by currently available isolation

methods. Furthermore, the cultivation of cells *in vitro* is artificial and does not entirely mirror the biological conditions.

In contrary, for EV biomarker studies on disease diagnostics, human body fluids should be used as source for EVs. In this case the EV source is much more complex, containing a plethora of EVs that originate from different cells and are mixed with many other components. For example, plasma, which is a common body fluid, contains abundant proteins like albumin, aggregates composed of different biomolecules like protein-bound RNA, and lipoproteins. Pure and reliable isolation of EVs is therefore not always possible when using biological fluids and the quality and composition of the isolate should be tested vigorously to ensure that EVs are selectively purified and contaminants successfully removed.

For both cell culture and patient samples, many factors, such as sample production, collection and storage, have important consequences on the subsequent EV preparation and isolation. Hence, it is of utmost importance to plan and define the strategy for sample preparation, collection, storage, and purification in advance to ensure consistency and reproducibility. When purifying EVs from cell culture, the cell's viability, growth rate and density are some of the important factors that will influence the secretion of EVs and ultimately the yield of EVs. The type of cell culture medium and the use of additives like fetal bovine serum are of particular interest in this regard, because serum contains abundant bovine EVs, which can easily bias results [30, 31]. Consequently, the use of chemically defined media without addition of fetal bovine serum is preferred. However this approach is only possible for cells that can survive without addition of serum. If this is not possible the use of EV-depleted serum is also an option, but a complete removal of EVs from serum is very difficult if not impossible to achieve with known methods [32]. A compromise of both strategies is often used for EV production by cells that are usually cultivated with serum, but able to survive for a few days without it. The medium of these cells is simply changed to serum-free medium for the time of EV production. But it has to be considered for all these approaches that the change of nutrients will trigger some response in the cells and might influence the composition of the secreted EVs [33, 34].

On the other hand, in EV isolation from body fluids, such as blood plasma, the time of blood collection, the choice of anticoagulant, the centrifugation parameters for plasma purification from whole blood samples, and the time and temperature of storage prior to EV isolation are some of the critical factors affecting the purification of EVs from plasma [35, 36]. The type of anticoagulants, such as EDTA, sodium-citrate, and sodium-heparin, commonly used to prevent coagulation of whole blood samples for plasma preparation was reported to greatly affect the EV content in plasma [37, 38]. Heparin, for example, can bind to EVs and thus influence their uptake

by cells, function and behavior. Plasma from EDTA treated blood has much higher MV counts than that from sodium-citrate treated blood. Moreover, the composition and procoagulant function of MVs was altered when blood samples were stored for 48 hours at room temperature or 4 °C. Consequently, factors such as the preparation, storage time and temperature in the processing of body fluids for EV extraction will have to be taken into consideration when planning studies. Protocols should be tested and optimized to achieve reliable and reproducible results in the downstream isolation and analysis procedures.

1.1.4 Methods of Isolation

Many different methods and protocols for EV isolation are currently used in the EV research field. They all have limitations and no optimal method, which could serve as standard method, has been found yet. This is mostly due to the heterogeneity of EVs in their biological and physical characteristics, which makes separation of individual EV types very complex. Furthermore, other biomolecules like proteins or lipoproteins have similar properties as EVs and thus can easily be co-purified during EV-isolation. Nevertheless, it is possible to reliably and reproducibly isolate EVs with the currently available methods, if all methodological limitations are taken into consideration. The choice of methods has to be made upon first defining the aim of the study and also considering the compliancy with the downstream analysis procedures and applications. Moreover, the isolation procedures and all influencing factors should be tested vigorously before commencing a study.

The here described isolation methods make use of the vesicle's size, density, and their specific or non-specific interaction with other molecules, like polymers or antibodies, for their separation from conditioned cell medium or biological fluids.

1.1.4.1 Centrifugation

Ultracentrifugation, differential centrifugation and density gradient centrifugation are the most commonly used methods for the isolation of EVs [39], despite many issues associated with these methods. In differential centrifugation protocols, as depicted in Figure 3a, sample solutions, like conditioned cell culture supernatant or body fluids, are typically first centrifuged at a low speed of ~300 g to remove cells. Then a centrifugation step at about 1,000 g is performed to remove cell debris and big vesicles, like apoptotic bodies. Next, high speed centrifugation or ultracentrifugation is performed depending on the vesicle type to be isolated. Larger vesicles are usually sedimented at a centrifugation speed ranging from 10,000 to 20,000 g, while smaller vesicles are sedimented at a much higher speed of 100,000 to 120,000 g. This is typically followed by a second round of centrifugation to wash the pelleted vesicles and remove contamination [40,

41]. Many factors are influencing the sedimentation efficiency of EVs during ultracentrifugation. First of all, the characteristics of the vesicles, like size, weight and density, play a major role, and they can all vary depending on the type or origin of the targeted EVs. Next, the conditions of the centrifugation itself have of course a big influence on the isolation efficiency. These include not only the speed and time of centrifugation, but also the type of centrifuge and rotor that is used [42]. Finally, also the viscosity of the medium from which the vesicles should be separated impacts their sedimentation. This is particularly important if EVs are isolated from complex mediums like body fluids with high viscosities. In such cases the sample fluid should be diluted before centrifugation [40]. However, the influence of the medium can also be utilized to improve purity of the EV isolates by combining ultracentrifugation with density gradients. Using density gradient centrifugation the sample components are separated according to their floating densities and vesicles stay in a certain fraction of the used density gradient and don't pellet, as illustrated in Figure 3b. This method can help to remove contamination by proteins, but other contaminants like different types of EVs or lipoprotein vesicles can still be copurified, because of their overlapping densities [43, 44].

As mentioned above, centrifugation based isolation methods have many disadvantages. For example, ultracentrifugation tends to cause vesicle aggregation due to the high forces exerted on them [45], resulting in low yields because the vesicle pellets are only partially resuspendable, making analysis of single vesicles impossible. Furthermore, as ultracentrifugation sediments EVs based on density or mass, other large biomolecules with similar properties also co-sediment with the EVs.

In summary, it can be stated that centrifugation based methods are not able to yield pure EV populations, but if the contamination level is not critical for the following downstream analysis, this could still be a useful method for vesicle enrichment.

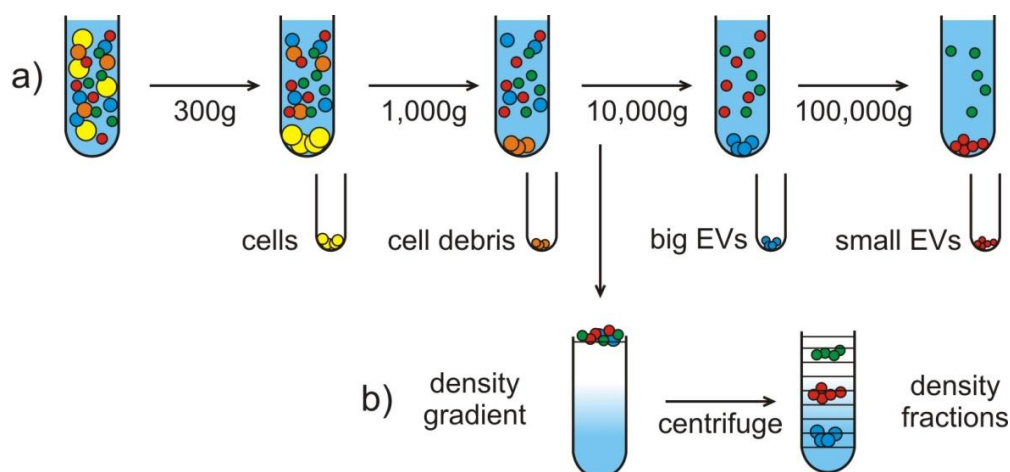


Figure 3 Schematics of a) a differential centrifugation protocol and b) a density gradient centrifugation procedure.

Figure adapted from [41].

1.1.4.2 Filtration

Filtration procedures separate molecules, particles or vesicles based on their different sizes. These methods are regularly used in combination with differential centrifugation and replace some of the low speed centrifugation steps. Filtration is therefore commonly used as a prepurification step to remove bigger compounds from the samples. For this purpose, filters with a pore size of 0.8 or 0.2 μm are used, depending on the size of the EVs that should be purified. In case of big sample volumes and low concentration of EVs, which might be the case if cell culture supernatant is used as EV source, it can be useful to use filtration methods, like tangential flow filtration, to concentrate the sample before further isolation steps. Still it has to be taken into consideration that using high pressure to force the sample through a filter may lead to disruption of large vesicles into small ones and thus may falsify the results. Furthermore, EVs could stick to the filter membranes, resulting in lower yields [8].

1.1.4.3 Size exclusion chromatography

Size exclusion chromatography also separates vesicles according to their size. In this method a chromatography column is filled with a porous material that allows only small molecules to enter the pores, while larger molecules cannot enter. Therefore, large molecules or particles will flow through the chromatography column faster than smaller molecules that are retained in the column. Size exclusion chromatography is currently the most promising method for total EV isolation, because this method is able to separate EVs from proteins and lipoproteins [46]. Furthermore the vesicles are not exposed to heavy forces and thus won't aggregate and keep their biological activity, which can be impaired otherwise. Nevertheless, the separation of certain EV types and subpopulations is still challenging, because of the overlapping size range of exosomes and microvesicles. Moreover, similar to the filtration process, EVs could attach irreversibly to the packed column materials and thus lead to lower yields.

1.1.4.4 Polymer-based precipitation

For precipitation of EVs with polymer solutions the sample fluid is incubated over night in a polymer mixture that often contains polyethylene glycol. The large molecule precipitate is then separated from the solution by low speed centrifugation [47]. The use of this method to isolate EVs from samples is very tempting, because it is a fast and easy procedure and the required materials are already available as kits for isolation of EVs or exosomes. However, the precipitation process is very non-specific and anything that interacts with the polymers will precipitate together with the vesicles, including proteins, RNAs or other biomolecules [8]. Furthermore, the polymer remaining in the isolate can interfere with downstream analysis methods.

1.1.4.5 Affinity capture

If specific populations of EVs should be isolated, that carry certain molecules on their surface, they can be readily isolated using affinity binding methods. These methods use the affinity of antibodies or other ligands for the target molecule on the surface of EVs to capture and isolate the EVs. The capture molecules are usually immobilized on a solid phase, for example surfaces in a packed column or magnetic or non-magnetic beads of different sizes, to facilitate the separation of the captured EVs from the sample medium. Magnetic particles and their bound target EVs can, for instance, be separated from the sample fluid by application of magnetic forces, as depicted in Figure 4. Non-magnetic particles, like polystyrene beads, can be easily pelleted by low speed centrifugation or separated by filtration [48, 49]. Compared to the above methods, affinity capture is much more specific and can yield much purer EV preparations. Furthermore, it can also be used to deplete a sample of undesired vesicles or contaminating molecules by using molecules specifically binding to these unwanted moieties and using the remaining supernatant for further analysis [8]. It should be noted that at this time point there are no general EV, exosomal or microvesicle markers that could be used for such isolation. Although tetraspanins, as mentioned above, are widely used in many commercial isolation and analysis kits for exosome purification, it is not definitive that tetraspanins are present only on exosomes and not on other EV types. Additionally, even if EVs that carry cell type-specific molecules are isolated, it is unclear if all of the EVs from this cell type would carry the targeted molecule and in what amount or density.

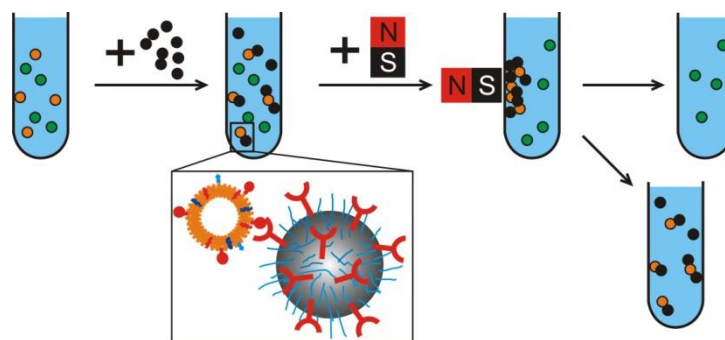


Figure 4 Schematics of affinity based isolation with magnetic beads.

Furthermore, it has to be considered that the removal of the vesicles from the matrix used for isolation, e.g. beads or packed gel columns, can be very complicated. Reversible binding of high affinity interactions is often impossible or can only be achieved under harsh conditions that likely affect the integrity of the EVs. Hence, such isolation methods could be problematic if the function of vesicles is to be studied. However, if only the molecular composition is of interest, removal from the isolation matrix by, for instance, lysis of vesicles won't influence downstream analysis methods and results.

1.1.5 Methods of Analysis

Analysis of EV samples serves not only to study and identify new components or functions in EVs, it is also crucial for testing the quality and purity of the isolated material. As EVs are highly heterogeneous, the analyzed EV sample should be clearly defined in terms of its source, preparation, EV isolation protocol, and other biophysical parameters such as density, size distribution profile, etc. to facilitate comparison among the research community [9]. As for the isolation methods, the biggest challenge in EV analysis is their heterogeneity and small size. Hence, some methods can only detect bigger particles and most likely miss the majority of small EVs, while others are able to detect small ones, but have a narrow dynamic range. Therefore, these methods are only capable of analyzing monodisperse samples, and face limitations when EVs of a wide size distribution are present in samples. Also, there are analysis methods that are examining only the bulk EV sample, giving a rough overview of the general characteristics, but not going into differentiation of EV subgroups. On the contrary, single particle analysis methods are able to analyze and quantify EVs individually, but often suffer from high detection limits and low signals induced by individual EVs, resulting in overlooking smaller vesicles.

When choosing methods for the analysis of EVs it has to be kept in mind that the isolation method and the associated impurity of EV samples can highly influence and bias analytical results. Thus, the procedures for isolation and subsequent analysis have to be concerted and harmonized. Methods for the assessment of the most frequently studied characteristics or parameters of EVs, that are their size, concentration, composition, and zeta-potential (particle surface charge), are discussed in the following sections.

1.1.5.1 Microscopy

Due to the nanometer size range of EVs, regular light microscopy, which is routinely used in life sciences, cannot be used to examine EVs. For this purpose high-resolution and -magnification microscopy techniques have to be employed. Super-resolution microscopy was just recently proposed as a novel imaging method for examination of EVs [50], but due to its novelty this method is still limited to highly trained researchers and not yet useful for a broader range of studies. On the contrary, electron microscopy or atomic force microscopy are already well established imaging methods with extremely high resolution, that belong to the most used analysis methods in EV research [39]. In electron microscopy an electron beam is made incident on the sample and the effects of the sample on the electron waves are measured. When the electrons hit the sample, they can be reflected, scattered, transmitted or their energy can be taken up and released again as x-ray radiation or secondary electrons, etc. The different techniques of

electron microscopy are optimized to measure some of these effects and enable to make assumptions on the sample structure, composition, electron density and surface characteristics.

In transmission electron microscopy (TEM) the electron waves that are transmitted through the sample are detected and create an image that depicts where more or fewer electrons travelled through the specimen. For this procedure, biological samples, including EVs, have to be prepared and processed with rather harsh methods that can lead to artifacts, as for example the cup-shape-like morphology of EVs that resulted from the dehydration process and was mistakenly described as EV characteristic in many reports [16] (see Figure 5a). Such dehydration and fixation steps can be avoided by using cryo-TEM. In this method a small volume of liquid sample is frozen instantaneously by exposure to liquid nitrogen resulting in a very thin section that can be examined by TEM [51]. Through this immediate and very quick freezing, the built ice crystals stay small and don't harm the sample material. Hence the vesicles' morphology is not changed and EVs keep their round shape (see Figure 5b and c). To gain more information from TEM methods, gold nanoparticles are employed for labeling of vesicles [52]. Nanoparticles, that are conjugated to specific antibodies or other ligands for specific binding to EVs, are incubated with the EV sample before sample preparation procedures for TEM are performed. The high electron density of the metallic nanoparticles leads to high contrast and visibility of the nanoparticles in the TEM images and yield qualitative information on the composition of the examined EVs (see Figure 5c).

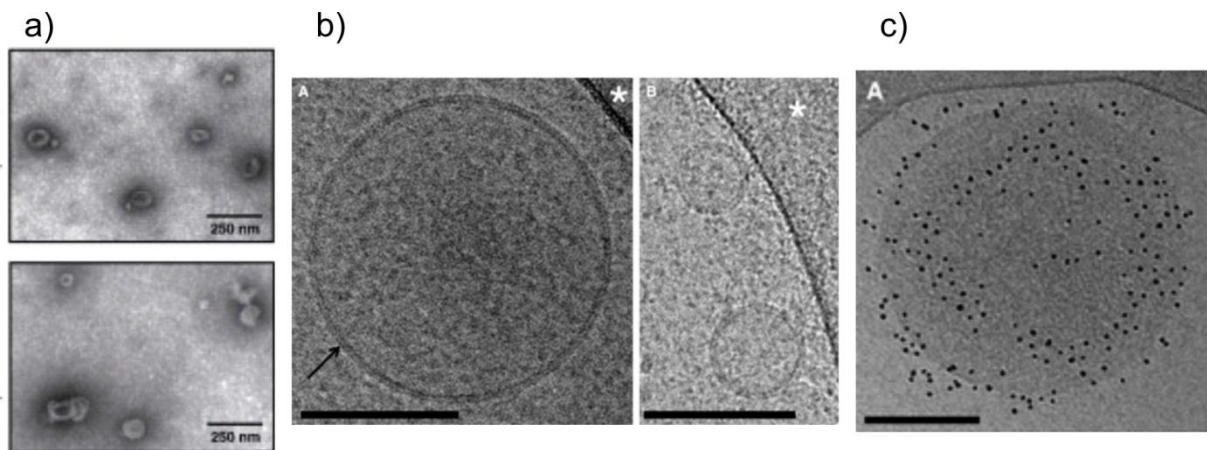


Figure 5 Electron microscopy images of EVs. The images were generated by TEM (a) and cryo-TEM (b and c). In c) the vesicles were labeled with gold nanoparticles conjugated to Annexin V. a) is reprinted from [53], b) and c) from [51].

Scanning electron microscopy (SEM) is another imaging method for EV visualization. This type of electron microscopy measures the secondary electrons that are emitted from the sample after exposure to the electron beam, which is used to scan across the sample. Thus, SEM allows making a topographical image of the surface. A disadvantage of SEM is that biological samples

need to be coated with an electrically conductive material, hence alterations due to sample processing can occur [52]. Atomic force microscopy (AFM) is another microscopic method that yields topographic information of a sample surface. In AFM a cantilever with a sharp tip is moved across the sample in very close proximity to the surface and its deflection caused by the interaction forces of the tip and the sample is monitored. Besides the topographical information AFM can also generate information of chemical and mechanical properties. For biological sciences and EV research, the most important advantage of AFM is that EVs can be examined directly in liquid samples, meaning that no sample preparation is required, except for the immobilization of the vesicles on a surface [52, 54]. However, a high level of expertise is required to examine lipid vesicles in solution by AFM, because the soft nature of the EVs makes them prone to deformation and rupture by too high pressures exerted by the AFM tip.

High-resolution microscopic methods, and especially TEM, are well-suited tools to gain information on the morphology and composition of EVs and contributed to EV-research since the first discovery of these small lipid vesicles [5, 55]. However, when it comes to quantification of EVs and examining size and size distribution these imaging methods are limited. Even though, it is possible to count EVs and measure their size in microscopic images per area and calculate concentration values from this, the generated data have to be handled with caution, because the size can be affected from sample processing procedures. Additionally, only small numbers of EVs are usually examined, because of the lengthy handling time, and the number of EVs can be biased by the EV collection on the EM grids [52, 56].

1.1.5.2 Dynamic light scattering and nanoparticle tracking analysis

The term light scattering summarizes the deflection of light waves when a light beam is hitting an object. This principle can be used to detect nano-sized particles in suspensions and track them over time, while they are moving through the suspension due to Brownian motion. The speed of the particle movement is dependent on the size of the particles, the viscosity of the suspension and the temperature. If the two latter conditions are known, the particle size can be determined from the velocity of the particles that is determined by tracking the scattered light intensity in a defined area. Dynamic light scattering (DLS) and nanoparticle tracking analysis (NTA) use this principle to analyze size, size distribution and concentration of nano-sized objects including EVs and NTA additionally visualizes the analyzed particles by light microscopy [52, 57]. A schematic of a NTA setup is presented in Figure 6. Both methods are very useful in the analysis of monodisperse suspensions, meaning samples with particles of a narrow size range, but face severe limitations when polydisperse samples are examined, due to their narrow detection range. First of all, the scattering caused by bigger particles is much stronger compared to that of small

particles, hence the high intensity of scattered light from big particles can mask smaller particles. Furthermore, for the same reason, the results of these measurements are highly dependent on the instrument settings and measurement parameters, since strongly scattering particles can be detected with high threshold settings, but weakly scattering particles need lower thresholds for detection [58]. Moreover the scattering ability of particles is strongly affected by the difference in refractive index between the particles and the solution they are suspended in. For example, solid nanoparticles, that are often used for calibration of the instruments or as reference, have strong scattering properties and can be easily detected down to small nanometer sizes. Lipid vesicles like EVs, on the other hand, are composed mainly of water and biomolecules and therefore have a very similar refractive index to water, which results in very weak scattering abilities and a higher detectable size cutoff of 50-100 nm in diameter [52, 59]. Another limitation for light scattering based analysis methods is the low specificity, since every particle present in the sample suspension, including lipoproteins, protein aggregates, and even salt crystals, can scatter light and thus will be counted by the detector [8]. Consequently, the analysis results are also dependent on the purity of the EV sample. Moreover, vesicle aggregates cannot be discriminated from single vesicles and will be categorized as one big particle, instead of several small ones. Nevertheless, the incorporation of fluorescence detection in NTA instruments can enhance specificity, sensitivity and add information on the composition of the analyzed EVs [60]. By binding of fluorescent tags and labels to the vesicles via specific antibodies or other ligands, subpopulations of EVs can be analyzed and their specific size distribution and concentration can be determined. Furthermore, by using the fluorescence signal for detection, instead of the scattered light, the performance of NTA in detection of EVs can be improved [60]. But of course, this is only an option if a certain subgroup of EVs carrying a specific molecule should be studied and not the general EV population.

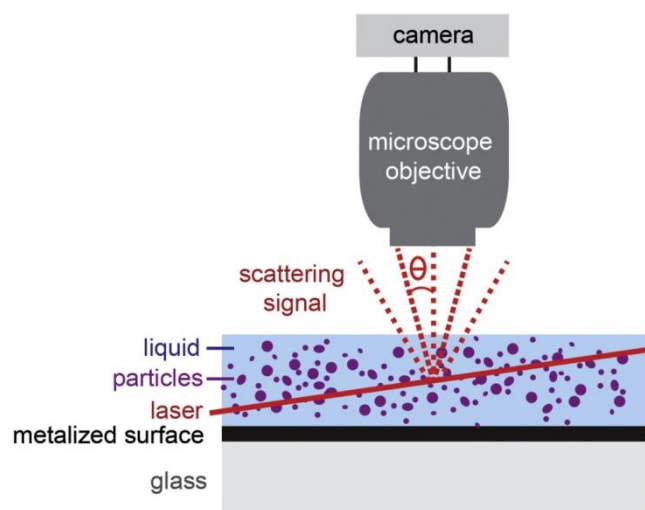


Figure 6 Illustration of a nanoparticle tracking analysis setup. Figure reprinted from [52].

In addition, instruments for DLS and NTA are capable of determining the zeta-potential of vesicles, by examining the particle motion when electrical fields are applied. The velocity of the particles within the electrical field is related to the vesicle's surface charge, which again can give information on its composition [52].

1.1.5.3 Flow cytometry

In flow cytometry (FC) particle suspensions are flowed across a laser beam and the scattered light is detected, yielding information on the size and the number of particles passing the laser. As the name indicates, this method was developed and optimized for analysis of cells, which are much bigger in size than EVs, but in recent years FC has been adapted and improved for EV analysis as well. Besides improvement of the detection limit by instrumental developments, also the methodology changed from light scattering to fluorescence based detection.

Due to the weak light scattering properties of lipid vesicles, as already explained for DLS and NTA above, conventional FC is only able to detect vesicles down to a diameter of 300-600 nm [59], leading to the finding that just ~1 % of EVs in platelet free plasma are detectable by FC when compared to the vesicle counts from cryo-EM [51]. When using the fluorescence signal for thresholding and detection of vesicles in FC, vesicles with sizes ranging from 100 to 150 nm in diameter are detectable [61]. For the determination of EV concentration, this leads to a 50 fold higher value when analyzing plasma vesicles fluorescently labeled with AnnexinV-Cy5 conjugates with fluorescent triggering compared to light scattering mode [61]. However, the detection limit is highly dependent on the number of fluorophores present on the vesicles, which again depends on the number of the moieties available for fluorescent labeling on the vesicle's surface. This is shown beautifully by Arraud et al. who analyzed different subpopulations of plasma EVs and saw that concentrations were increased 15, 40 or 75 fold when comparing fluorescence to scattering mode, depending on the surface marker of the vesicles that was used for labeling [62]. As mentioned above, FC was designed for single cell analysis and therefore the fluidic system is built to separate cells and analyze them individually. This means that the fluidics are in the size of micrometers allowing just one cell to pass the laser at a time, but not separating EVs. Consequently, the so called swarm detection has to be taken into consideration when analyzing EVs by FC. This means that several vesicles, that are passing the laser at the same time, are detected as one vesicle with higher intensity and thus bigger size. Even though this is a severe problem during FC measurements, it can be solved quite easily by dilution of the samples to lower concentrations, in which only single EVs pass the laser [63, 64].

Generally FC is very useful for the concentration determination of EVs, if the right settings and techniques are used. Currently only detection with fluorescence thresholding gives trustworthy

results, because also smaller vesicles are detectable. But with further development of the FC instruments, in future, also light scattering detection will be feasible for EV analysis. Another advantage of FC is the ability to detect several surface markers simultaneously and thus get information on EV's composition and subpopulation characteristics. The determination of size distribution of EVs by FC is more complicated, because this requires calibration with standards in order to calculate the size of a particle from its scattering intensity measured by FC [52]. These reference samples usually contain beads in different sizes made from polystyrene or silica and thus have different scattering properties compared to EVs, because of their different material and refractive index. If these differences are not considered, the accuracy of the size determination is very poor.

Imaging FC is a recently developed method that combines FC with microscopy and enables to image every particle that triggers a scattering or fluorescence signal when passing the laser beam. By these means it was already shown that the interaction or at least the attachment of specific EVs with certain cells can be examined [37]. This further improvement of FC holds great potential for a more detailed and precise analysis of EVs and their cargo molecules.

1.1.5.4 Tunable resistive pulse sensing

The method of tunable resistive pulse sensing (TRPS) is based on the fact that an electrical current through a membrane pore changes or becomes partially blocked, when a particle travels through this pore [65]. In this method the electrical current between two electrodes in a conductive electrolyte solution is measured continuously. The two electrodes are separated by a nonconductive membrane that harbors a single pore, through which the so called trans-membrane current travels. As soon as a particle or vesicle is entering the pore, the electrical current through the pore decreases, because it's blocked by the particle that has a lower electric conductivity than the electrolyte solution in which it is suspended. The extent and intensity of this current decrease, or also called resistive pulse, relates to the size of the particle. The bigger the resistive pulse intensity, the bigger is the particle or vesicle that travels through the pore. By analyzing the resistive pulse events over time, the particle concentration of a sample solution can also be determined. But both, size and concentration determination, rely on the calibration with standards of known size and concentration, because the measurement conditions and therefore the electrical current and the pulse intensity vary depending on the pore geometry [65]. In order to measure particles of different sizes the size of the pore has to be adjusted, because if the particles are too big in relation to the pore, they would not be able to pass through and clog the pore, or if the particles are too small they would travel through the pore without triggering a resistive pulse and therefore without being detected [66], as illustrated in Figure 7. In TRPS, the

pore size adjustments are achieved by decreasing or increasing the strain exerted on the membrane. Therefore the pore size correlates directly with the sensitivity of the instrument, meaning that a smaller pore size can detect smaller particles. Currently, the TRPS is able to detect vesicles down to 35 nm in diameter, but only at instrument settings that make the measurement system very unstable because of many pore blockages [66].

The above mentioned pore blockages occur when particles or vesicles, that are too big to pass through the pore, get stuck and block the pore. These events can be reversed by inverting the sample flow, but they still lead to instability of the measurement system, which affects usability of this analysis method [66]. Also the unspecific binding of vesicles or molecules to the membrane or pore highly influences the measurements, because the current baseline and also the resistive pulse intensity will be affected by any kind of change resulting from specific or unspecific interactions. However, with standardized protocols TRPS is capable of accurately and reproducibly determining EV concentrations, which has been tested in a comparative multi-center study [67].

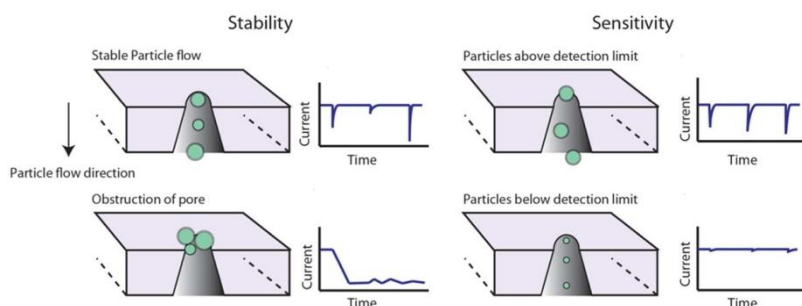


Figure 7 Illustration of stability and sensitivity of tunable resistive pulse sensing and resulting signals. Figure reprinted from [66].

By application of an electric field across the membrane pore, also the zeta-potential or surface charge of vesicles can be determined by TRPS. In this case the velocity of the vesicles moving through the pore and within the electric field correlates to the intensity of the resistive pulse and therefore the surface charge can be calculated.

1.1.5.5 Protein and nucleic acid bulk assays

In addition to the above described methods that are capable of analyzing individual EVs, there are also several methods commonly used that analyze the bulk characteristics of EVs in a sample. These methods mostly serve to determine the composition and cargo molecules of vesicles and are routinely used and well established in biological laboratories.

The total protein concentration is often determined in order to quantify EV samples. The most common methods are based on colorimetric measurements and differ in the chromogen used. Two commonly used assays are the Bradford assay [68], that uses Coomassie Brilliant Blue G-250

for staining of proteins and the BCA assay [69] utilizing bicinchoninic acid for protein concentration determination. Even though these methods are used routinely, there are still limitations and variations in results depending on protein amino acid composition and comparability to the used standard solutions. Especially, the determination of total protein concentrations in complex samples like EVs is challenging, as the different chromogens interact differently with proteins of varying purity and composition, leading to divergent result [70]. Even though, the total protein concentration values are commonly used as a surrogate for EV concentrations. However, its usefulness is very limited, because of co-purified proteins that bias the results and the unknown amount of protein per vesicle [71].

The presence and amount of certain proteins in isolated EVs is often determined by Western blot and enzyme linked immunosorbent assay (ELISA) [39, 72]. Western blotting relies on the lysis of isolated EVs and subsequent separation of the contained proteins by molecular weight through gel electrophoresis. Then proteins are transferred from the gel onto a nitrocellulose membrane and certain proteins are consecutively labeled with specific antibodies that are then detected via colorimetric, chemiluminescent or fluorescent systems [72]. Western blotting is a semi-quantitative method, because it can only quantify differences in protein levels between samples, but doesn't yield absolute concentration values. However, the comparison of the results with standard solutions and a calibration curve can provide such information, but this is typically very tedious, because Western blot is not useful for big sample numbers. In ELISA target molecules of intact or lysed EV samples are immobilized on a surface functionalized with specific capture antibodies. After washing away unbound particles and molecules, another set of specific antibodies is used for the detection of the proteins of interest in a so-called sandwich assay [72]. As for Western blot the detection can be performed with colorimetric, chemiluminescent or fluorescent approaches. The concentration of the target protein is determined by comparison to the signal resulting from standard solutions, which most commonly comprises of the free protein. In this context, it has to be taken into consideration that EVs, if intact, have much slower diffusion rates and therefore will have different binding kinetics to the functionalized surface compared to the standard solutions containing the free protein. If EV samples are lysed and the target molecules are free, this limitation can be circumvented.

Both methods are very useful for proving that certain molecules or markers are present or absent in the samples to verify the identity of EVs and their vesicular nature or endosomal origin. Furthermore, they can be used for comparative studies to examine whether proteins are present at different levels in EV samples harvested from different conditions, for instance healthy compared to disease. However, these methods are not able to determine the distribution of the measured molecule on the EVs [52]. Consequently, from these analyses it is not inferable if the

examined protein is only present in a subpopulation of EVs or in all of them. Along the same lines, when different levels of the target molecule are observed, it cannot be known whether these differences result from a higher number of EVs carrying the molecule or if the same population of EVs is carrying more of the molecule. Furthermore, Western blot and ELISA cannot differentiate between potentially co-purified free proteins or protein aggregates and truly EV-associated molecules of the same kind [8]. Hence, these methods are highly dependent on the quality of the isolation method used for the sample preparation. Through engineering of the used antibodies to be specific for certain epitopes on the proteins, the specificity of these methods can be improved and more information on the EV sample and the protein localization can be gained. For example, by using antibodies specifically binding to extracellular or intracellular epitopes of a transmembrane protein, it can be brought to light whether such proteins are oriented in the EV membrane in the same manner as in the cellular membrane or whether EV's lipid bilayers are intact. If a broader range of proteins should be examined or new EV-associated markers identified, broader proteomic approaches like mass spectrometry are applied [73]. These methods yield big datasets and by usage of bioinformatics tools all proteins present in a sample can be examined. The actual value of such newly identified proteins for use in research or clinics has to be validated with independent methods, because a general problem of big data sciences is the identification of correlations that are statistically significant, but biologically irrelevant and therefore unusable.

In similar ways, the nucleic acid content of EVs is determined by RNA or DNA isolation from EV samples and subsequent analysis with quantitative (reverse transcriptase) PCR [11]. By these means the presence and expression levels of certain nucleic acid molecules (e.g. messenger RNA, micro RNA, long noncoding RNA, genomic DNA) can be determined. For more exploratory approaches and identification of new nucleic acid molecules present in EV samples, next generation sequencing is regularly used [11]. As discussed above for the bulk assays for protein detection, these methods have the same limitations concerning the determination of the amount of molecules per EVs and their localization within, outside or not associated with EVs.

All of the bulk assays mentioned above, are at least semi-quantitative, making quantification of the analyzed molecule possible. However, in this regard normalization between samples to achieve comparability is the biggest challenge for these assays. As no general EV markers, on neither protein nor nucleic acid side, are known yet, molecules that are found in EV isolations at stable levels over all experimental conditions have to be identified for each study, before quantitative experiments and comparisons can be performed.

Besides the fact that the bulk analysis assays cannot differentiate which kind of EVs in the often very heterogeneous EV samples are carrying the analyzed molecules, they are very useful tools to verify the presence or absence of certain compounds in EV samples, including contaminating particles and molecules, hence yielding valuable information on the quality of EV samples and used isolation methods.

1.1.5.6 Emerging techniques

To overcome issues of time-consuming and labor-intense procedures for analysis and isolation of EVs, microfluidic devices, that are capable of detecting EVs by simpler means, have been developed. These so-called “lab-on-a-chip” devices rely mostly on affinity binding of antibodies to molecular components of EVs for capturing and detection of vesicles. One of the first microfluidic chips, called ExoChip, was presented by Kanwar et al. in 2014 [74], who incorporated both isolation and detection of EVs in one device by first capturing the EVs within small chambers on the chip utilizing antibodies specific for CD63, a surface marker present on many EVs, and then labeling the vesicular membrane with a lipophilic fluorescent dye. By the special design of the microfluidic channels, depicted in Figure 8a, the sample’s retention time within the small chambers is increased giving the vesicles more time to interact with the functionalized surface. Furthermore the channels connecting the chambers change the fluid velocity, thus leading to mixing of the sample and higher efficiency of vesicle capturing.

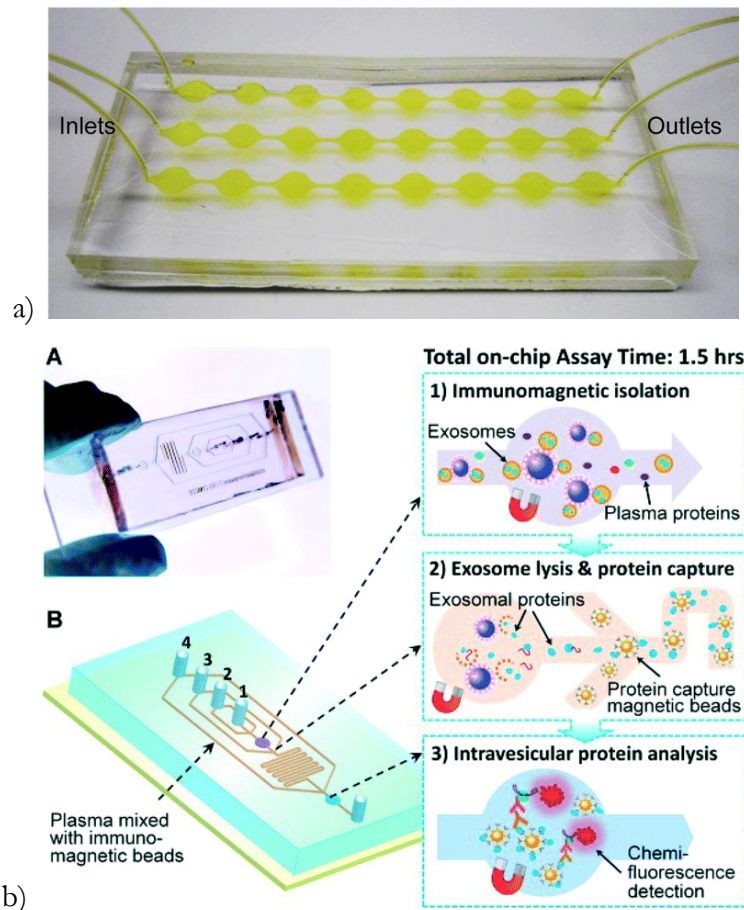


Figure 8 Microfluidic devices for EV isolation and detection. a) Design of ExoChip, reprinted from [74], b) Schematics of the working principle of on chip magnetic-bead based isolation and detection of EVs, reprinted from [75].

A different approach uses magnetic beads for immuno-capturing of EVs via different antibodies specific for molecules present on the surface of EVs [75]. The magnetic beads are pre-incubated with the EV samples and then collected in the microfluidic chip by application of a magnetic field. Consecutively, the captured EVs were lysed within the flow cell and intravesicular molecules were analyzed by an ELISA-like assay via immobilization of the molecules onto newly introduced magnetic beads. The schematics of the microfluidic chip and the steps of the procedure are illustrated in Figure 8b. This microfluidic device was further improved by incorporation of the pre-incubation step into the chip [76]. In this improved version, the sample was directly injected into the microfluidic chip and was mixed with the functionalized magnetic beads while flowing through a Y-shaped microfluidic channel. After capturing, the surface markers of EVs were detected by an on-bead ELISA.

Moreover, chips have been designed that rely on the isolation of EVs by their size. These devices make use of consecutive filtration steps that separate big from small particles. In this regard, ExoDisc [77] was introduced that enriches EVs in the size range of 20 to 600 nm, which can be either collected from the device and used for subsequent analysis or analyzed directly on the chip

by ELISA for surface markers. Another very different approach was presented by Lee et al., which used acoustic purification to separate EVs by their size in a microfluidic device [78]. Based on the radiation forces acting on the vesicles resulting from the ultrasound waves, the EVs move differently in the acoustic field depending on their size. Thus, differently sized EV populations can be spatially separated while flowing through a channel and collected in separate chambers after passing through the acoustic field.

Besides microfluidic technologies that mostly improve already existing methods in regard to their usability, advances in the field of nanosciences have also shown promising results for the application to EV analysis. For instance, EVs were specifically coupled to magnetic nanoparticles and subsequently analyzed by a miniaturized nuclear magnetic resonance (NMR) system that was incorporated into a microfluidic chip [79]. The binding of the magnetic nanoparticles to vesicles via surface molecules changed their magnetic behavior and resulted in an increased decay rate of the NMR signal. This change in decay rate is proportional to the amount of magnetic nanoparticles bound to EVs, therefore enabling to quantify certain EV populations that carry the targeted molecule. Another example is the development of a nanomechanical assay that uses cantilevers made from gold and measures the mass of EVs binding to their surface [80]. Through functionalization of the cantilever surface with antibodies specific for proteins present in EVs, as depicted in Figure 9, the amount of EV subpopulation carrying the targeted molecule can be determined and by consecutive binding of gold nanoparticles the signal can be further enhanced.

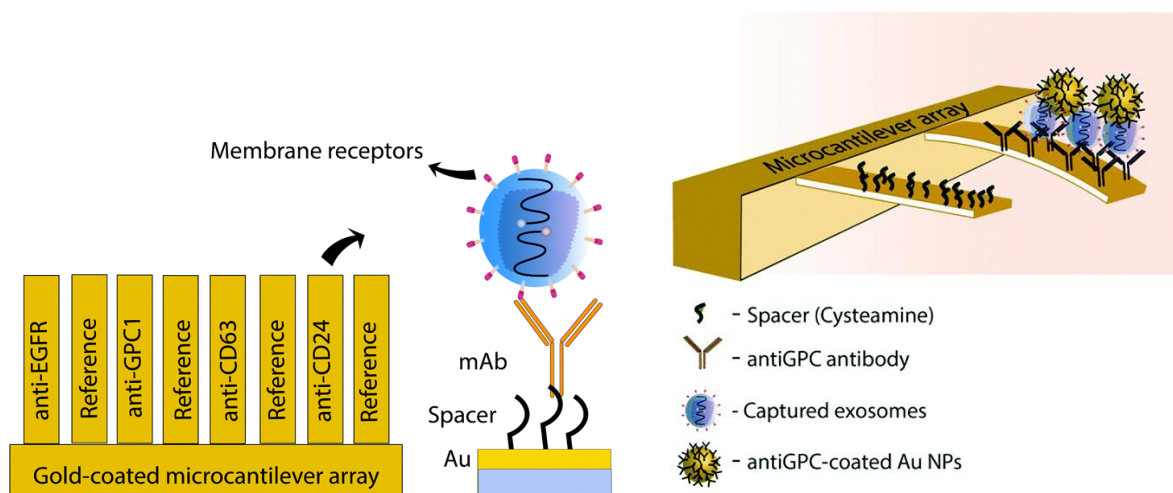


Figure 9 Schematics of a nanomechanical sandwich assay for the detection of EVs. Figures reprinted from [80].

A similar assay approach by immunocapturing of EVs for their detection is used in surface based optical devices that utilize evanescent fields on thin metal surfaces. Grating coupled interferometry sensors are measuring the changes in the phase shift of a light wave after it travelled through a waveguide. The area of the waveguide can be functionalized, just as the cantilever surface described before, and thus specifically capture certain EV populations [81]. The

binding of EVs to the waveguide surface influences the phase shift of the light wave in a quantitative manner and thus the amount of bound EVs can be determined via measuring the shift. Another such optical method using evanescent fields is surface plasmon resonance, which was used for EV detection by several different approaches and is discussed in much more detail in sections 1.2 and 1.3. The advantage of these optical methods is that they work in a label-free manner and enable to measure the EV interactions with the sensor surface real-time.

Raman spectroscopy is another very promising optical method that has been introduced for the analysis of EVs recently. This method is able to determine the chemical composition of EVs by monitoring the Raman scattering [82]. The characteristics of the spectrum of the Raman scattered light are dependent on the composition of the particle that scatters the light and thus by comparison of the Raman spectra different compounds in a sample can be identified. By utilizing laser tweezers Raman spectroscopy it is even possible to determine the composition of single vesicles [83]. Furthermore, EVs can be analyzed by this method without any labeling and in solution, meaning that results are not influenced by any interactions with labeling molecules or surfaces. Thus, this method holds great potential for the further characterization of EVs and their chemical composition.

All in all, new tools and methods with the potential to improve EV research are constantly developed and already showed how EV isolation and analysis can benefit from them. However, further studies are required to develop standard procedures and easy-to-use instruments.

1.1.6 EVs in Cancer

EVs not only have important functions in the intercellular communication between healthy cells, they also play key roles in pathological conditions. They are involved in many critical processes of cancer development and progression and thus have been studied intensely over the last decades. In the earlier years of this research field, the subgroup of EVs that originate from cancer cells and transfer oncogenes to promote cancer growth and spread, were named oncosomes. In later studies, the so-called large oncosomes were classified as a new group of EVs formed by blebbing from the plasma membrane. These vesicles are a special type of MVs, because they are much bigger in size than most EVs, ranging from 1 to 10 μm in diameter, and are only secreted by cancer cells [84]. Despite the fact that many pathways and processes are not entirely understood yet, there is plenty of evidence that EVs are crucial for the bilateral interaction of cancer cells with its microenvironment, but also with distant sites. The exceptional interest of researchers in EV's functions in cancer is fuelled by the great potential for clinical application of such EVs, on the one hand as biomarkers for diagnosis, prognosis and prediction of response to therapy, and

on the other hand as therapeutic target, in immunotherapy or as biological vehicle for drug delivery.

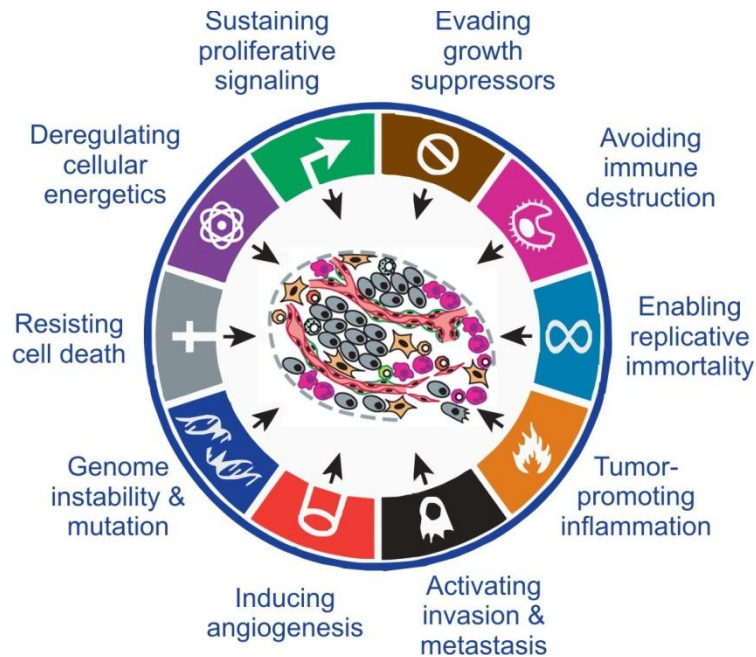


Figure 10 Established and emerging hallmarks and enabling characteristics of cancer. Figure adapted from [85].

To get a better view on how central and broadly distributed the functions of EVs in cancer development are, the following section discusses EVs and their so far reported roles in regard to their relation to the hallmarks of cancer, which are the most important characteristics and functions that cells have to develop during carcinogenesis [85] and are illustrated in Figure 10. Subsequently, the clinical applications of EVs as cancer biomarkers and in cancer therapeutics are presented. Since cancer is a very heterogeneous disease and the discussion of all different types would exceed the limits of this work, both sections focus on highlighting the findings about EVs in ovarian cancer, which was the focus of many research studies so far. For better understanding first, a brief description of this disease is given below.

Ovarian cancer (OC) is the leading cause of death among gynecological cancers with a five-year-survival rate of about 46 % [86]. However, this survival rate is the average for all patients, of which only ~25 % are diagnosed with OC at early stages. In the early stages, when the disease is still localized to the ovarian tissues, therapy is usually effective with 5-year-survival rates of 70-90 % [86]. On the contrary, in ~75 % of patients OC presents at late stages, when effective treatment is almost impossible, resulting in 5-year-survival rates of 10-30 % [86]. The most common type is epithelial OC, which comprises about 90 % of all cases [87] and it can be assumed that studies examining OC focus on this type, if not otherwise stated. Based on the histological characteristics, epithelial OC can be further discriminated into serous, endometrioid, clear cell or mucinous, with incidence rates decreasing from almost 70 % for the serous type to

10-20 %, 10 % and 3 % for the other types, respectively [88]. The so-called FIGO stages [89] are used to categorize OCs depending on their disease progression with stages I and II being considered as early stages, where the cancers are still localized in the original tissues, while stages III and IV are OCs that started to invade the surrounding tissues and formed either near (stage III) or distant (stage IV) metastases. The latter are considered as late stages associated with poor survival rates, as discussed above.

The late diagnosis of OC in most cases is due to the asymptomatic course of disease and the lack of specific and sensitive biomarkers and screening methods. Currently, clinicians still rely on diagnostic methods introduced in the 1980s, which are the transvaginal ultrasound and the serum-level of cancer antigen 125 (CA-125) [90]. Since the transvaginal ultrasound is an imaging method of tissues and organs it suffers from the inherent limitation that the cancer needs to reach a certain size to be imaged and detected, thus leading to a lack in sensitivity. The determination of CA-125 levels, on the other hand, greatly lacks specificity, because CA-125 is often elevated in benign conditions or even in healthy women, due to hormonal fluctuations in their menstrual cycle [90]. Over the last years, many studies have been conducted to identify new biomarkers for a more reliable diagnosis of OC, but so far none of them has reached clinical application [91]. Consequently, improvements of diagnostic biomarkers and detection methods to achieve an earlier diagnosis of OC are urgently needed. Besides the limitations in diagnosis, also the currently used therapies, consisting of surgery and chemotherapy, have only a minor impact on the overall survival of patients, because in most of the cases the cancer recurs after a first line of chemotherapy and the patients typically and quickly develop resistance to the therapy [92]. The study of EVs and their function in cancer, and particularly in OC, could yield novel ways for improved diagnosis and therapy of this disease.

1.1.6.1 Function of EVs in ovarian cancer

One of the most prominent characteristics of cancer cells is their fast and continuous proliferation, which is based on the ability to sustain proliferative signaling. So far EVs have been shown to transfer proliferative phenotypes to cells by, for example, induction of signaling pathways via receptor tyrosine kinases, transfer of oncoproteins, or micro RNAs [93]. In EVs isolated from serum of OC patients the oncogenic epithelial growth factor receptor vIII was identified [94], which indicates that this molecule could be transferred to other cancer cells to increase proliferation, as already shown for glioma cells [95]. The proteomic analysis of EVs derived from two OC cell lines showed that the vesicles are highly enriched in proteins related to signaling pathways associated to cell proliferation and carcinogenesis, including among others the

EGF receptor, FGF receptor, and Wnt signaling pathway, as well as the PI3 kinase, Ras, and P53 pathway [73].

In addition to the active stimulation of proliferation, cancer cells also need to avoid growth suppression. To date, there is only little known about the role of EVs in evasion of growth suppressors by cancer cells. So far studies suggest that cancer cells might down-regulate tumor suppressors by secreting and removing them from the cell through EVs [93]. Furthermore, there is some evidence that EVs loaded with micro RNAs that target tumor-suppressor protein expression in recipient cells could play a role in these processes [93].

Related to the evasion from growth suppression is the need to circumvent cell death during carcinogenesis. Cappellesso et al. [96] found that the anti-apoptotic and pro-cancerogenic properties of OC cells are also found in their secreted EVs. Specifically, high levels of miR-21 and low levels of programmed cell death 4 protein, which could result in apoptosis avoidance, were identified in both cells and secreted EVs. The prevention of cell death is especially immanent when it comes to resisting to therapy. In this regard several studies identified a role of EVs in chemo resistance and the ability to transfer this capability from resistant cells to cells that are sensitive to chemotherapeutic agents. For example, OC cells are able to export cisplatin through endosomal vesicles, thus lowering the drug concentration and cytotoxicity within cells [97]. Furthermore, the transfer of paclitaxel-resistance by vesicular transport between OC cells was discovered, which depends on the transfer of the P-glycoprotein, that enables cells to export chemotherapeutic drugs [98]. Pink et al. showed that EVs derived from an OC cell line, that was resistant to cisplatin treatment, were able to induce resistance in a cisplatin-sensitive cell line [99]. A different strategy to evade cell death from chemotherapeutics, which typically attack the upregulated processes of cell proliferation in cancer cells, is to enter senescence. Through this the therapeutically targeted proteins and pathways are downregulated and cancer cells are not affected by the drugs anymore. This connection was shown in OC cells, in which induction of cellular senescence was mediated by the overexpression of micro RNA 433 and resulted in resistance to paclitaxel. The transfer of senescence and thus of chemo resistance to neighboring cells via EVs was shown and micro RNA 433 was suggested as mediator, because it is present in the secreted vesicles [100].

Besides sustaining proliferation, cancer cells also need to reach replicative immortality, meaning that the limitation of total cell cycles a cell can undergo, which is caused through the shortening of telomeres on chromosomes, is avoided by telomerase activity. The interaction of EVs with this enzyme, which elongates telomeres, is not yet known, but as some factors that activate

telomerase, c-myc, b-catenin or p53, were already identified in EVs, a functional relation is possible and should be explored in future [93].

Like every tissue, cancers also need nutrients to fuel their growth and as they grow in size the formation of blood vessels to deliver such nutrients is crucial for their survival. In this context, EVs were identified to play key roles in the communication between cancer and endothelial cells, which are responsible for the formation of blood vessels or angiogenesis. The vascular endothelial growth factor (VEGF), which induces endothelial cell activation and growth, was identified in EVs secreted from OC cell lines. In the work of Taraboletti et al. [101] VEGF was found inside the vesicles and therefore cannot bind to the extracellular receptor on target cells. However, these EVs burst in the acidic cancer microenvironment to release VEGF that can bind the extracellular VEGF receptors on endothelial cells and activate angiogenesis. Similarly, studies showed that the expression of CD147 in EVs from OC cells was required for the successful induction of a pro-angiogenic phenotype in endothelial cells [102]. This is most likely associated with the function of CD147 as an activator of matrix metalloproteinases to degrade the extracellular matrix in order to create space for the formation of new vessels. A more complex pathway to activate endothelial cells via OC derived EVs was described by Al Thawadi et al. [103]. The EVs first cleaved E-cadherin on the surface of endothelial cells via matrix metalloproteinases carried by the EVs to induce the intracellular release of β -catenin. At the same time, the EVs were also taken up by the recipient cells via interaction of phosphatidylserine in the vesicular membrane and lactadherin and integrins present in the cellular membrane. This internalization lead to the phosphorylation of the released β -catenin within the cells and then its transfer to the nucleus where it induced a pro-angiogenic program. Since the isolation method used in this study does not discriminate between subtypes of EVs, it is possible that the different EV functions are actually performed by separate vesicular subpopulations.

As the disease progresses, cancer cells start to invade tissues surrounding its primary tissue site before crossing the endothelial barriers of blood vessels to enter the blood system and metastasize at distant tissues. In this process of migration, invasion and metastasis formation EVs have also been implicated. In regard to OC, matrix metalloproteinases (MMPs) carried by EVs have been the focus of several studies. MMP9 and MMP2, for example, have been found in EVs isolated from OC cell lines and also from ascites of patients with OC. These MMP-containing EVs have been shown to be active in degrading extracellular matrix components and enhancing cell's migratory and invasive behavior [104-106]. Beside proteins, MMP messenger RNA, e.g. MMP1 messenger RNA, was also found in EVs from OC cell lines [107]. When these EVs were administered to mouse models bearing OC, the tumor size was not affected, but the metastatic

burden was significantly higher compared to controls. The function of these EVs in promoting metastasis is linked to the destruction and apoptosis of mesothelial cells, which build the outer border of organs and has to be breached to enable invasion to neighboring and distant tissues. Another study that examined the nucleic acid content in OC cell line derived EVs found that molecules of the micro RNA let-7 family are present in high levels in vesicles derived from cell lines with higher invasiveness [108], supporting the hypothesis that cells secrete the tumor suppressor micro RNA let-7 via EVs to maintain their invasive phenotype. Moreover, OC derived EVs are also capable of inducing epithelial to mesenchymal transition by gene regulation in human embryonic kidney cells and enhancing their invasive and migratory behavior [109]. Finally, vesicles not only promote invasive phenotypes in cells, they also take part in preparation of metastatic niches in distant organs for future metastasis formation. This was examined by Hoshino et al. [110] who studied EVs derived from several cancer types and found that the EVs bind to cells in different organs to form pre-metastatic niches and that the different integrin types carried by different EV subpopulations determined in which organ these niches were formed and subsequent metastasis occurred.

The immune system in humans identifies foreign compounds in the body and eliminates them by a combination of a plethora of cellular functions and a mesh of different interacting pathways. It is well known that immune cells also counteract the development and growth of cancer cells, but cancers have found ways to avoid the detection by and the activation of the immune system and its response. In this regard, studies reported that OC cell line derived EVs carry the Fas ligand, which binds to the Fas receptor on immune cells, causing apoptosis of these cells [111, 112]. Additionally, the T cell signaling cascade, which is a major part of the activation of the immune response, can be inhibited via the interaction of the cells with the phosphatidylserine present on EVs isolated from ascites of OC patients [113]. Furthermore, EVs carrying the NKG2D ligand are able to reduce the cytotoxic effect of natural killer cells, by binding to the NKG2D receptor, that is found on the surface of natural killer cells, and thus preventing the attachment of these immune cells to cancer cells, which again prevents the killing of cancer cells [114]. Another different approach to escape the immune system by OC derived EVs is to induce regulatory T cells via IL-10 and TGF β 1 to downregulate the overall immune response [115].

However, cancer cells not only suppress the immune system, they also make use of it in their own interest. For instance, cancer cells use macrophages to degrade the extracellular matrix surrounding them to make more space for cancer growth. Ying et al. found that OC derived EVs are also involved in this process and are capable of inducing polarization of macrophages and change their phenotype to tumor-promoting M2 type macrophages [116].

As already known for a long time, cancer cells need to acquire many genetic mutations to gain all these functions described above. This requires a certain degree of genome instability, which is why it was defined as an enabling factor for cancerogenesis [85]. So far EVs were shown to induce phenotypical transformation in normal and cancer cells, for instance inducing epithelial to mesenchymal transition, by triggering of cell signaling cascades, delivery of signaling molecules, messenger RNAs, micro RNAs, oncogenes or proteins, but if such EV-triggered changes are sustained and lead to genomic instability or mutations is not known yet [93]. Also the deregulation and reprogramming of the energy metabolism in cancer cells by EVs has not been studied yet.

1.1.6.2 Clinical applications of EVs in ovarian cancer

Since EVs are involved in many processes associated with cancer development, studies on their use in clinical applications were conducted early at the onset of this research field. Generally, these studies can be divided in two groups: those studying EVs as biomarkers and those focusing on the use of EVs in cancer therapy.

In many stressful situations that the human body experiences, cells react by secreting more EVs. So higher levels of EVs in the circulation of people with different diseases, including cancer, compared to healthy individuals were often identified [117, 118]. Hence, simply the EV concentration in, for instance, blood plasma could be used as marker for irregularities or diseases. However, such a marker would be rather unspecific, as an upregulation of EV production appears to be a general effect of stress on cells [24]. Consequently, the cargo molecules of EVs have to be studied to identify potential biomarkers. By these means it is possible to define the cancer-derived or at least cancer-associated EVs and discriminate them from other EVs present in the body. At this point, it is also important to mention that EVs secreted by cancers are capable of entering body fluids and thus also circulate through the human body via the blood stream. Since cancer-derived EVs carry cancer-specific molecules and are present in body fluids, they could serve as liquid biopsy, which means that diagnostic information on the cancer can be gained by a simple blood collection instead of open surgery and consecutive examination of the removed cancer tissue.

The group of Altevogt was one of the first to study known OC markers in EVs and found that the proteins CD24 and epithelial cell adhesion molecule (EpCAM) were present on EVs isolated from ascites of OC patients [106]. Furthermore, they found that EVs secreted to the cancer proximity were also present in the patient's circulation, by examination of EVs from paired ascites and blood samples of OC patients [119]. Thus, they could prove that EVs have the

potential for application as a diagnostic marker of OC via detection of cancer associated proteins on EVs isolated from patient's blood samples.

Since EpCAM is a transmembrane protein and present on the surface of cells and EVs, it can be used for isolation of EVs based on affinity binding of antibodies to the extracellular domain of EpCAM. This property was utilized by Taylor et al. [120] who isolated EVs from blood serum by coupling the vesicles to magnetic particles via antibodies specific for EpCAM. By comparison of the amount of EVs isolated by these means from serum of healthy women, women suffering from benign lesions or from malignant ovarian cancers, the group found that the total protein concentration, as a measure for the EV amount, increased from healthy to benign to malignant and with the progression of malignancy. Furthermore, this study identified 8 micro RNAs in the EpCAM-positive EVs as a diagnostic signature for ovarian cancer.

The presence of EpCAM in EVs and its usefulness as diagnostic marker for OC were examined in several studies that found a correlation between elevated levels of EpCAM-carrying EVs and ovarian cancer malignancy [76, 121-123]. However, contradictory results were also found when EVs from normal ovarian epithelial cells were compared to those derived from OC cell lines and no difference in the EpCAM levels between normal and cancer cell derived EVs was examined [124].

In addition to EpCAM, other proteins were also identified as specific for OC derived EVs and as potential biomarker. For example, claudin-containing EVs were found in the plasma of OC patients and claudin-4 bearing EVs were identified as potential diagnostic markers with high specificity (98 %), but medium sensitivity (51 %) in a panel of 63 OC patients compared to 50 healthy volunteers [125]. In another study EVs, isolated from plasma of OC patients, individuals with benign masses and healthy women, were examined and higher levels of exosomal protein concentration were found in patients with OC compared to benign diseases or healthy people [126]. In this study also TGF- β 1 and MAGE3/6 were identified as EV cargo proteins with potential as diagnostic biomarker. Moreover, the lipid phosphatidylserine, which is found in cancer derived EVs, was proposed as a diagnostic marker, since its plasma levels are increasing from healthy women to women with benign lesions to women with OC [127]. Besides studying the vesicular protein and RNA cargo, recently more studies on the glycosylation patterns of EVs were conducted. One of these studies identified a glycosignature specific to EVs derived from OC cell lines compared to the cellular membranes [128]. Such signatures also hold potential as OC biomarker.

That EVs not only have potential as diagnostic marker was proven by Vaksman et al. [129], who identified a micro RNA signature in EVs from malignant effusions of OC patients as prognostic

marker. Furthermore, the potential of four micro RNA molecules, carried by EVs, for diagnosis and prognosis of ovarian cancer were examined by Meng et al. [130]. They found that levels of exosomal micro RNA-200b and -200c were elevated in serum from patients of advanced stages of OC, thus indicating a potential as prognostic biomarker. Moreover, since EVs are involved in the resistance of cancer cells to chemotherapy, as discussed in detail above, their specific detection could also serve for better prediction of treatment efficacy.

Cancer therapy and in particular ovarian cancer therapy is very difficult, because of the complexity of this disease, its progression, metastasis, and the frequent emergence of resistance to chemotherapies. EVs were studied over the last decades in regard to their utility in cancer therapy. First of all, EVs can be new therapeutic targets, since EVs clearly have major pro-cancerous functions. A specific example is the capacity of OC cell line derived EVs of transferring cisplatin-resistance to sensitive cells and the loss of this capability after treatment with curcumin [131]. Hence, this could be a new approach to prevent chemoresistance in ovarian cancers. However, the complex interplay between different cells and subpopulations of EVs and therefore the effect of targeting EVs in therapy by, for instance, disabling their biogenesis, is by far not fully understood yet. So the efficacy and especially the safety and side effects of such therapeutic approaches need to be studied in much more detail, before EV-mediated functions can be targeted in cancer therapy.

The application of EVs in immunotherapy was also studied in regard to OC treatment. Macrophages, which were stimulated with TWEAK, for example, secreted EVs loaded with micro RNA-7 and thus inhibited metastasis formation of OC tested *in vitro* and *in vivo* [132]. EVs from cancer cells could also serve as cancer specific antigens to elicit an immune response by the host. This was suggested by Li et al. [133], who found that EVs isolated from ascites of OC patients were taken up by dendritic cells, which enabled them to present cancer specific antigens that again induced T-cell mediated tumor specific cytotoxicity.

EVs also can be used as therapeutic agents, which was shown in many studies that used mesenchymal stem cell derived EVs for tissue regeneration. A similar approach could also serve as cancer therapeutic agent. Namely, mesenchymal stem cell derived EVs and their micro RNA content induced apoptosis signaling, reduced cell viability, restrained proliferation, and impaired wound-repair and colony formation ability of ovarian cancer cell lines [134].

As mentioned in the chapter above, EVs could prepare metastatic niches and thus define where cancer cells will invade to build metastases. This capability of attracting metastasizing cancer cells to certain tissues is utilized in the so-called M-trap introduced by de la Fuente et al. [135]. This implant was first coated with EVs isolated from ascites of OC patients and then implanted into

the peritoneum of ovarian cancer bearing mice. Through the specific interaction of OC cells with the EVs embedded in the M-trap, the cells adhered to the implant and metastasis formation at other sites of the peritoneum as well as at distant sites was prevented. By these means, the overall survival of the OC bearing mice was improved.

Finally, EVs are studied as new drug-delivery system that has the great advantage of being of biological origin, hence making these vesicles biocompatible. Furthermore, the targeted delivery of drugs to specific cells could be achieved by usage of EVs that are naturally programmed to target certain cells. Among others, Hadla et al. [136] used EVs loaded with doxorubicin to treat mice with breast cancer or OC. By the packaging of the drug into EVs they achieved an increase in the therapeutic effect, because the packaged doxorubicin avoided heart toxicity and thus the administration of higher dosages of this drug were possible.

All in all, EVs show great potential in many clinical applications and settings, but there is still a great lack in reliable and standardized methods for their isolation and analysis, which might bias results and make comparisons between studies difficult. Consequently, in order to achieve the successful application of EVs in clinical settings better techniques are required. But also the complexity of EV functions and interactions has to be elucidated.

1.2 Plasmonic Biosensors

The discovery of the phenomenon of surface plasmon resonance (SPR) dates back to 1902 [137], but only after 60 more years it was possible to completely explain its physics background [138, 139]. From then onwards, SPR was employed in many sensing applications and gained much interest in the field of life sciences after the description of the first SPR-based biosensor by Liedberg et al. in 1983 [140]. Nowadays, the use of plasmonic biosensors is the gold standard for monitoring biomolecular interactions in real-time in a direct, label-free manner. The strongly confined field of surface plasmons makes this a highly sensitive method, which enables to measure analytes down to pM concentrations and by application of surface plasmon-enhanced spectroscopy methods even lower concentrations could be detected [141].

Plasmonic biosensors are based on the probing of the sensor surface by the surface plasmon field that can be excited on the interface between a metal surface and a dielectric medium. The surface plasmon field, illustrated in red in Figure 11, is sensitive to changes in the refractive index of the dielectric in close proximity to the metal surface, also referred to as the sensor surface. By functionalization of this surface with capture molecules, illustrated in green in Figure 11, the specific binding of the target analyte, illustrated as yellow circles in Figure 11, to the sensor surface can be directly monitored via the changes in the refractive index.

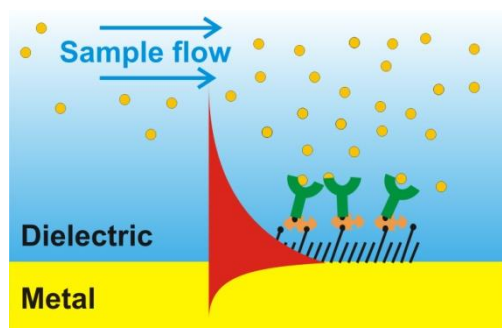


Figure 11 Schematic of a plasmonic biosensor illustrating the surface plasmon field at the metal-dielectric interface and the binding of the target analyte to the functionalized sensor surface.

In the following paragraphs and sections an introduction to the theory of SPR and its application in sensing, the implementation and characteristics of different biosensors, and several methodological topics are discussed. This chapter is based on two comprehensive books, that give a detailed explanation on the physical background and the application of SPR in biosensors [142, 143], and a few review articles that are cited in the text. Besides a general discussion on plasmonic biosensors related topics, the focus is drawn to explain those methods and sensors in more detail that were used in the studies presented in the later chapters. Practical examples of different plasmonic biosensors are presented in chapter 1.3.

1.2.1 Principle of Surface Plasmon Resonance

Surface plasmons are defined as *propagating electron density waves occurring at the interface between metal and dielectric* [144]. These oscillations can build an electromagnetic field that penetrates into the two adjacent media in a perpendicular direction to the interface and decays exponentially while propagating along the metal surface. It is important to note that the evanescent field penetrates much deeper into the dielectric medium than into the metal. For sensing application this means that mostly changes in the dielectric medium will influence the signal response. The coupling of the incident photons with electron density oscillations on the metal-dielectric interface and therefore the resonance of the excited surface plasmons is influenced by many parameters. These include the wavelength of the light beam, the angle of incidence, the thickness of the metal layer as well as the type of metal used, but also the temperature and the refractive index of the two media building the interface. For sensing applications, the changes in one of the SPR parameters can be monitored, while the others are kept constant. Hence, for example, changes in the refractive index of the dielectric medium will result in changes of the resonance characteristics and thus can be directly tracked by monitoring one of the other parameters. Therefore, surface plasmons, which penetrate into the dielectric medium, can be utilized to probe this medium for changes caused by the binding of molecules to the surface that result in a refractive index change. This principle is the basis for the use of SPR in biosensors.

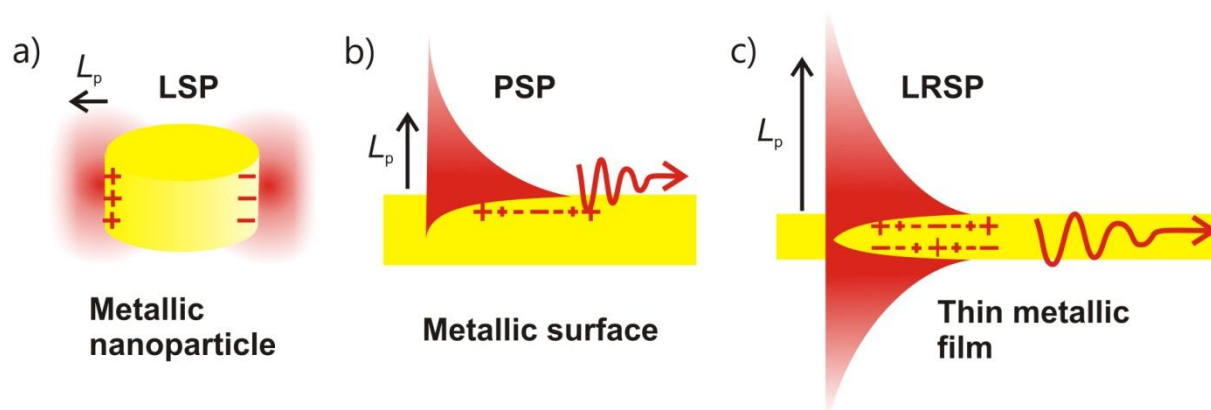


Figure 12 Schematics of different surface plasmon modes. a) localized surface plasmons (LSP), b) propagating surface plasmons (PSP), c) long range surface plasmons (LRSP) (L_p – penetration depth). Figure adapted from [4].

Three different types of surface plasmons exist: localized surface plasmons (LSPs), propagating surface plasmons (PSPs), and long-range surface plasmons (LRSPs) (see Figure 12). The first can be excited on metallic nanoparticles that are suspended in a dielectric. These plasmons have a very small penetration depth in the range of tens of nanometers and are therefore used to examine very thin films or small molecules. PSPs are excited at the metal-dielectric interface on

thin metal layers and compared to the localized surface plasmons exhibit a longer penetration depth of around 100 nm. In contrast, long range surface plasmons are a combination of two propagating surface plasmon modes that are excited on two metal-dielectric interfaces in parallel. This is achieved if a metallic layer is in contact with a dielectric medium on both sides. By coupling of these two surface plasmon waves a stronger electromagnetic field is built that reaches a penetration depth of several hundreds of nanometers up to one micrometer, thus enabling to measure big particles or thick layers of molecules. Since only the propagating surface plasmons were used in this project, the following sections will focus on this kind and will refer to them as surface plasmons (SPs) for simplicity.

1.2.2 Sensing Modalities and Instrumentation

To monitor the changes in SP excitation several approaches can be used that track either the angle of incidence or the wavelength of the light beam at which the maximum SP excitation is achieved. These two approaches rely on measuring the intensity of the light beam reflected from the metal surface over a range of angles or wavelengths and from the resulting spectra the resonance angle or wavelength is determined. The third approach also measures the intensity of the reflected light beam, but at a fixed angle and wavelength, which is simply referred to as reflectivity measurement. The angle and wavelength in such settings are chosen to measure the intensity changes close to the maximum resonance conditions, to achieve high sensitivity. In Figure 13 the schematics of these three methods for SP monitoring are depicted. In all three approaches the examined parameter is directly influenced by the refractive index n of the dielectric medium and thus changes in n result in changes in the resonance angle θ , the resonance wavelength λ , or the reflectivity intensity R , respectively. The output of the different modalities and the measured changes caused by a change in refractive index from n to $n+\Delta n$ are also illustrated in Figure 13. By measuring the spectra or the reflectivity repeatedly over time, it is possible to measure changes in refractive index and thus binding of molecules to the sensor surface real-time, which is one of the most important advantages of plasmonic biosensors. The output of such real-time measurements is depicted in the lower panel of graphs in Figure 13.

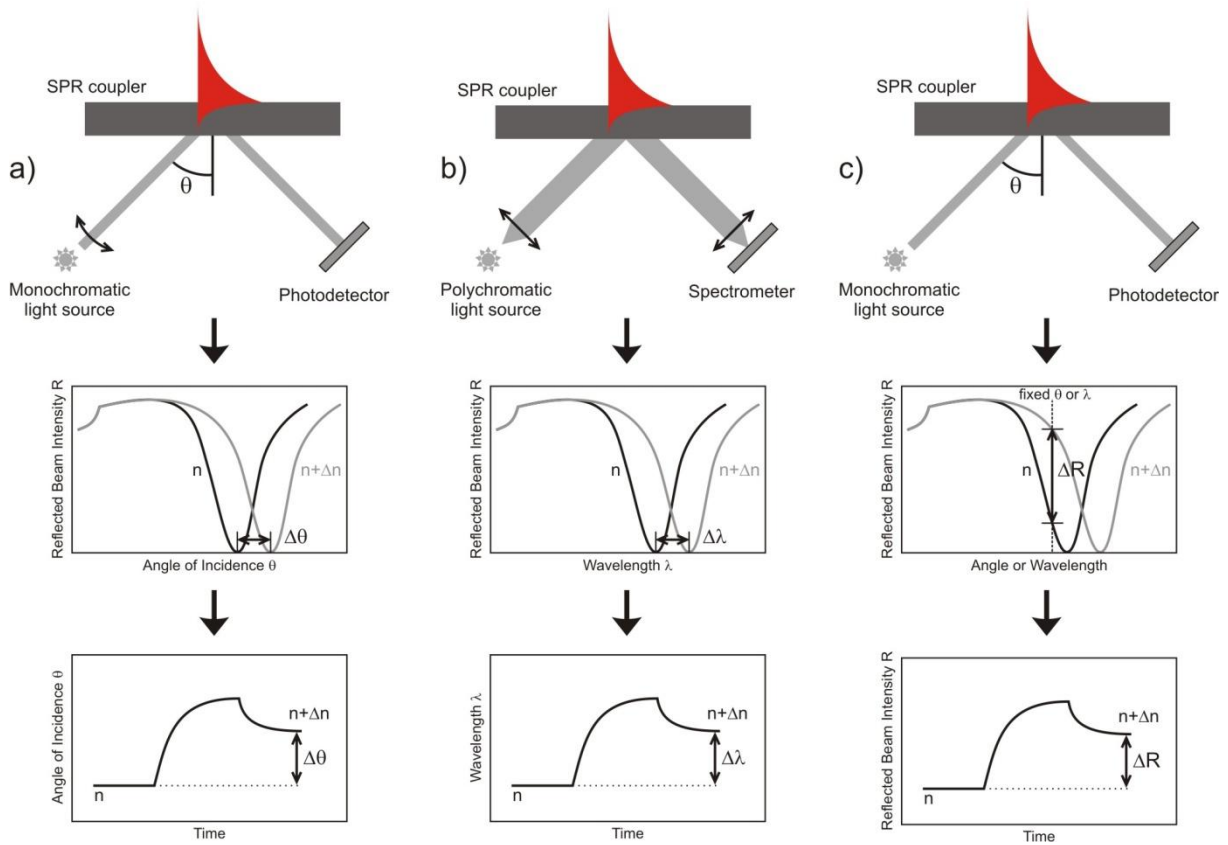


Figure 13 Schematics of the different modalities for monitoring of surface plasmons. (a) angular modulation, (b) wavelength modulation, (c) reflectivity measurement at fixed angle and wavelength (n – refractive index). This figure is based on figures in [142] and [143].

Since angular modulation, in most of the applications, requires the change of the angle of incidence of the light beam, the instrumentation involves moving parts, which can be prone to disturbances and wear and tear. This is avoided in wavelength modulation sensors that use a polychromatic light beam that is made incident at a fixed angle. However, for both measurement modalities complex algorithms have to be used to automatically calculate the resonance angle or wavelength from the measured spectra over time, which can be especially challenging in terms of the computing capacity, if highly time-resolved measurements are performed. The reflectivity measurements are much simpler, since angle and wavelength are kept constant and the intensity value is measured directly. But these simple reflectivity levels are not as precise as tracking the resonance angle or wavelength. Furthermore, by not tracking the spectra a lot of valuable information is lost that could help for data interpretation and potential troubleshooting. To achieve higher accuracy and sensitivity, in all modalities several measurements over time are typically averaged.

Another approach to SP detection is SPR imaging [145]. Instead of a photodetector or spectrometer a camera is installed to collect the reflected light and generate a microscopic image of the sensor surface. On the images intensity differences can be visualized as bright or dark

areas. This method is often used for the parallel monitoring of several measurement points. For example, individual spots on the sensor surface that are functionalized by different capturing molecules in a microarray format can be monitored simply by taking images of the whole sensor surface. Just as for the regular reflectivity measurements, also for SPR imaging a drawback is the lack of spectral data, because only the reflectivity values are tracked, but new developments are tackling this problem and SPR imaging devices that can follow the angular shifts were already introduced.

In order to excite SPs, so-called SPR couplers have to be used. The most common method for SP coupling is the attenuated total reflection (ATR) configuration with Kretschmann geometry, which is schematically depicted in Figure 14a. In this system a high refractive index glass prism is attached to the backside of the metallic layer. The light beam is made incident through the prism onto the metal-dielectric interface where the photons couple to the metallic electrons resulting in the excitation of the evanescent field and SPs. Since this method works with thin and plain metal layers, it has the advantage of simple sensor chip preparation, in which only the metal film has to be deposited on a substrate. However, the optical setup is more complex in this system, due to the required optical matching of the sensor chip with a prism, and even smallest changes in the alignment of the light path, prism and sensor chip by, for example, vibrations, can influence the measurement and bias results [146].

SP excitation can also be achieved by usage of diffraction grating coupling, in which a light beam is made incident on a metallic film that harbors a periodic grating structure and results in diffraction of light waves that are then able to couple with SPs, as illustrated in Figure 14b. This optically simpler system is less sensitive to changes in the alignment, but the fabrication of the sensor chips is more elaborate, since it involves nanofabrication of grating structures [146]. Nevertheless, with new developments in nanotechnology the production of such sensor chips in a cheap manner suitable for mass-production is possible. An important limitation of grating coupled SPR is the fact that the light beam passes through the dielectric medium, so through the sample solution, before it hits the sensor surface. This can lead to a decreased stability of the sensor signal. Also, bigger flow-cells have to be used to avoid internal reflection effects between the metallic surface and the glass of the flow-cell. However, the capability of tuning the SPR, by adjusting the period Λ and architecture of the grating structure, enables to tailor the resonance parameters. Furthermore, since the light beam is made incident on the front side of the sensor surface, the backside is free for the incorporation of additional sensing modalities.

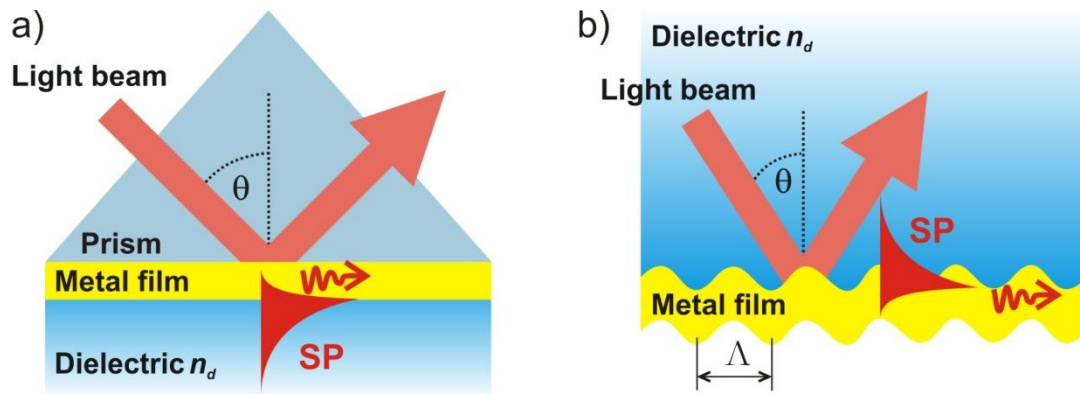


Figure 14 Schematics of the systems for surface plasmon (SP) excitation. a) Attenuated total reflection configuration with prism-coupling, b) Grating coupling (Λ – period of grating structure). Figure adapted from [147].

Both SPR coupling methods can be used for the monitoring with angular or wavelength modulation and with reflectivity measurements. The combination of these systems is summed up as the optical system of SPR biosensors, which is only one of the components of plasmonic sensing instruments. Other components are the sensing chip and its surface architecture for specific detection of a target analyte, the microfluidic system including the flow cell attached to the sensor chip, and the electronics to enable data acquisition and processing. Exemplarily, a typical setup for reflectivity measurements and angular spectra using the ATR configuration is schematically depicted in Figure 15 and the different components of such an instrument are illustrated.

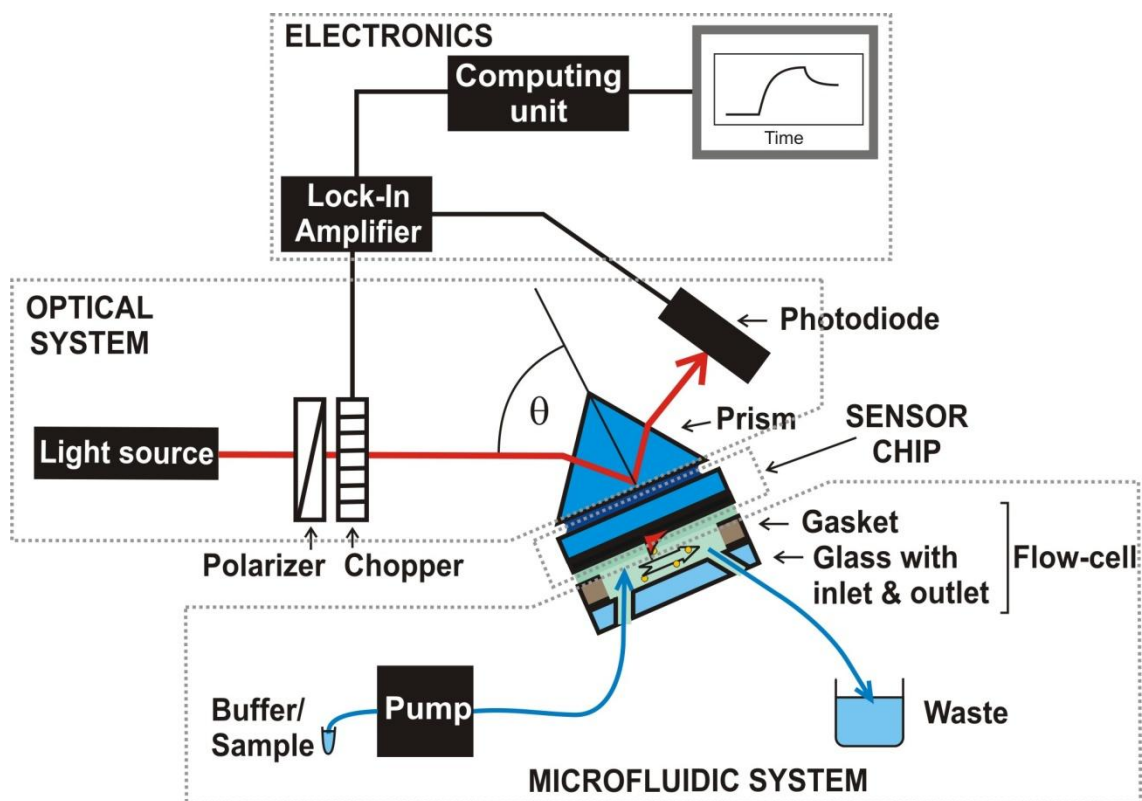


Figure 15 Schematic of a SPR biosensor setup in ATR configuration for angular modulation and reflectivity measurements.

The microfluidic system, or also called liquid handling system, comprises of a pump and a flow-cell that allows bringing solutions and the sample into contact with the sensor surface. Even though such systems can be made very complex for multiplexing of many parallel measurements, the flow-cells used in the here presented studies are very simple. They consist of a silica glass that contains an inlet and an outlet port and a gasket made from a polymer, for example polydimethylsiloxane (PDMS). Both parts are clamped to the sensor chip and taken together these three components enclose a small volume that forms the flow-cell. Through using different thicknesses and dimensions of the gasket the volume of the flow-cell can be tailored. The inlet and outlet of the flow-cell are connected to the pump and the sample solution vial or a waste container via tubes and thus enable the flowing of solutions across the sensor surface. The electronics for data acquisition rely on a detector, which is part of and dependent on the optical system used and in this case a photodiode, connected to a signal-processing device, like a lock-in-amplifier, that averages the measured light intensities over time and yields the signal values for the computing unit. Finally the processed data are written out as output graphs in the software. More details on the instrumentation of different types of plasmonic biosensors can be found in [148, 149]. The last part, not mentioned yet, is the sensing chip or surface and its architecture, which are explained in more detail in the following section.

1.2.3 Sensor Chip Architecture

Besides the optical system that enables to excite and monitor SPs, the sensor chip is just as important for successful biosensing. For better understanding let us discriminate here two parts of the sensor chip: the physical chip with the layers and structure crucial for the excitation of plasmons, and the sensor surface and its architecture or functionalization that enables to probe for specific molecules. The components of exemplary plasmonic sensor chips are depicted in Figure 16.

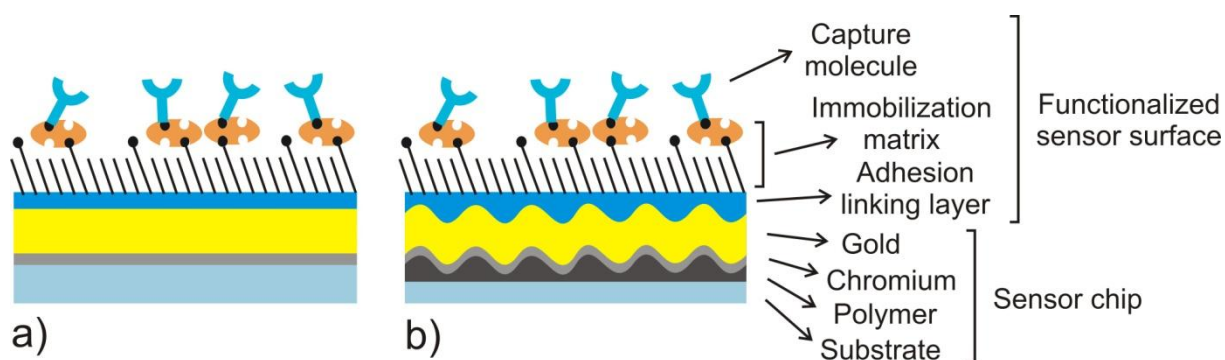


Figure 16 Schematics of an exemplary plasmonic sensor chip and its surface architecture used for a) ATR couplers or b) grating coupling.

The chip itself is typically made up of a substrate, for example simple BK7 glass or silicon wafers, to which either a metal is directly deposited to form a homogeneous thin layer on the substrate, or the metal is deposited onto a nanostructure that is first built on the substrate. Which type of chip is required depends on the kind of SPR coupler that is used for the sensor, as explained above. The formation of nanostructures like diffraction gratings is commonly performed by lithographical methods applying top-down synthesis approaches, in which parts of bigger pieces of materials are removed to build a new, smaller structure. Common nanofabrication techniques are summarized by Lindquist et al. [150] and some of them are discussed below. In conventional lithography a photosensitive or electronsensitive material, a so-called resist, is first coated on a substrate like glass or silicon. Then a pattern is formed in this layer by exposing the resist to light or electron beams while a patterned mask covers some of the resist layer. Consequently, only those parts of the resist material, that were exposed to light or electrons, are degraded and can be easily removed by, for example, chemical solvents, thus unveiling the produced pattern. Since the production of a highly accurate mask and the multiple exposures make such methods very complicated and expensive, this is mostly used for the fabrication of complex structures and patterns. For the production of simple and periodic patterns, like linear gratings or arrays of nanoparticles, easier and cheaper approaches have been developed, including optical interference lithography. In this method the pattern is directly transferred into the photoresist layer by exposure to an optical beam at a certain angle of incidence that generates interference patterns in the resist material. Hence, this method has the advantage of not requiring patterned masks, but it is only capable of producing periodic patterns, which is, however, no problem in most of the plasmonic applications. If arbitrary patterns should be fabricated without the use of masks, electron-beam lithography can be employed that can “write” a pattern to the resist layer. As for the conventional lithography, the pattern in the resist layer has to be unveiled by removing the exposed and degraded portions. This can be performed by chemical procedures, so-called wet-etching, by physical techniques or by plasma etching, also termed dry-etching.

A very different set of lithographic techniques is covered by the term of soft lithography. These methods rely on soft and elastic stamps that are used to print or mold patterns onto a substrate and include, for example, nanoimprint lithography. This method includes the approach to transfer the structure present on a hard model stamp to a polymer by employment of heat or UV light for curing of the polymer. In this approach the working stamp is in direct contact with the polymer while the polymer is cured by either exposing it to the curing temperature or to UV, respectively. The polymerized, soft stamp can then be used for other wet lithographic techniques, for instance for molding of the pattern to another polymer that is coated onto a substrate.

In many applications a combination of different lithographical methods are used to fabricate the targeted structures to achieve optimal quality while saving resources and time. As example of such a combined application of lithographic techniques, the steps performed for the fabrication of the diffraction gratings, used in the studies presented below, are depicted in Figure 17. The procedure starts with UV laser interference lithography (steps 1-3) to create a model, that is afterwards used in thermal nanoimprint lithography (step 4) to transfer the pattern onto a soft PDMS stamp, that again is employed for replica molding with UV-curing (steps 5-8) to finally yield the same pattern on the sensor chip as it was built on the model.

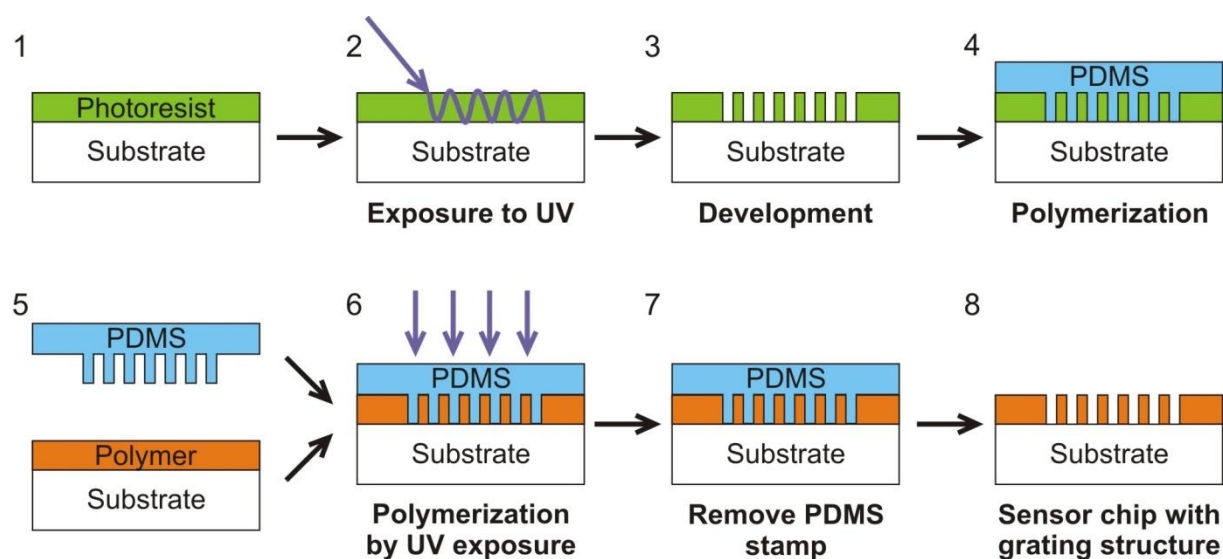


Figure 17 Example for application of lithography. Fabrication procedure of diffraction grating sensor chips (PDMS – polydimethylsiloxane). Figure is partially based on [150].

As mentioned above, a metallic layer, crucial for SP excitation is deposited either on the chip substrate directly or on the fabricated nanopatterns. For the optimal sensing performance the right choice of the metal type is important. Silver yields the highest field intensities of SPs, but is unstable and sensitive to chemical changes and thus impractical for sensing purposes in which the sensor is in contact with different chemical reagents and solutions. Gold is the second best material for SP excitation in physical terms and it is an inert metal, hence it is much more stable compared to silver and therefore also the most common metal used for plasmonic sensor chips. Not only the material itself, but also the layer thickness plays a critical role in plasmonic sensing performance and has to be optimized for the specific application. Furthermore, the roughness of the metal layer can also influence the sensing quality, where a higher surface roughness results in lower sensitivity [146]. This roughness can be controlled by using the right method for metal deposition. Several methods are available for deposition of thin metal layers on substrates including evaporation, which heats up a metal source thermally or by an electron-beam and the metal vapor condenses and solidifies on the substrates located opposite to the metal source. Also

sputtering can be used to form a metal layer on a substrate by targeting a metal source with ion gases, which leads to ejecting of metal molecules that condense again on the target surface. Evaporation and sputtering yield rather rough surfaces, while metal layers with a minimized surface roughness can be prepared by template stripping [151]. For this approach the metal is first coated on a substrate that has a very flat surface and low adhesion properties to the metal. Afterwards the metal is coupled to a different substrate material on the opposite side with high adhesion forces via a high performance adherence layer. Subsequently, the first substrate with low adhesion to the metallic layer is stripped off and thus leaving a super flat metal layer adhered to the other substrate behind.

1.2.4 Sensor Surface Architecture

The surface on top of the thin metallic layer is the sensor surface, which requires a certain architecture of several layers to enable sensing of biological molecules and samples [152]. As depicted in Figure 16, first of all an adhesion linking layer is coated onto the metal surface. This layer has two central functions: passivation of the metal and introduction of linking elements for further functionalization. The metallic surface is usually incompatible with biomolecular ligands and sensing of specific interactions between molecules, because the solutions and molecules used in biosensing are, in the majority of applications, present in a hydrated state and thus would not be able to attach specifically to the inert metal layer. Thus, a bioinert layer that creates a hydrophilic surface is needed to cover the metal film. Furthermore, gold surfaces also have the property of adsorbing any kind of biomolecule unspecifically. To circumvent these effects the metal layer is covered with a material that on the one hand forms a barrier to avoid the unspecific interaction of the molecules present in sample solutions with the metal, which is also called passivation, and on the other hand creates a hydrophilic environment. This second function also includes linking the sensor chip with a specific sensing material that will only detect the target molecule. This linking is performed via incorporation of functional groups, like carboxylic or amine end groups, within the adhesion linking layer. On metal surfaces, this linking layer very commonly consists of thiols that spontaneously form self-assembled monolayers on metals, because of the strong affinity between the metallic surface, that acts as an electron pair acceptor, and thiol, disulfide or thioether molecules, that act as electron pair donors. Such self-assembled monolayers can achieve high packing densities and by using thiols with unreactive endgroups, like hydroxyl groups, optimal aqueous passivation layers can be formed. Furthermore, by addition of thiols with functional endgroups, like carboxyl or amine groups, the self-assembled thiol layer can also be used for linkage with specific analyte immobilization layers.

After this conversion of the inert metallic surface to a biocompatible hydrophilic surface, the next layer assures further passivation of the surface and more importantly is responsible for the specific linkage and binding of the capture molecules that will specifically interact with the target analyte. This so called immobilization matrix can be, for example, a three-dimensional hydrogel that creates a thick layer with many interaction points for binding of ligands distributed across the whole volume of the hydrogel (see Figure 18a). Such hydrogels consist of a mesh of polymers that can be tailored to exclude molecules of certain sizes from entering the matrix and thus not being able to interact with the specific binding sites. Hence only smaller sized molecules, including the target analyte, could enter and bind to the capture molecules, thus triggering a SPR signal. Therefore, such a polymer hydrogel can be employed for passivation too. Moreover, very high densities of capture molecule and hence high immobilization capacity of the target molecule can be achieved by three-dimensional immobilization matrices, because their height can be tailored to fit the penetration and hence sensing depth of the SPs, so that the whole volume that is probed by SPR can be utilized for binding of target molecules leading to higher signals. Two-dimensional surface architectures can be used for applications that require lower immobilization capacities, which for instance is the case, if kinetic measurements are performed or bigger molecules should be detected. Such layers can also be comprised of polymers, but they are much thinner compared to the three-dimensional matrices.

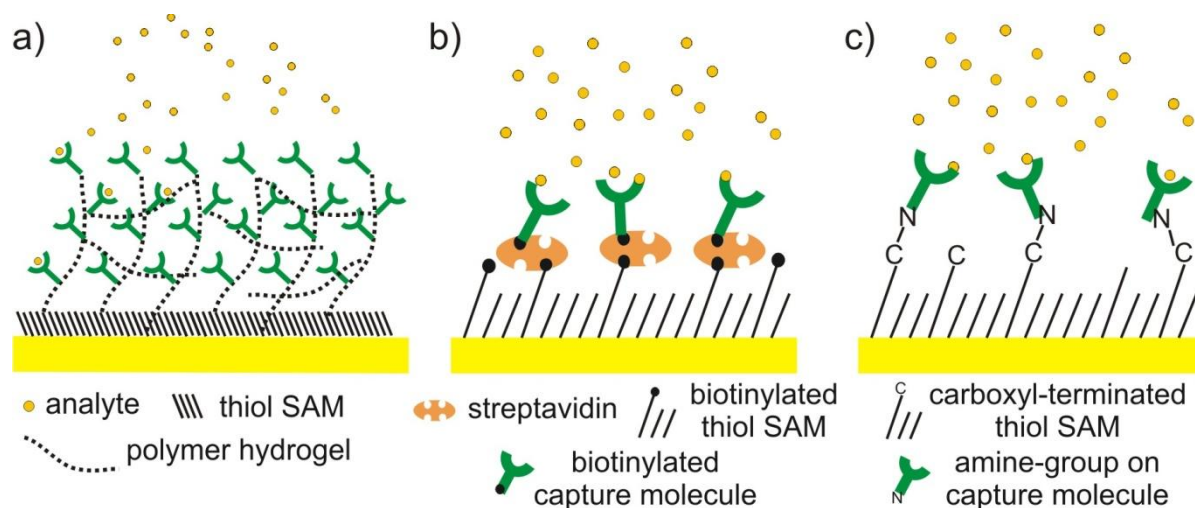


Figure 18 Schematics of sensor surface architectures with a) 3-D immobilization matrix, and incorporated adhesion and immobilization layer with thiol-PEG-molecules using b) streptavidin-biotin coupling or c) amine coupling for surface functionalization.

It is also possible to omit the separate immobilization matrix or layer and incorporate its immobilization function into the first adherence and biocompatibility layer. This can be easily conducted by building a self-assembled monolayer with thiols that contain a sulfide-group and carbon-chain at one end of the molecule for attachment to the metallic surface, several polyethyleneglycol (PEG) groups as linkers to achieve hydrophilicity and improved surface

passivation, and functional groups at the other end of the molecule, that are capable of immobilizing the capture molecules (see Figure 18b and c). To tailor the immobilization capacity of these layers, a mixture of thiol-PEG molecules without a functional group and thiol-PEGs that carry functional groups at the end is often used. By adjusting the ratio of functional to non-functional thiols the amount of capture molecule ready to immobilize the target analyte can be controlled and optimized [153]. Also steric hindrances can be avoided by using longer PEG-linker chains in the functionalized thiol-PEG molecules, so that the functionalized groups extend out of the passivation layer of unfunctionalized thiol-PEGs.

The often mentioned functional groups present on either the thiol-layer or the immobilization matrix are used to couple or immobilize the capture molecule onto the sensor surface. This step is also called the surface functionalization, because the capture molecule is responsible for the specific binding of the target analyte and thus the function of the plasmonic sensor surface. The specificity of plasmonic biosensors is fully dependent on the specificity of the sensor architecture, because the SPR response itself does only indicate a refractive index change, but cannot differentiate what kind of molecule or particle initiated this change. Thus, the specificity of the interaction between the capture molecule and the target analyte additionally to the passivation capacity of the sensor surface determine how specific a plasmonic biosensor can detect the target analyte. Very well established methods to couple the capture molecule to the surface are available today. The most common examples are amine coupling and biotin-streptavidin coupling, as depicted in Figure 18b and c. In amine coupling a peptide bond is formed between a carboxylic and an amine group. In most applications the carboxylic group is found on the sensor surface, as mentioned for thiol layers or hydrogel matrices, and by chemical activation builds a covalent bond with amine groups that are present on the amino acid side chains present in proteins that are utilized as capture molecules. The second most commonly used approach for surface functionalization is the usage of the streptavidin-biotin interaction. This method makes use of the extremely high affinity between streptavidin and biotin that in biosensing applications could be seen as equally strong as covalent bonds. In this approach, biotin molecules are attached to the immobilization layers as functional groups, then streptavidin is bound to the surface, and since each streptavidin molecule harbors four binding sites for biotin, capture molecules that carry another biotin can be immobilized to the surface-bound streptavidin.

The most commonly used capture molecules are antibodies that can be designed to specifically bind a target analyte. But of course any kind of molecule that specifically interacts with the molecule of interest can be used for functionalization. Besides protein based capture molecules that are usually used to probe for protein targets, also nucleic acid strands can be immobilized to

the sensor surface to study interactions with other nucleic acid molecules or proteins, for example [154].

1.2.5 Operation of Plasmonic Biosensors

As described already, plasmonic biosensors monitor changes in light wave characteristics that are caused by a change of the SP excitation, which result from refractive index changes in the dielectric medium that is in contact with the metallic surface. These changes in intensity, SPR wavelength or SPR angle are triggered by any kind of solution exchange in the overall dielectric medium, also called the bulk solution, and in particular in the close proximity to the sensor surface within the SP penetration depth. By keeping the refractive index constant in the bulk solution, a target analyte, that interacts with the functionalized sensor surface and thus increases the analyte concentration only at the surface, can change the refractive index within the SP field and therefore result in a specific SPR response. These changes in close proximity of the sensor surface are examined in plasmonic biosensors to determine, among others, the binding characteristics of certain molecule interactions, the thickness of adhered layers or the concentration of a target analyte in a sample solution. For applications that only focus on the examination of layer thicknesses, for instance, simple end-point measurements can be employed. If, in contrary, the interaction between two molecules and the binding kinetics should be studied, monitoring of SPR changes over time is required. Both of these scenarios can be achieved by the measuring modalities, described in section 1.2.2, that allow to monitor SPs and their resonance not only before and after a binding or adsorption event to the sensor surface, but also in real-time during the binding process.

A typical measurement cycle in plasmonic biosensors involves the establishment of a stable baseline in the SPR signal while flowing running buffer across the functionalized sensor surface, followed by the introduction of the target analyte, and a subsequent washing step with buffer. The sensorgram of such a cycle is depicted in Figure 19 and looks in principle the same for all sensing modalities. During the second step, in which the target analyte is exposed to the sensor surface, the SPR signal increases, because the molecules bind to and accumulate on the sensor surface. Since a concentration increase of biomolecules, like proteins or nucleic acids, in aqueous solutions leads to an increase of the refractive index, the plasmon resonance is shifted towards longer wavelengths or higher angles of incidence and higher reflected beam intensities, as visualized in the graphs in Figure 13. After reaching a plateau at which the signal is stable again, the running buffer is flowed across the surface again and the dissociation of bound molecules occurs. This step leads to a decrease in the SPR signal. In the end a stable signal at the level of the original baseline is reached again, when all analyte molecules are removed from the surface.

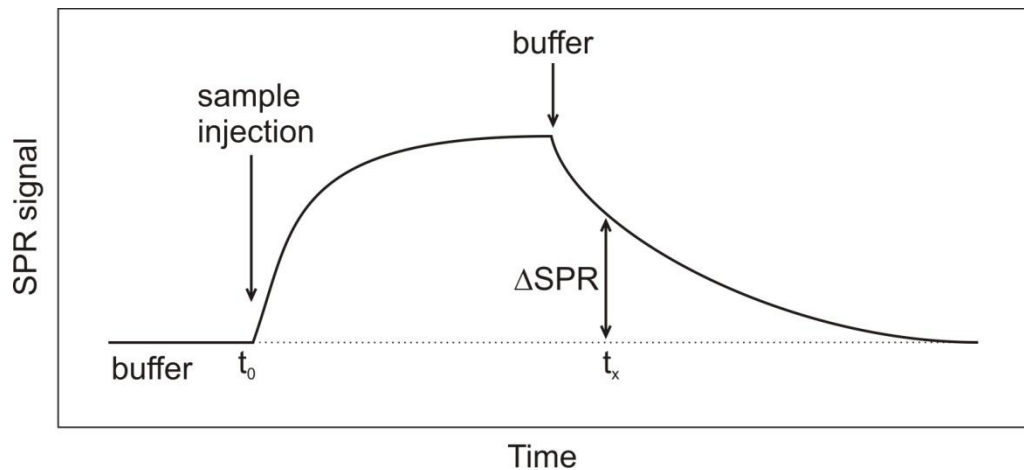


Figure 19 Sensorgrams of a plasmonic biosensor measurement cycle over time (t_0 – time point before sample injection, t_x – time point for concentration determination).

By different analysis of the sensorgram the analyte concentration or its binding kinetics can be determined. The comparison of the original baseline level (see t_0 in Figure 19) and the level at a set time point after washing (see t_x in Figure 19) yields the SPR response (ΔSPR in Figure 19) as angular $\Delta\theta$, wavelength $\Delta\lambda$ or intensity ΔR shift. These signal shifts are used to determine the concentration of the target analyte in samples. The curve characteristics and slopes, on the other hand, are employed for the determination of the binding kinetics, since the rate of signal increase upon sample injection relates to the rate of binding of the target analyte to the surface and the rate of signal decrease upon washing to the rate of dissociation of the target analyte from the surface, respectively. These rates are characteristic for the affinity between the target analyte and the capture molecule on the sensor surface.

To explain the correlation between the SPR response and the concentration of the target analyte in the bulk solution and the kinetics of such binding events, the principles of the interaction of molecules in solution with surfaces have to be discussed [155]. In order to do so, most importantly the two required steps for the binding of the target analyte to the sensor surface have to be defined: first the transport of the target molecule from the bulk solution, pumped through the flow cell, to the sensor surface, second the binding of the target analyte to the capture molecule on the surface. These two processes, illustrated in Figure 20, happen at different rates and whichever is the slower one will define the molecule-surface interaction. Therefore, two regimes are differentiated: mass-transfer limited or reaction-limited.

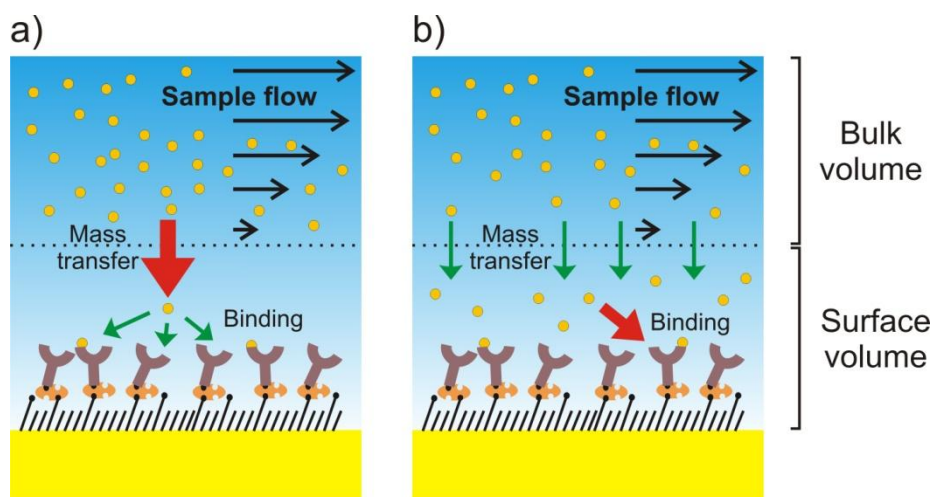


Figure 20 Schematic of the transfer of target analyte and its binding to the sensor surface in a) the mass-transfer limited and b) the reaction-limited regime. The slower and therefore limiting step is illustrated as red arrow and the faster as green arrows, respectively.

In the mass-transfer limited regime the interaction between the analyte and the capture molecule (see red arrow in Figure 20a) is much faster than the transport of the analyte from the bulk to the surface (see green arrows in Figure 20a), hence the overall speed of the binding event is only dependent on the mass-transfer rate. The mass-transfer rate is dependent on the concentration of the transported molecule in the bulk solution and close to the surface, on the diffusion coefficient of the molecule in the solution, and on the flow of the bulk solution. To describe the effect of the latter, a two-compartment model can be applied. This approximation divides the fluid in the volume in close proximity to the surface and the adjacent bulk volume, as illustrated in Figure 20 by a dotted line parallel to the sensor surface. In the volume close to the surface the velocity is equal to zero, because of the friction of the flow at the interface, while the rest of the solution flows at the bulk speed, which corresponds to the flow rate at which solutions are pumped through the flow-cell. Furthermore, the concentration of the analyte in the fluid close to the sensor surface, i.e. surface volume in Figure 20, equals zero, because the analyte is binding to the surface faster than being transported to the surface. Consequently, the transfer of molecules from the bulk volume to the surface volume is only dependent on the diffusion and the concentration of the molecule in the bulk solution. Since the diffusion of a molecule depends on parameters that can be determined and kept constant, namely the size of the target analyte, the temperature and the solution's viscosity, only the concentration of the analyte in the bulk solution, i.e. the sample solution, influences the binding of the analyte to the sensor surface. Therefore, the SPR shift caused by the binding of molecules in the mass-transfer limited regime can be used for determination of analyte concentrations in unknown samples. Since the target analyte dissociates from the sensor surface over time during washing, it is important to keep the

incubation times for analyte binding and washing constant over all measurements and calculate the SPR shift always between t_0 and t_x (see Figure 19), to achieve comparable results.

On the contrary, in the reaction-limited regime the reaction rate of the target molecule binding to the surface (see red arrow in Figure 20b) is slower than the mass-transfer rate (see green arrows in Figure 20b). Hence molecules can accumulate in the volume above the surface and are not bound to the sensor surface immediately. Under these conditions the association and dissociation rates of the target analyte to the capture molecules on the sensor surface are independent of the mass-transfer rate and therefore solely depend on the affinity between the examined molecules. Therefore the binding kinetics of such interactions, namely k_{ON} and k_{OFF} as well as the equilibrium constant, can be determined by fitting of the binding curves, yielded from the SPR signal monitoring, to the appropriate kinetic models for the specific interaction examined.

In order to reach either the mass-transfer limited or the reaction-limited regime, the flow rate, the bulk concentration of the target analyte and the density of capture molecules, i.e. binding sites, on the surface have to be adjusted and optimized. As described, the flow rate and the bulk concentration influence the mass-transfer, with an increase in both resulting in an increased mass-transfer rate. The reaction rate is influenced by the affinity of the molecular interaction, but it can also be adjusted by changing the ratio of molecules available in solution and binding sites available on the surface. High densities of immobilization sites on the surface and low molecule concentrations in solution result in faster reaction rates and vice versa.

Additionally to the analysis of analyte concentrations and binding kinetics, also the density of molecules attaching to the sensor surface and the layer thickness can be determined. These measurements are commonly performed to examine the characteristics and quality of the different metallic or biocompatible layers attached to the sensor surface for SP excitation, passivation and functionalization. Both values rely on endpoint measurements, which are based on the comparison of the level before and after the immobilization step. The density of molecules can be calculated from the shift in the plasmon resonance yielding the surface mass density (mass per area), if certain parameters, like the molecular weight of the adhered molecule and its refractive index are known. Similarly, the thickness of a certain layer can be determined from the SPR spectrum, when all other parameters of the different layers are known, including refractive indices and material characteristics.

1.2.6 Signal Enhancement with Nanoparticles

In order to induce a measurable SPR signal change, the binding of a molecule to the sensor surface needs to result in a sufficiently strong refractive index change, which nowadays typically

equals to $\sim 10^{-7}$ RIU when high-end commercially available devices are used [156]. This fact limits the sensitivity of plasmonic sensors, which can be defined as the minimal measurable refractive index change or sensor resolution [146]. Hence, if molecules have a too small molecular weight, they might not be able to trigger such a measurable change and consequently cannot be detected by plasmonic biosensors. For such cases sensitivity enhancing methods have been developed.

One approach is to use molecules or particles with a higher molecular mass that are bound to the target analyte and are capable of inducing an additional refractive index change and consequently an amplified SPR response. By such means also the presence and concentration of formerly undetectable molecules can be determined indirectly. For example, the target analyte can be first immobilized to the sensor surface via the capture molecules, while the SPR signal shows no change, and subsequently a detection molecule is used, that also specifically binds to the target analyte, in order to trigger the signal change, which again is proportional to the concentration of the target analyte. Just as for capturing also for detection antibodies are often employed, because of their high affinities and tailored specificity to the target molecules. To achieve an even higher sensitivity enhancement, such detection antibodies can also be coated onto nanoparticles that have much higher mass, compared to biomolecules, and thus are capable of plasmonic signal enhancements. Furthermore the use of metallic nanoparticles (gold or silver) leads to the excitation of LSPs that couple with the PSPs that are present on the sensor surface. These coupling modalities can lead to signal amplifications of several orders of magnitude, depending on the size and shape of the used nanoparticles [157].

Besides metallic nanoparticles also carbon-based nanostructures, e.g. carbon nanotubes, latex nanoparticles, liposome nanoparticles or magnetic nanoparticles can be employed for signal enhancement [141]. Carbon nanostructures enhance the SPR signal by transferring charge to the sensor surface and thus increasing the evanescent field intensity, which leads to higher SPR responses. Latex and liposome nanoparticles act, just as antibodies, by enlarging the mass bound to the surface and thus triggering a higher refractive index change. Magnetic nanoparticles induce a SPR signal enhancement by the same means, but additionally their magnetic properties can be used for a further sensitivity increase. By application of a magnetic field on the backside of the sensor surface the magnetic nanoparticles can be attracted and collected at the surface very efficiently. Hence, the diffusion limited transfer of nanoparticles to the sensor surface, which is limiting the amount of nanoparticles being able to interact with the surface for signal enhancement, can be overcome, resulting in higher sensitivities [158]. If the target analyte is first bound to the magnetic nanoparticles and then introduced to the plasmonic sensor, also the target analyte can be pulled to the sensor surface in a more efficient way and thus avoiding diffusion limited transfer of big sized analytes [159].

1.2.7 Surface Plasmon-Enhanced Fluorescence Spectroscopy

In addition to the SPR readout of plasmonic sensors, fluorescence detection can be incorporated into plasmonic systems. The capability of SPs to enhance fluorescence signals up to 10^3 -fold makes this a very attractive approach for the application in highly sensitive biosensors [147]. Similar to the nanoparticles used in the SPR enhancement methods described above, plasmonically enhanced fluorescence (PEF) biosensors also use detection molecules that bind to the already captured analyte on the sensor surface and carry fluorophores.

Fluorescence occurs during the transition of fluorophores from an excited energy level to their ground state, which is accompanied by the emission of photons. This is illustrated in more detail in the Jablonski diagram, depicted in Figure 21, which shows the energy transitions of fluorophores in the free space (black arrows) and in proximity of a metallic surface with SPs (red arrows). In free space a fluorophore is elevated from its ground energy state to an excited state by absorbing a photon of the excitation wavelength λ_{ex} and releases this energy spontaneously by non-radiative or radiative decay to fall back to the ground state. The radiative decay involves the release or emission of photons at the emission wavelength λ_{em} , which is detected as signal in regular fluorescence assays. If such fluorophores are getting close to a metallic-dielectric interface where SPs are present, the metallic surface and the plasmons impose several effects on the energy transitions [147, 160]. First of all the strongly confined electromagnetic field of SPs and its very high field intensity can excite fluorophores faster, hence enabling to have a higher emission intensity, which results in higher fluorescence signals reaching the detector in a biosensor. Furthermore, fluorophores can also emit their energy to SPs, which can be out-coupled from the surface by the same means used for the SP excitation and targeted to the fluorescence detector. This can again lead to an increase in the fluorescence signal intensity. Additionally, the radiative decay rate is enhanced in comparison to the non-radiative decay through the coupling to SPs and hence the quantum yield of a fluorophore, that is the ratio of the radiative to the non-radiative decay, is increased. A second surface associated decay channel is only possible at very short distances from the metallic surface (<15 nm) and due to the Förster energy transfer from the fluorophores to the metal electrons. This energy transition is a non-radiative decay and quenches the fluorescence signal, if the fluorophore gets too close to the surface, and thus has to be avoided in PEF biosensors.

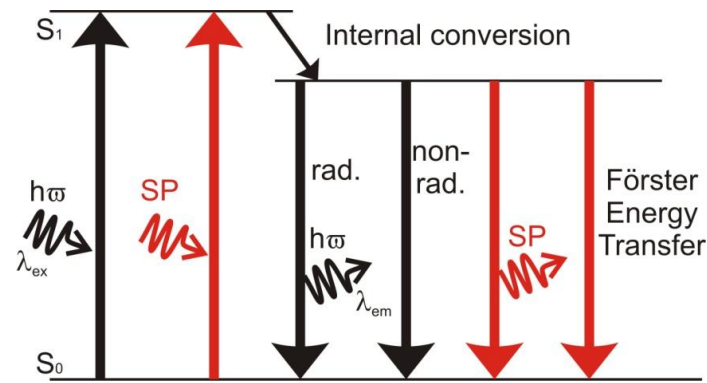


Figure 21 Jablonski diagram of the energy transitions by fluorophores in free space (black arrows) and in proximity to a metal surface (red arrows) ($h\omega$ – photon, λ_{ex} – excitation wavelength, λ_{em} – emission wavelength, SP – surface plasmon, rad. – radiative decay, non-rad. – non-radiative decay). Figure adapted from [147].

Taking these effects together, the emission of photons by fluorophores in the vicinity of metallic-dielectric interfaces can be enhanced (i) by the increased excitation levels through the high intensity electromagnetic SP field, (ii) by the energy transition to SPs that are out-coupled to the far field in a certain direction, and (iii) by the increased quantum yield.

The implementation of PEF for biosensing is achieved by the already known SPR coupling instruments. Most of the applications use the ATR configuration and add instrumentation for the fluorescence detection on the sensor chip's side opposite of the prism, measuring the fluorescence that is emitted through the flow-cell, which has to be made of a transparent material in this case. The schematic of such an ATR configuration for SPR and PEF readout is depicted in Figure 22. Additionally to the photomultiplier for detection of the fluorescence intensity at λ_{em} , optical filters are installed to remove background signals from λ_{ex} and only let λ_{em} pass through.

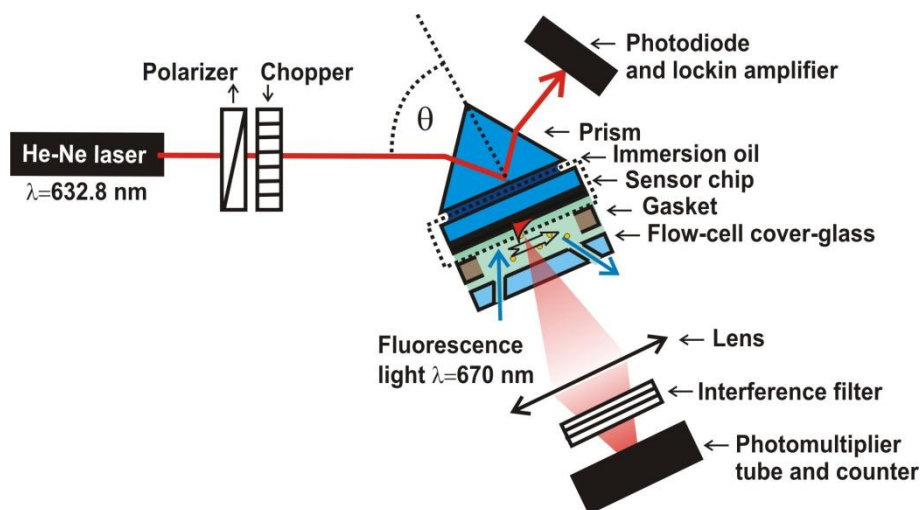


Figure 22 Schematic of a combined plasmon-enhanced fluorescence and surface plasmon resonance biosensor in the ATR configuration. Figure reprinted from [147].

Moreover, diffraction grating coupled SPR can be used for PEF application. For these instruments the so-called epi-fluorescence geometry is utilized, in which the same beam path is

used for the incoming λ_{ex} and the outgoing λ_{em} light beam, see Figure 23. A very attractive feature of grating-coupled SPR for fluorescence enhancement is that by optimization of the grating structure on the sensor surface, the direction of the emitted fluorescence through SPs can be controlled in a much more defined way than in the ATR configuration. Hence it is possible to concentrate the emission towards specific angles in which the detector is positioned [161]. The direct comparison of the ATR and grating couplers, showed that grating coupled PEF results in an about 10- to 4-fold higher fluorescence enhancement compared to ATR coupling, based on simulation studies and measurements of a fluorescence detection assay, respectively [162].

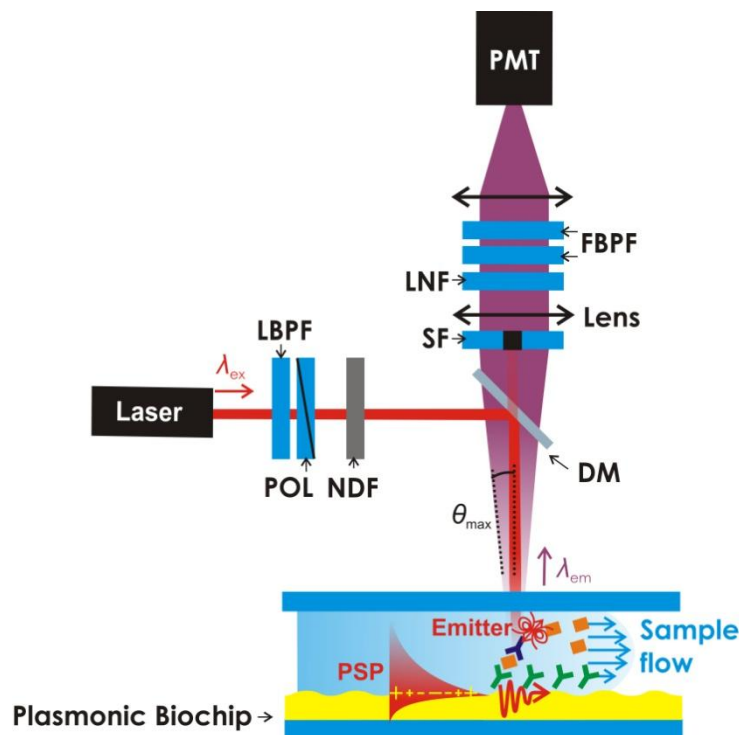


Figure 23 Schematic of a combined plasmon-enhanced fluorescence and surface plasmon resonance biosensor using diffraction grating coupling and epi-fluorescence geometry. Figure adapted from [161].

A factor that has to be considered in all PEF applications is the matching of the fluorophore's λ_{ex} with the resonance wavelength. Thus, the conditions of the SP coupling have to be optimized to fit the requirements for fluorophore excitation as well. For a maximal enhancement of emitted fluorescence by SPs, both resonance and excitation wavelength should be the same, since the field intensity and the coupling are strongest at the maximal excitation of SPs. For such purposes the choice of fluorophore, the wavelength of the monochromatic light source, the angle of incidence and the grating structure can be adjusted and tailored to the needs of the individual application.

1.3 Plasmonic Biosensors for EV Analysis

The adsorption of lipid vesicles to sensor surfaces was first primarily studied in the context of creating lipid surfaces in biosensors for the examination of interactions between lipid-bilayers and proteins or transmembrane protein functions [163]. In these applications the vesicles only served as tools to functionalize the surface and thus the studies focused on the physical characteristics of the vesicles attaching and spreading on the sensor surface. But still findings on the vesicle's behavior are important for today's interpretation of results. Only three years ago in 2014 the first plasmonic biosensors for the detection and analysis of EVs were introduced. Since then several different plasmonic techniques and approaches have been discussed to better characterize and quantify EV samples.

An important characteristic of plasmonic sensors is their limited probing depth of a distance of around 100 nm away from the surface for conventional PSPs. Hence, only molecules or particles that are within this probing depth can be detected by plasmonic biosensors. Since the currently used methods for EV analysis cannot detect vesicles smaller than 100-200 nm, as discussed in detail in section 1.1.5, plasmonic biosensors could serve as additional tool to analyze exactly these small vesicles that are missed by other methods. So far the detection of EVs with plasmonic biosensors, which monitored their affinity binding via certain EV cargo molecules to the sensor surface, proved that such biosensors are capable of analyzing EV subpopulations and their cargo in a qualitative manner [121, 164, 165]. Furthermore the relative quantification of EVs carrying specific cargo molecules and the comparison of protein levels between different EV populations was examined in these studies. However, the absolute quantification of vesicle subpopulations by SPR biosensors is more complex, even though in theory possible. The challenges of vesicle quantification are mainly caused by the size heterogeneity of EV samples and by the complex interaction of lipid vesicles with functionalized surfaces, as they can spread out and thus influence the signal response. So far, most studies, that give a concentration value as limit of detection or sensitivity of plasmonic biosensors for EV analysis, used other methods, like total protein concentration measurements or NTA, for the determination of the concentration and related this to the dilutions examined in the plasmonic biosensor [121, 166]. Only one group worked intensely on the methodology and data interpretation to determine the absolute concentration of EVs by SPR measurements [167, 168], which is discussed in the following paragraphs.

Regarding quantitative SPR measurements, the surface mass density, which is the quantitative output of plasmonic biosensors, of vesicles bound to the sensor surface can only be calculated from the induced refractive index change and SPR response, if the thickness of the layer and the refractive index change per amount of vesicles is known [52]. The later can be approximated by

combining already determined refractive index changes from the individual biomolecular components of EVs, like lipids, proteins and nucleic acids. The definition of the layer thickness that is formed on the sensor surface is more complex, due to the heterogeneous size of EVs and the possible flattening of vesicles when they are binding to the surface. The size distribution of an EV sample can be determined by other techniques, like nanoparticle tracking analysis, but it has to be considered that the errors and limitations afflicted with such methods are transferred also to the calculated SPR results. Moreover, it is important to differentiate between the overall size distribution of an EV sample and the one of the vesicle subpopulation that harbors the target molecule that will affinity bind to the functionalized plasmonic sensor surface, as this can vary strongly. Another approach to determine the absolute concentration of EVs with plasmonic biosensors is to monitor the binding rate of vesicles to the surface in the mass-transfer limited regime. Under these conditions the binding rate is only dependent on the concentration of target analyte in the sample solution and on the diffusion rate of the analyte to the surface. Therefore, the concentration can be determined from the binding rate, if the diffusion is known, which depends on the size of the analyte. Hence, for this approach the size distribution of the analyzed EVs has to be known in advance, which again can bias the calculated results from the SPR response.

Using a conventional SPR sensor relying on PSPs on flat gold surfaces, Rupert et al. [167] were able to determine the concentration of EVs carrying CD63 as the surface bound mass with an accuracy of about 50 % when using an estimated refractive index increment per vesicle concentration and approximating the thickness of the bound layer via the vesicle size, which again was measured by NTA. Furthermore, it was assumed that all vesicles present in the sample carry CD63 and are able to bind to anti-CD63 antibodies on the sensor surface. The used surface functionalization and a measured sensorgram are depicted in the following image.

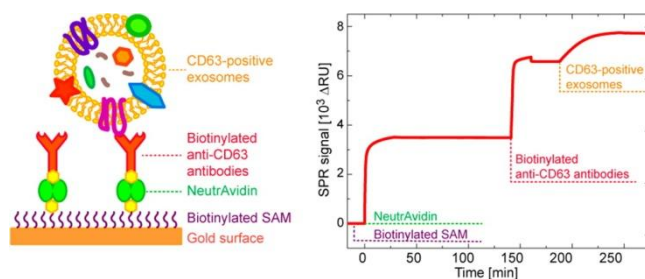


Figure 24 Schematic of the surface architecture and assay used for the quantification of EVs by SPR and the resulting sensorgram. Figures reprinted from [167].

The main reason for the error in concentration calculations resulted from the vesicle deformation when binding to the surface, which was not considered in the estimation of the bound layer thickness. Through the attachment to several binding sites on the surface, the vesicles, which

consist of a soft and flexible lipid bilayer, are flattening and thus their mass comes closer to the sensor surface [169]. Since the SPR sensitivity is increasing in the proximity to the interface, this vesicle flattening directly influences the measured and calculated surface mass. To improve the performance of plasmonic biosensors for the direct quantification of EVs Rupert et al. used dual-wavelength SPR to determine the EV size and concentration in parallel [168]. This approach simultaneously measures the SPR response from two SP fields that are excited by light beams with different wavelengths and the schematic setup is depicted in Figure 25a.

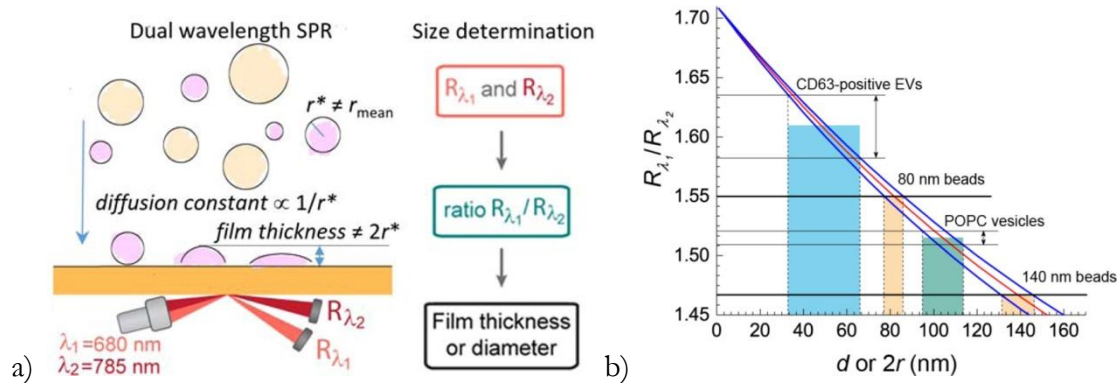


Figure 25 a) Illustration of the sensing setup of the dual-wavelength SPR sensor for EV analysis and b) the relation of the measured response ratio to the vesicle size (given as diameter). Figures reprinted from [168].

Through calculating the ratio of these two SPR signals, it is possible to determine the thickness of the layer that bound to the sensor surface and hence determine the size of the adhered vesicles, as illustrated in Figure 25b. This can be achieved, if the sensitivity, the refractive index increment per vesicle amount, and the SP penetration depth are known. By these means the actual film thickness of the bound vesicles can be used for the calculations of the EV concentration. Therefore the deformation, which caused inaccuracy in the previous SPR concentration measurements, is taken into account in the calculations, leading to a highly improved concentration determination with an error of only about 10 %. However, the knowledge of the size distribution of the CD63-carrying EVs is still required and determined by NTA, which can bias the concentration determined by the plasmonic biosensor. Moreover, the conversion of the mass concentration resulting from the SPR response to a particle number concentration is very complex and requires knowledge of the exact molecular composition and mass of the examined vesicles. Nevertheless, when the limitations of this method are taken into consideration, plasmonic biosensors have the capability to determine the absolute concentration of EVs and prove useful to complement currently used quantification methods.

The deformation of vesicles when in contact with surfaces was studied intensely by Jackman et al., who developed a biosensing platform based on LSPs to examine the kinetics of the adsorption process of liposomes on metallic surfaces [170, 171]. Besides an elaborate discussion

on the quantification of vesicle deformation by interpretation of the SPR response, the studies showed that the vesicle deformation decreased with an increase in surface coverage, because in densely packed layers there is less free space for vesicles to flatten on the surface, compared to spatially separated vesicles. Furthermore, the size of vesicles influenced the vesicle deformation, with big liposomes deforming stronger than small ones, because of the differences in membrane curvature and thus flexibility. Finally, liposomes were diluted in buffers with varying ionic strength and the influence of the osmotic pressure on the deformation of adsorbed liposomes was examined. If liposomes were suspended in high ionic strength buffer the SPR response indicated a much higher deformation compared to liposomes in low ionic strength buffer. This results from the greater membrane flexibility of such liposomes caused by the internal volume decrease resulting from the liposome's reaction to balance and equalize the osmotic pressure across its membrane. Even though these studies were primarily performed to yield a better understanding of the formation of supported lipid bilayers by vesicle adsorption to surfaces, the results could also aid in the interpretation of data derived from plasmonic biosensors for EV detection.

Besides quantification, plasmonic biosensors have been used to study the composition of EVs by examining their binding behavior to antibodies specific for different molecules that are associated to vesicles in general or to specific populations that derive for instance from cancer cells. For this purpose, a nanohole array sensor was developed, that relies on LSPs, by Im et al. [121]. In Figure 26 electron microscopic images of the sensor surface are depicted that show the measures of the nanohole arrays and the vesicles bound to the surface.

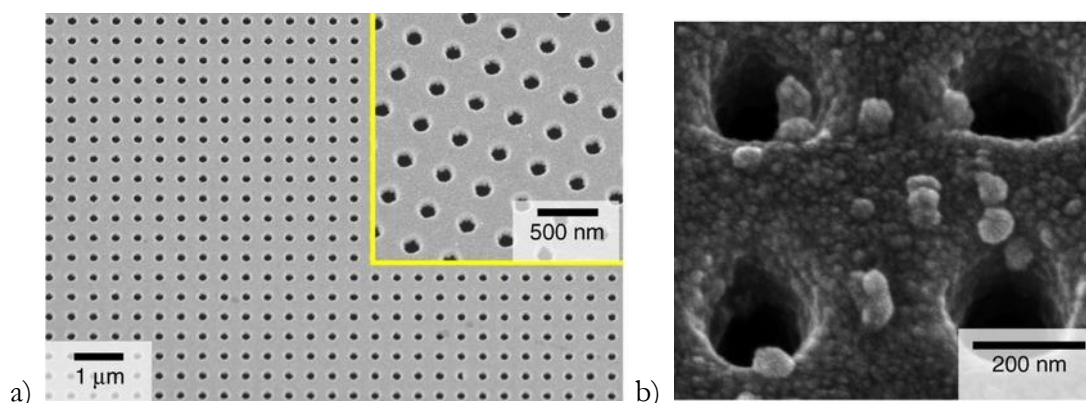


Figure 26 Scanning electron micrographs of a) the nanohole array sensor surface and b) EVs bound to the surface.

Figures reprinted from [121].

This sensor enabled to measure EVs binding to anti-CD63 antibodies with higher sensitivity compared to ELISA or Western blot and achieved a lower detection limit of 670 aM, while the concentration of EVs was determined by NTA. By binding of gold nanoparticles to the captured vesicles, the SPR response was amplified even further. Moreover, it was shown that this sensor

was capable of measuring not only purified EVs suspended in buffer, but also directly from body fluids that were only filtered through 0.2 μm pores to remove bigger particles. For analysis of the presence of several target proteins associated to EVs and cancer, a multiplexed format with 12 channels was developed in which different antibodies were used for the specific detection. The SPR response measured for the targeted proteins was normalized to the response of the channel in which the more general marker CD63 was probed, in order to compare levels of EVs carrying the target proteins between different samples. Since it is not known whether EVs from different samples carry the same amount of CD63 and it is also unlikely that all EVs carry CD63, this normalization step could potentially bias the results. However, the group was able to identify potential markers that could be used in the diagnosis of ovarian cancer by these means.

To achieve even higher throughput and screen many protein targets for their presence on EVs in parallel, SPR imaging was utilized by Zhu et al. [164]. In this approach an array of sensing spots, each functionalized with different specific antibodies, was printed on the sensor surface, which was probed by an expanded light beam that excited SPs across all sensing spots. The schematics of the sensing platform can be seen in Figure 27. By monitoring the reflected beam intensity over the whole beam area with a CCD camera, the SPR response for each sensing spot was determined. The SPR imaging biosensor allowed detecting not only purified vesicles, but also EVs present in the conditioned cell culture medium of cancer cell lines without prior purification steps. The comparison of the binding patterns of EVs secreted from different cell lines with differing metastatic potential to the SPR imaging antibody array chip revealed that more vesicles were present and bound to the sensor surface when the conditioned medium of the highly metastasizing cell line was analyzed. This proves the ability of plasmonic imaging sensors to determine differences in EV protein levels.

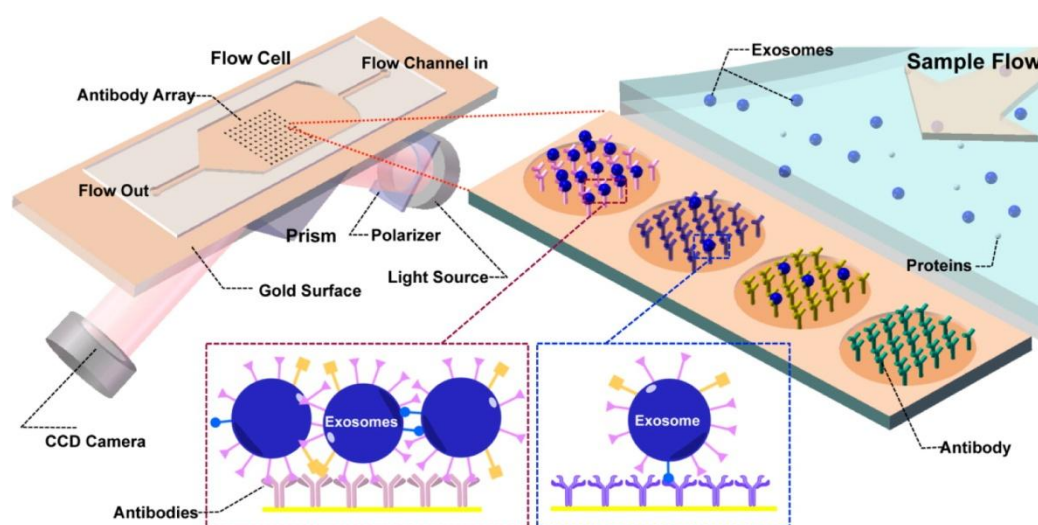


Figure 27 Schematics of the SPR imaging platform for multiplexed EV analysis. Reprinted from [164].

The presentation of the PAMONO-sensor (plasmon assisted microscopy of nano-objects) for examination of EVs, showed a potential alternative way for size determination and quantification of EVs by plasmonic sensors [172]. This method is also based on SPR imaging, but uses an image processing software to identify and count EVs that bind to the sensor surface and trigger a SPR response. Additionally a convolutional neuronal network algorithm was used to determine the size of detected particles. As illustrated in Figure 28 an image of EVs similar to a microscopy image can be produced based on the difference in reflected light intensity and from this image the size of the bound vesicle can be determined. By analyzing several images over time the binding of EVs was monitored in real-time and the binding events were counted, thus yielding the vesicle number bound to the surface within a certain time, or in other words the counting rate. From this the EV concentration in the sample could be calculated, when considering the kinetic conditions, as explained above. The determination of the size of particles with the PAMONO-sensor was so far only tested with polystyrene beads of known sizes. Even though this is a very promising tool, there are some limitations afflicted to this study. First of all the used EV samples were isolated by ultracentrifugation at 100,000 g, which almost certainly resulted in vesicle aggregation, thus the examined vesicle of a diameter of 5 μm , depicted in Figure 28, is most likely an aggregate and not a single vesicle. But by improvements of the resolution, it could be possible to detect EVs directly without prior purification, which has not been tested yet. Also the size determination was so far only performed for polystyrene beads, because the neuronal network algorithm requires training with a calibration set of known size and results are highly dependent on the characteristics of the training set. Therefore, the size determination of a heterogeneous EV sample would be a big challenge.

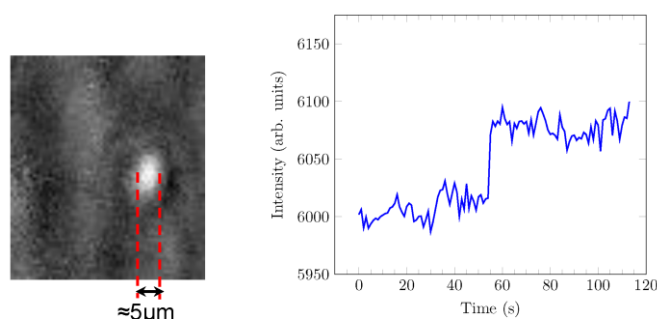


Figure 28 Image of EV bound to the PAMONO-sensor surface and the corresponding increase in the SPR signal.

Figures reprinted from [172].

Finally regular SPR spectroscopy is also useful to study the interaction of EVs with certain molecules or structures. This ability was used by Di Noto et al. [165], who studied the binding ability of EVs to the extracellular matrix component heparin. The measurements showed that EVs isolated from serum of patients with multiple myeloma interacted much stronger with the heparin coated surface, compared to EVs from serum of healthy individuals. This sensing

approach could help elucidating the processes involved in the attachment of vesicles to their target cells.

All in all plasmonic biosensors are promising tools for improved analysis of EVs, because of their high sensitivity, their ability to detect small EVs, and the capability of quantification of specific EV subpopulations. However, there are certain limitations, outlined above, that should be addressed in future studies to further enhance the functions and capabilities of plasmonic biosensors for EV analysis.

2 Aim of the Project

Since in the majority of cases ovarian cancer is diagnosed at late stages when the disease has already spread, a successful therapy is often not possible, leading to low five-year survival rates of only 10-30 % for those patients diagnosed at advanced stages. On the contrary, the few people, who are diagnosed with ovarian cancer when the disease is still contained within the ovaries, have much higher chances to get cured, resulting in five-year survival rates of 70-90 %. Consequently, an earlier diagnosis of this disease would improve the treatability and hence result in tremendously improved survival of patients.

Over the last years extracellular vesicles (EVs) have been shown to be involved in many processes of cancerogenesis. These small lipid vesicles have diverse functions in cell communication and transfer biomolecules or signals between cells across the whole body through body fluids. As they carry molecules that are specific for their cell of origin, they became very interesting as new source of biomarkers. The isolation of EVs from, for example, blood plasma and their subsequent analysis for the presence of cancer-derived EVs through detection of cancer specific moieties could serve as liquid biopsy and be used for diagnosis of ovarian cancer. However, there is still a lack of reliable methods for isolation and analysis of EVs, hence limiting the identification and clinical application of EV biomarkers.

The aim of this project is to identify new EV-based biomarkers for the diagnosis of ovarian cancer, on the one hand, and develop methods for their sensitive detection, on the other hand. In order to achieve the former goal, a biomarker discovery study was performed that is presented in chapter 3. Since currently used EV-isolation methods suffer from high levels of contamination, the study reports on a new approach for vesicle isolation based on lipid-binding proteins.

Plasmonic biosensors were pursued to achieve the highly sensitive detection of EVs. These sensors were chosen, because they enable to measure trace amounts of their target analyte, which is extremely important if small amounts of cancer-derived EVs should be detected in the majority of blood cell derived EVs present in blood. The developed sensor platforms for detection of EVs are presented in chapters 4 and 5.

3 Identification of EV-based Biomarkers for the Diagnosis of Ovarian Cancer

This chapter presents data that were published in [1] and uses text and figures from this publication. Some additional, unpublished data are also included.

As outlined in the introductory section 1.1.6, ovarian cancer is the deadliest among gynecologic malignancies, which is mostly due to the asymptomatic disease progression resulting in diagnosis at advanced stages and to the lack of reliable biomarkers. Over the last few years, extracellular vesicles (EVs) have gained a lot of interest as potential sources of biomarkers in many diseases including ovarian cancer, because the secreted vesicles and their cargo resemble their cell of origin and additionally EVs can be easily accessed and isolated from any of our body fluids [16]. Since the collection of body fluids is generally less invasive than conventional tissue biopsy, the possibility of using EVs as liquid biopsy is very favorable. In several studies of ovarian cancer EVs, cancer derived vesicles have been identified in blood plasma, serum and ascites of patients and presented a unique set of cargo proteins and RNAs with great potential as new diagnostic, prognostic and predictive biomarkers [173, 174].

However the current methods to isolate EVs from body fluids for protein biomarkers are particularly challenging for several reasons. First, the proteome of most body fluids is complex and protein concentrations have a dynamic range that exceeds 10^{10} . For example, the proteome of plasma or serum is dominated by several high abundance proteins. It is estimated that of the approximately 10,000 proteins in the serum, only 21 proteins (among others albumin, IgG, transferrin, apolipoproteins, and complement components) constitute >99% of the serum protein mass [175]. As such, any technique that aims to isolate candidate biomarkers will have to isolate the remaining 1% from the bulk of high abundance proteins. Hence, common EV isolation methods based on biophysical parameters, described in section 1.1.4, such as high speed centrifugation or filtration, would inevitably be contaminated with the high abundance proteins [8, 45]. Second, in addition to proteins many body fluids contain large lipoprotein complexes that are similar in size and density to EVs and thus are often co-purified and mistaken as EVs by common analysis methods [43, 176]. Third, individual classes of EVs, for instance exosomes or microvesicles, are very difficult to discriminate, because they overlap not only in their physical characteristics like size or density, but also in their cargo molecules [44]. Consequently this lack of distinguishing criteria makes the isolation of pure vesicle populations almost impossible with currently used methods. Additionally, recent publications suggest that even within the earlier

defined classes of EVs there are more subclasses of vesicles with distinct cargo and functionality [177] adding another layer of complexity.

To overcome some of these obstacles a new strategy for vesicle isolation using proteins with high specific binding affinity for membrane lipids has been proposed. In this approach, vesicles are isolated based on their membrane lipid composition, which resolves the problem of protein contamination and introduces a new way of classifying vesicle populations. The proteins used for isolation are Annexin V (AV), Cholera Toxin B-chain (CTB) and Shiga Toxin B-chain (STB), which have a high specific binding affinity for phosphatidylserine, ganglioside GM1 and globotriaosylceramide, respectively. By combining these lipid-binding ligands with magnetic particles, distinct populations of EVs, that can be bound by each of the lipid ligands, were purified and characterized from conditioned medium of mesenchymal stem cells [49]. This lipid-based isolation approach was also used to successfully identify protein biomarkers in EVs isolated from human plasma for diagnosis of preeclampsia [178].

The aim of this part of the project was to examine the potential of ascitic fluid derived EVs as markers for ovarian cancer using this new vesicle isolation method based on specific binding of lipids present in the vesicle membrane. First the isolation method was tested for successful isolation of EVs from ascites and then the protein cargo of different EV populations isolated from ascitic fluid of patients with ovarian cancer and cirrhosis was analyzed in regard to the presence of cancer associated molecules.

3.1 Material and Methods

3.1.1 Patient samples

Ascites of patients with ovarian cancer and cirrhosis was collected at the Medical University of Vienna (Austria). Patients with ovarian cancer were recruited in the time from September 2013 to January 2015 and included in the study, if ascites was present and no treatment was performed before sample collection. Patients with cirrhosis were recruited between July and August 2015 and were excluded, if the cirrhosis was due to hepatitis C. All patients signed an informed consent before sample collection, which has been approved by the ethical review board of the Medical University of Vienna (no. 793/2011). The ascites samples of ovarian cancer patients were collected at the first presentation of the disease, before therapy or during debulking surgery.

After collection the ascitic fluid was centrifuged at 1,000 g for 10 min. and the supernatant was centrifuged a second time at 3,000 g for 10 min. to remove remaining cells and cell debris. Subsequently the supernatant was filtered through a 0.22 µm filter (Merck Millipore, USA),

aliquoted and stored at $-80\text{ }^{\circ}\text{C}$ for further analysis. The cell pellet of the first centrifugation at 1,000 g was used for cell smears which were consecutively fixed and stained with Giemsa and PAP by standard protocols. The presence of different cell types (cancer cells, lymphocytes, neutrophil granulocytes and mesothelial cells) in the ascites samples was assessed by microscopy by a pathologist using routine procedures. The abundance of each cell type was classified as 0 = no cells, 1 = very few cells, 2 = moderately abundant cells, 3 = many cells.

3.1.2 EV isolation with lipid binding ligands

The EV isolation procedure was performed as described earlier [49]. Briefly, 1.5 ng of biotinylated lipid binding ligand were used per μl of ascites. The ligands AV, CTB or STB were mixed with ascites in binding buffer (10 mM HEPES, 2.5 mM CaCl_2 , 140 mM NaCl, PBS pH 7.4) and incubated for 30 minutes at room temperature (RT) with shaking. Then 0.1 μl per μl ascites starting volume of pre-washed Dynabeads M280 Streptavidin (Thermo Fisher Scientific, USA) were added to each reaction mixture and incubated again for 30 minutes at RT with shaking. The beads were separated from the liquid with a magnet, the supernatant was discarded and the beads were washed twice with PBS. Finally, the bead bound fraction was resuspended in PBS or lysis buffer depending on the subsequent analysis method. The starting volume of ascitic fluid for EV isolation was adjusted for each analysis method and is stated in the respective sections. As negative control for unspecific binding to the magnetic beads the same isolation procedure was performed without addition of a lipid binding ligand.

3.1.3 Western blot

Standard western blot analysis was performed by denaturing the EV samples isolated from 250 μl of ascites and loading them onto 4-12% NuPAGE Bis-Tris Gels in reducing conditions (Thermo Fisher Scientific, USA). After gel electrophoresis the proteins were transferred to a nitrocellulose membrane. The membrane was then probed with a primary antibody followed by a HRP-conjugated secondary antibody. The primary antibody was detected using a chemiluminescent HRP-substrate (Super Signal West Solution, Thermo Fisher Scientific, USA). The chemiluminescent signals were analyzed with Image Lab software (Bio-Rad Laboratories, USA). The band intensities of each individually analyzed protein were quantified by subtracting the background signal and normalizing to the corresponding β -actin band intensity. Results were given as protein to β -actin ratio. The primary antibodies were mouse antibodies against the human proteins β -actin (C4), β -catenin (E-5), CD71 (H68.4), CD9 (C-4), Alix (1A12), CD59 (H-7), EpCAM (0.N.276) (Santa Cruz Biotechnology Inc., USA), CD63 (H5C6) (BD Biosciences, USA), and FN1-EDA (IST-9) (abcam PLC, UK). All primary antibodies were used in a 1:50

dilution, only anti-FN1-EDA was diluted 1:500. The secondary antibody was a goat anti-mouse IgG-HRP conjugate (sc-2031, Santa Cruz Biotechnology, USA) and diluted 1:1,250.

3.1.4 Zymography and MMP9 ELISA

The presence of gelatinases in the EV isolates was analyzed using Novex Zymogram Gels (Thermo Fisher Scientific, USA) according to the manufacturer's instructions. The EV isolations from 500 μ l ascites and 1 μ l of ascites without isolation were diluted in the loading buffer and resolved on a 10% zymogram (gelatin) gel in non-reducing conditions. After protein renaturation and developing the gel over night at 37 °C, the gel was stained with Coomassie Blue staining solution (40 vol% methanol, 7 vol% acetic acid, 0.25 mg/ml Brilliant Blue R (all Sigma Aldrich, USA), in water) for 30 min. at 80 °C and then for 4 hours at RT with agitation. Then the gel was washed in destaining solution (40 vol% methanol, 7 vol% acetic acid, in water) for 10 min at 80 °C and RT alternately.

The obtained images were analyzed with Image Lab software (Bio-Rad Laboratories, USA). The band intensities were quantified by extracting the background corrected volume density and normalized to the number of pixels of the analyzed band. For quantification of MMP9-levels only the 92 kDa band was analyzed.

MMP9-levels of ascites or EV isolates were quantified by ELISA. The samples were lysed with the Mammalian Cell Extraction Kit (BioVision, USA) and subsequently analyzed with the Quantikine ELISA human MMP-9 kit (R&D, USA) that were both performed according to manufacturer's instructions; except the sample incubation conditions in the ELISA were changed to overnight at 4 °C.

3.1.5 Cryo electron microscopy and AV gold labeling

For cryo-electron microscopy (EM) experiments, ascites samples were labeled with 4-nm gold nanoparticles (NP) conjugated to AV as follows. An 8 μ L aliquot of ascites was mixed with 1 μ L 20 mM CaCl₂ and 1 μ L $1-4 \times 10^{16}$ NP/L AV-gold-NP and incubated for 15 min. Then 4 μ L were deposited on an EM grid coated with a perforated carbon film and quickly frozen in liquid ethane. EM grids were mounted on a Gatan 626 cryoholder and transferred into a Tecnai F20 (FEI) microscope operated at 200 kV. Images were recorded with an USC1000-SSCCD camera (Gatan). For the synthesis of AV-gold-NPs, refer to Arraud et al.[51].

3.1.6 Statistical analysis

The statistical analysis was performed in the software R. The 2-sided, unpaired Mann-Whitney-Wilcoxon test was used for the comparison of MMP9 levels measured by zymography or ELISA between different patient groups. The correlations were calculated with the Spearman method and for the relation between Zymography and ELISA results only the range from 0 to 100 pg of MMP9 was used. Correlation coefficient (ρ), as well as p-values were given as results and p-values ≤ 0.05 were considered as statistically significant.

3.2 Results and Discussion

3.2.1 Patient Cohort

The patient cohort comprised of 17 patients with ovarian cancer and 10 with cirrhosis, respectively. The former had a median age of 61 years (39-83 yrs) at diagnosis and recruitment to the study. The later had a median age of 66 years (53-77 yrs). The clinicopathological characteristics of the ovarian cancers – histological type, FIGO stage, grade – were assessed by a pathologist after routine surgical removal of the cancer tissue. All clinical details of the ovarian cancer patients are given in Table 1.

Table 1 Clinical characteristics of ovarian cancer patients; na = not available, *these samples were only used in the pool, because the detailed clinical characteristics were not available. Table reprinted from [1].

Patient number	Histological type	Age at diagnosis	FIGO stage at diagnosis	Grade at diagnosis
1	carcinosarcoma	na	IIIC	3
2	serous papillary	60	IV	3
3	serous papillary	52	IV	3
4	serous papillary	46	IIIC	3
5	carcinosarcoma	na	IIIC	3
6	serous papillary	67	IV	2
7	serous papillary	83	na	2
8	serous papillary	60	IV	2
9*	na	na	na	na
10	serous papillary	39	IV	3
11	serous papillary	70	na	3
12*	na	na	na	na
13	serous papillary	73	IIIC	3
14	serous papillary	63	IIIC	2
15	serous papillary	60	IIIC	3
16	serous papillary	62	IIIC	3
17	clear cell	61	IIIC	3

3.2.2 Isolation method testing

In this study, EVs were isolated by incubating the ascites fluid with biotinylated lipid binding protein ligands, AV, CTB, and STB. Vesicles bound by these biotinylated ligands were extracted with streptavidin coated magnetic beads and thus could be separated from proteins or other vesicles present in the sample. As this method was only used for EV isolation from conditioned cell culture medium and plasma before [49, 178], we determined if these ligands could also isolate EVs from ascitic fluid by examining the isolates for the presence of tetraspanins CD9 and CD63, the Transferrin Receptor or CD71 and a cytosolic protein, Alix. All these proteins are associated with EVs and generally used as EV markers [16]. β -actin was used as loading control and for band intensity normalization. As shown in Figure 29, CD9 and CD63 were detected only in the AV- and CTB-binding EVs from ascites. CD71 and Alix were detected in all three vesicle populations. As a negative control for unspecific binding of ascites proteins to the magnetic beads the same isolation procedure was performed without addition of a ligand (Figure 29, lane 4). Even though some unspecific binding to the magnetic beads occurred, especially for β -actin and CD71, the level of the proteins in the negative control was very low compared to the EV isolations, suggesting specific enrichment of the tested proteins in the isolations. As CD9 and CD63 are tetraspanins with 4 transmembrane domains, their presence in the isolates were definitive evidence that all three isolates were lipid membrane vesicles. The different distribution profile of the four proteins relative to β -actin among the three EV isolates further suggested that each of the three EV isolates were unique. For example, the absence of CD9 in STB-binding EVs showed clearly that these EVs are different from both CTB-binding and AV-binding EVs [49]. Taking these results together, AV, CTB, and STB are capable of isolating unique EV populations from ascites.

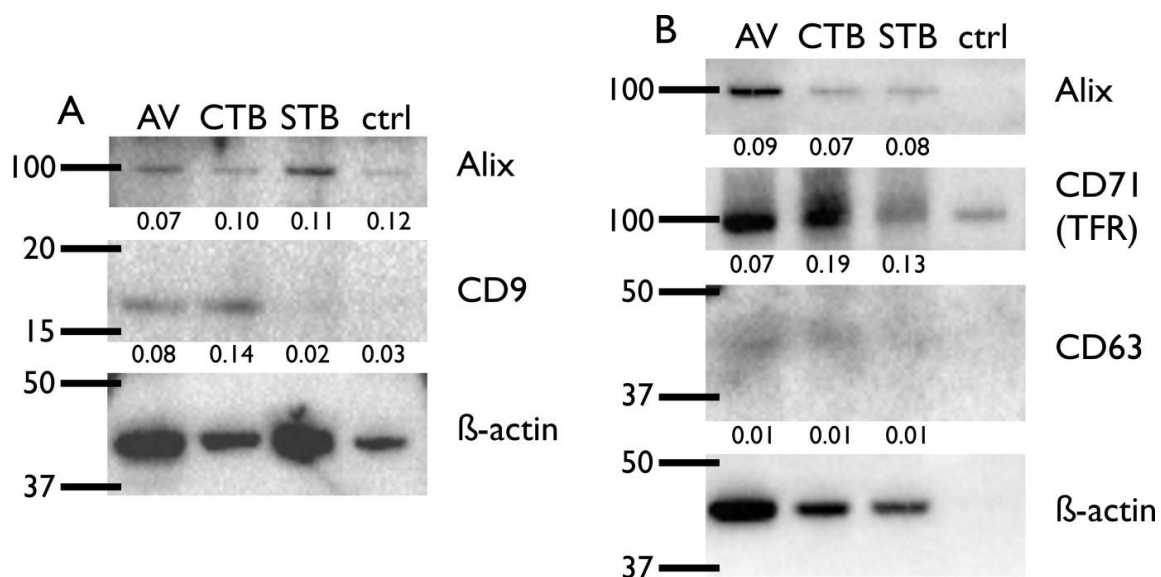


Figure 29 EV isolation from ascites. EVs were isolated from ascites with the ligands AV (lane 1), CTB (lane 2), or STB (lane 3) and analyzed by western blotting. As negative control no ligand was added (lane 4). 250 μ l of pooled ascites from 6 (A) or 16 (B) ovarian cancer patients were used as starting material. The tetraspanin proteins CD9 and CD63, the transferrin receptor (CD71) and the cytosolic protein Alix were examined and β -actin was used as loading control. The normalized band intensities of the analyzed proteins are given below each band. The molecular weight markers are indicated on the left side of the images in kDa. Figures reprinted from [1].

3.2.3 Cancer marker search

Next, AV-, CTB-, and STB-binding vesicles isolated from pooled ovarian cancer ascites or from pooled portal-hypertensive ascites were probed for the presence of cancer markers. The rationale for using ascitic fluid instead of plasma for discovery of EV-associated ovarian cancer biomarkers is that ascites, being in direct contact with the cancer, is more likely to carry cancer biomarkers [179-183]. Once candidate EV-associated ovarian cancer biomarkers are identified, we will next determine if these ascites EV-associated candidate biomarkers can be found in plasma as well. This strategy will enhance the chance of identifying ovarian cancer biomarkers where the signal-to-noise ratio will be higher than that in the plasma, where the vast majority of EVs are derived from blood cells. The following cancer associated proteins were selected for analysis in the EV isolations based on literature search: cellular fibronectin (FN1-EDA), protectin (CD59), epithelial cell adhesion molecule (EpCAM), β -catenin, and gelatinases matrix metalloproteinase 2 and 9 (MMP2/9).

FN1-EDA, also called cellular fibronectin, is a splice variant of fibronectin and an important component of the extracellular matrix. It is highly expressed during embryogenic development, but barely found in adult tissues in contrast to the soluble fibronectin isotype, which is constantly produced by hepatocytes and generally present in plasma [184]. FN1-EDA was found in a variety of cancer tissues [185] and plays an important role in angiogenesis and cell migration [184] which

are two processes crucial for carcinogenesis and metastasis. This protein was detected in all three EV types isolated from ascites of patients with ovarian cancer and was highly elevated in AV- and STB-EVs of the cirrhosis patients (Figure 30). The elevated level of FN1-EDA in EVs of patients with cirrhosis is consistent with the previous report of its important role in experimental hepatic fibrosis [186]. However, this observation eliminated the utility of FN1-EDA as an ovarian cancer marker.

CD59 is a GPI-anchored membrane protein that is expressed on the surface of cells to protect them from complement mediated cell lysis by inhibiting the assembly of the membrane attack complex. Many types of cancer including ovarian cancer express CD59 to escape the immune system [187]. Furthermore, CD59 has been found on EVs, which enabled them to protect themselves and other cells from complement attack [188-190]. Interestingly, it was previously reported that CD59 is not only present in ascites of ovarian cancer patients but that it is also associated with the phospholipid fraction [191]. Consistent with this, we not only detected CD59 in EVs from ovarian cancer ascites but we found that this protein was localized to AV-binding EVs (Figure 30, lane 1). Furthermore, these AV-binding EVs carried more CD59 than AV-binding EVs from portal-hypertensive ascites (lane 5) after correcting for β -actin, making CD59 a potential biomarker for ovarian cancer.

Among the recently identified EV-based biomarkers for diagnosis of ovarian cancer EpCAM is one of the most intensively studied. Several studies showed that the number of EpCAM-positive EVs in body fluids increases with disease progression [76, 106, 120-122]. However, in our EV isolations, EpCAM was not detectable (Figure 30). This could be due to the different isolation procedures used in the different studies, which result in different vesicle populations being analyzed, as well as highly variable contamination levels.

A well known protein which is overexpressed in many cancers is β -catenin. It acts via the Wnt/ β -catenin signaling pathway promoting cell growth and proliferation [192]. A recent study showed that β -catenin can be transferred between cancer cells via EVs and promotes cell motility and proliferation in the recipient cells [193]. This protein was identified in all vesicle populations from ovarian cancer ascites (Figure 30, lanes 1 to 3). Although the ratio of β -catenin to β -actin was higher in each of the three EVs in ovarian cancer ascites than those in the portal-hypertensive ascites this ratio was similar to that in the no ligand control suggesting that the signal is likely to be contamination.

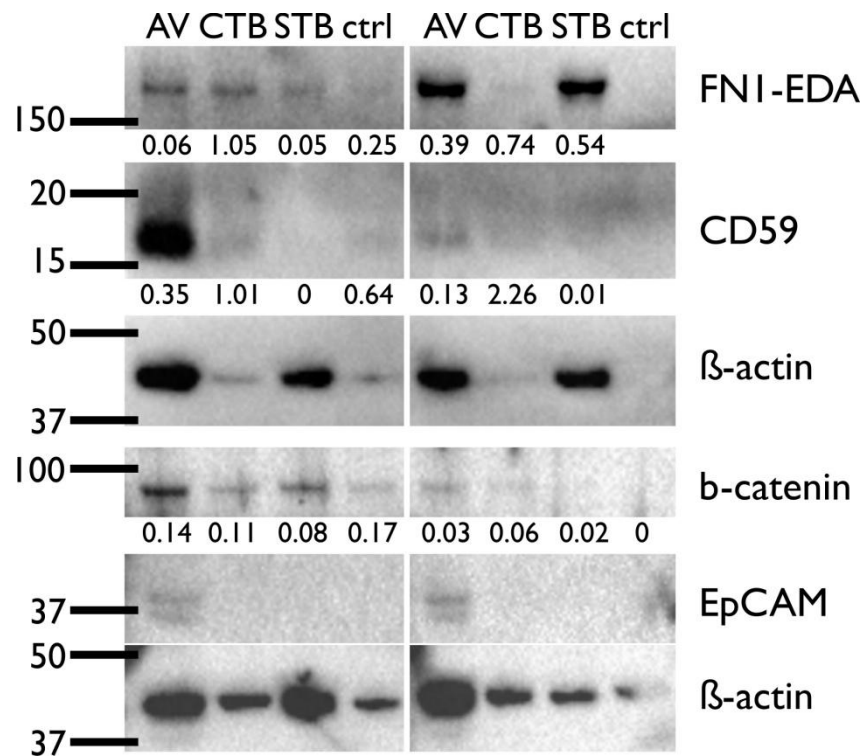


Figure 30 Western Blot of cancer proteins in EV isolations. EVs isolated from 250 μ l of pooled ascites from 6 ovarian cancer patients (lanes 1-4) or from 5 patients with cirrhosis (lanes 5-8) were analyzed by western blot. As before the ligands AV, CTB, or STB were used for isolation, no ligand was added as negative control. The proteins cellular Fibronectin (FN1-EDA), CD59, β -catenin, and epithelial cell adhesion molecule (EpCAM) were examined and β -actin was used as loading control. The normalized band intensities of the analyzed proteins are given below each band. Figure reprinted from [1].

3.2.4 MMP9 cargo of AV-binding EVs

The gelatinases MMP2 and MMP9 have crucial functions in cancer progression and have been identified in ovarian cancer tissues, ascites, and patient's circulation [194-196]. Using zymography in which the presence of both gelatinases in their active and inactive pro-form can be examined, we observed that relative to the portal-hypertensive ascites, the pooled ascitic fluid of ovarian cancer patients had a higher level of pro-MMP2 and pro-MMP9 with the molecular weights of 72 kDa and 92 kDa, respectively. Additionally, the pooled portal-hypertensive ascites had the 60 kDa active MMP2 which was not detected in ovarian cancer ascites (Figure 31, lane 1 vs. 6). The higher MMP-levels in malignant ascites are generally consistent with the often reported higher expression and secretion of MMPs in the cancer environment [197].

MMPs have already been reported to be present in EVs from ovarian cancer ascites and had been associated with a pro-invasive effect on ovarian cancer cells [105, 106]. Here we not only confirmed the presence of MMP9 in EVs, we further demonstrated that the enzyme was present in its inactive pro-form and was restricted specifically to the AV-binding EVs (Figure 31). This enzyme was not present in the CTB- or STB-EVs, or in any of the three EV types isolated from

the portal-hypertensive ascites. In addition to pro-MMP9 at 92 kDa, we observed two higher molecular weight MMPs at >200 kDa and 125 kDa in the AV-binding EVs from pooled ovarian cancer ascites. We hypothesized that the former could be multimers of MMP9 [198], while the latter could be a complex of MMP9 and neutrophil gelatinase B-associated lipocalin (NGAL) [198], which has been described in AV-binding EVs secreted by activated neutrophils [199].

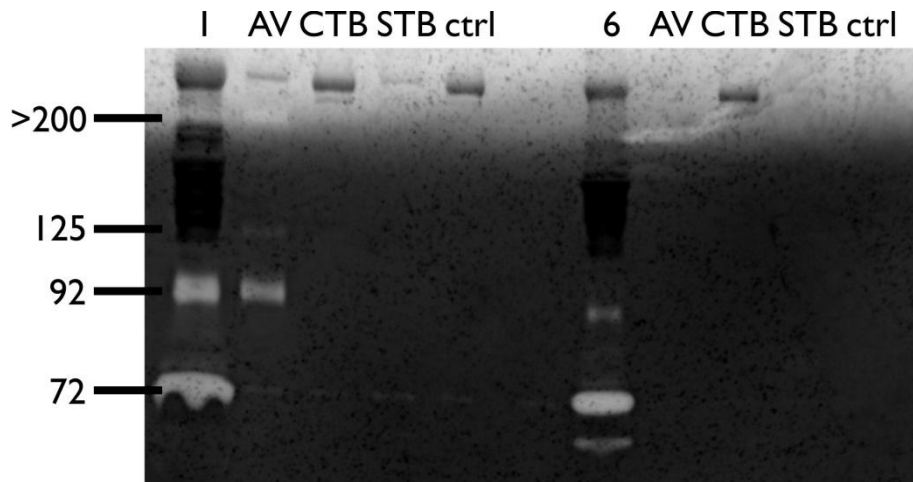


Figure 31 Zymogram of gelatinases in EV isolations. EVs isolated from 500 μ l of pooled ascites from 6 ovarian cancer patients or from 5 patients with cirrhosis were analyzed by zymography. As before the ligands AV, CTB, or STB were used for isolation, no ligand was added as negative control. The left part of the image (lanes 1-5) shows the ovarian cancer samples and the right part the cirrhosis samples (lanes 6-10). In lanes 1 and 6 1 μ l of the pooled ascites samples were analyzed. The molecular weight markers are indicated on the left side of the images in kDa.

Figure reprinted from [1].

To rule out any anomalies caused by pooling of ascitic fluids, we analyzed ascites samples individually with zymography. Interestingly, we did not detect MMP9 in the AV-EVs from ascites of patients with a carcinosarcoma or the clear cell histology. Instead, MMP9 was detected in AV-binding EVs of patients with high grade serous ovarian cancer (HGSOC) (Figure 32A). The analysis of the gelatinolytic band intensities revealed that MMP9-levels were significantly higher in AV-EVs from HGSOC ascites compared to ascites AV-EVs from patients with cirrhosis ($p=6*10^{-4}$) (Figure 32B).

For further evaluation of this finding, the MMP9 concentration in AV-binding EVs was quantified by a sandwich-ELISA. This was performed, because the detection range by zymography is very narrow. As shown in Figure 32C, the band intensities in zymography only correlated with MMP9-levels up to 100 pg MMP9 per 500 μ l ascites at Spearman's rho of 0.885 ($p=1.85*10^{-9}$). Based on the ELISA analysis, MMP9-levels in AV-EVs were statistically significantly higher in patients with HGSOC, when compared to patients with cirrhosis ($p=3*10^{-4}$) (Figure 32D).

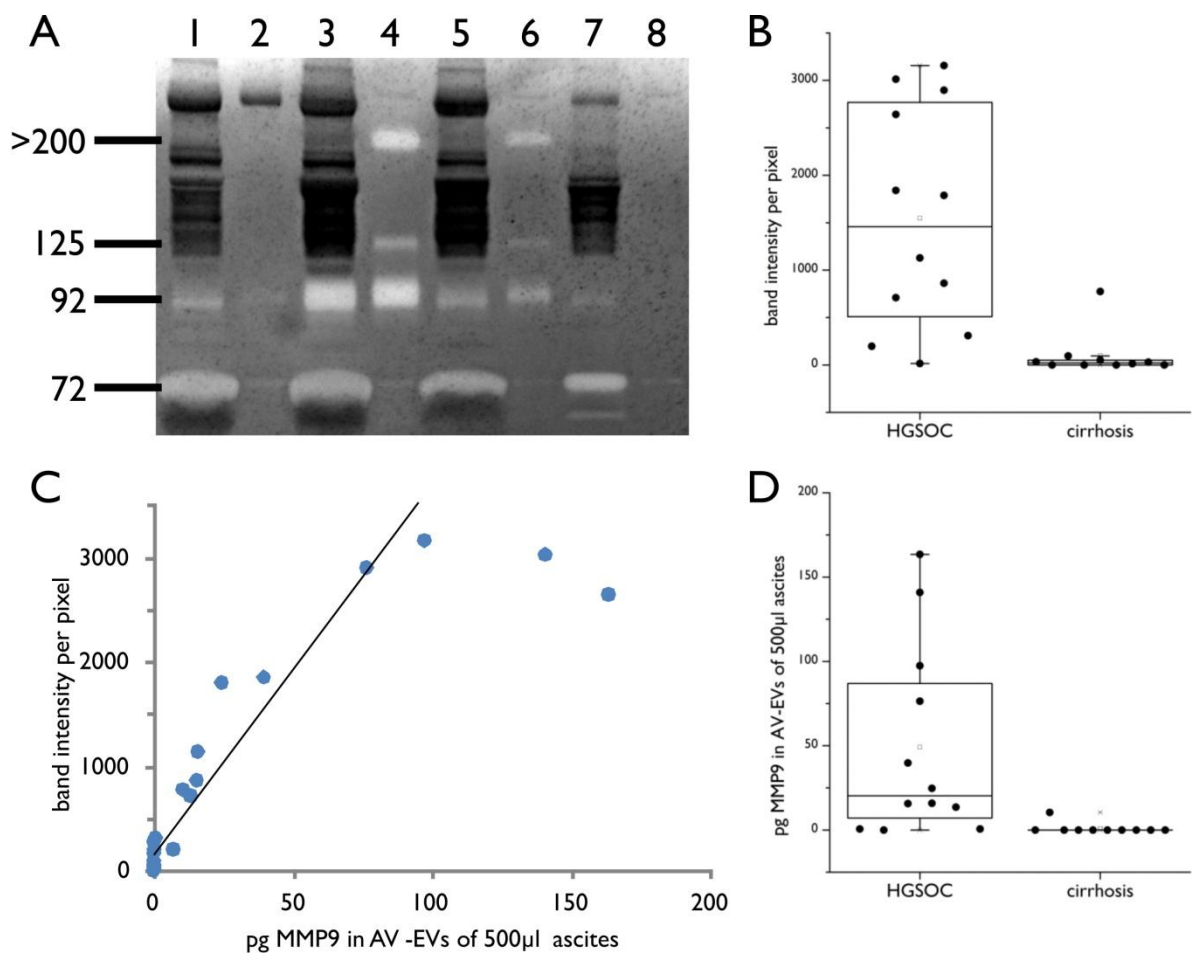


Figure 32 MMP9 presence and protein-level in AV-binding EVs from ascites. A Representative image of a zymogram to determine the presence of MMP9 in ascites samples from four individuals, where 1 µl of ascites (lanes 1, 3, 5, and 7), and AV-binding EVs from 500 µl ascites (lanes 2, 4, 6, and 8) were loaded. The sample in lanes 1 and 2 is from a patient with carcinosarcoma, the samples in lanes 3, 4, and 5, 6 are each from patients with HGSOC, and the sample in lanes 7 and 8 is from a patient with cirrhosis. B Boxplot showing the difference in MMP9 band intensity analyzed by zymography in AV-EVs isolated from different ascites samples. C Correlation graph of MMP9-levels measured with zymography (y-axis) and ELISA (x-axis), D Boxplot showing the difference in MMP9 amount analyzed by ELISA in AV-EVs isolated from different ascites samples (HGSOC = high grade serous ovarian cancer). Figures reprinted from [1].

To confirm that the lack of detectable MMP9 in AV-binding EVs from portal-hypertensive ascites was not due to the absence of AV-EVs, we examined ascites by labeling of EVs with AV-conjugated gold nanoparticles and imaging with cryo-EM [51]. In all of the examined samples, including those that did not have detectable MMP9 in AV-EVs, both AV-binding EVs and non AV-binding EVs were observed (Figure 33). In addition, both EV populations exhibited the characteristic lipid bilayer with a size range characteristic of EVs, i.e. 50 to 500 nm in diameter [16].

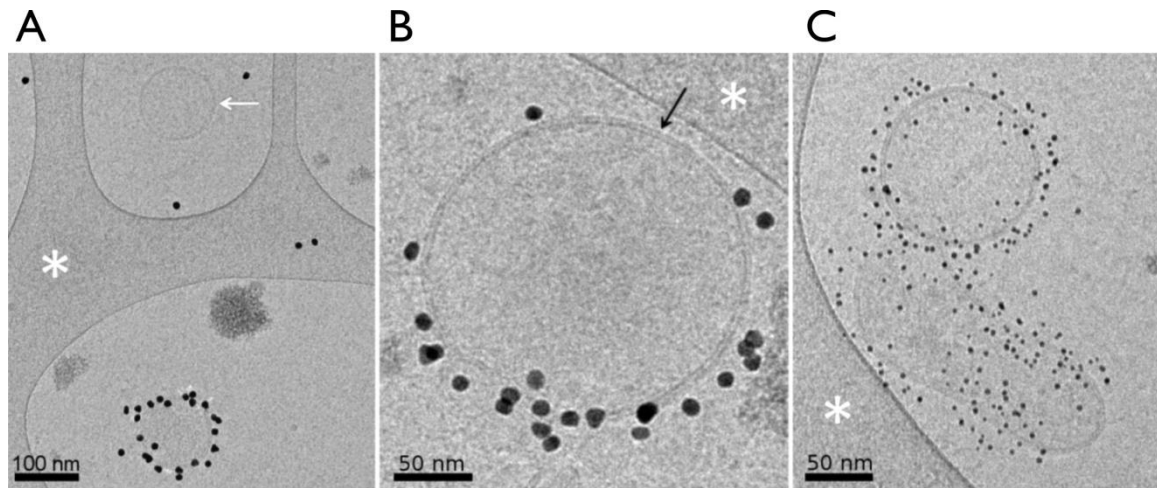


Figure 33 Cryo-EM images of individual EVs from ascites of patients with HGSOC (A), carcinosarcoma (B) or liver cirrhosis (C). The samples were labeled with AV-conjugated gold nanoparticles (10-nm diameter in A and B, 4-nm diameter in C). In A, a non AV-binding EV (white arrow) is seen, next to an AV-labeled EV. The lipid bilayer surrounding EVs is clearly resolved by cryo-EM (black arrow in B). The white asterisks point to areas of the carbon support film. Scale bars: 100 nm in A, 50 nm in B and C. Figures reprinted from [1].

As mentioned before and visible in Figure 31B and Figure 32A MMP9 was present in AV-EVs in different forms. One of them was the neutrophil-derived complex of MMP9 with NGAL, which was also identified in AV-binding EVs secreted by activated neutrophils [199]. This prompted us to examine the cellular composition of the ascitic fluid with special regard to the presence of neutrophils that might be the source of these PS-exposing and MMP9 carrying vesicles. Neutrophil granulocytes, lymphocytes, cancer cells and mesothelial cells were isolated from ascites by centrifugation, examined microscopically, and the abundance of each cell type was determined. When comparing MMP9 levels in the AV-binding EVs of each patient with the different cell amounts, there was no correlation between neutrophils, lymphocytes or mesothelial cells and the MMP9 levels observable (Figure 34B-D and Figure 35B-D). The comparison of MMP9 levels and the cancer cell amount including all patients resulted in a significant but weak correlation (Spearman $R=0.66$ for zymogram results (Figure 34A), Spearman $R=0.56$ for ELISA results (Figure 35A)), but this only resembled the already known difference between non cancer and cancer samples, i.e. absence of tumor cells and MMP9 carrying AV-EVs in non cancer and presence of both in cancer samples. To answer the question whether a higher number of cancer cells in the ascitic fluid correlates with higher levels of MMP9 in AV-EVs, we analyzed only the cancer patient samples for their correlation and found no significant correlation (Figure 36). Consequently the presence and increased concentration of MMP9 in AV-binding EVs in ascites of HGSOC patients could not be explained simply by the specific secretion of the EVs by a certain cell type present at higher levels in the ascites.

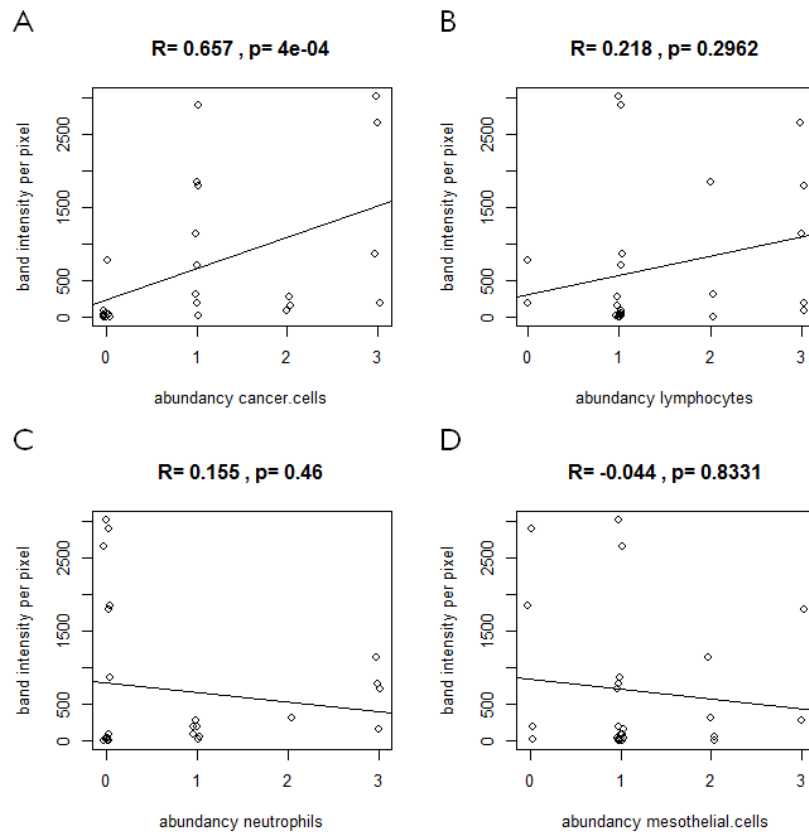


Figure 34 Correlation graphs of MMP9 levels in AV-EVs compared to the abundance of different cell types (A cancer cells, B lymphocytes, C neutrophils, D mesothelial cells) in ascites of all cancer and non cancer patients. MMP9 levels in AV-EVs were measured by band intensity analysis of zymography. The correlations were calculated with the Spearman method; Spearman R values and p-values are indicated on top of each plot. For better illustration of the correlations a line of a linear regression model is displayed in each plot.

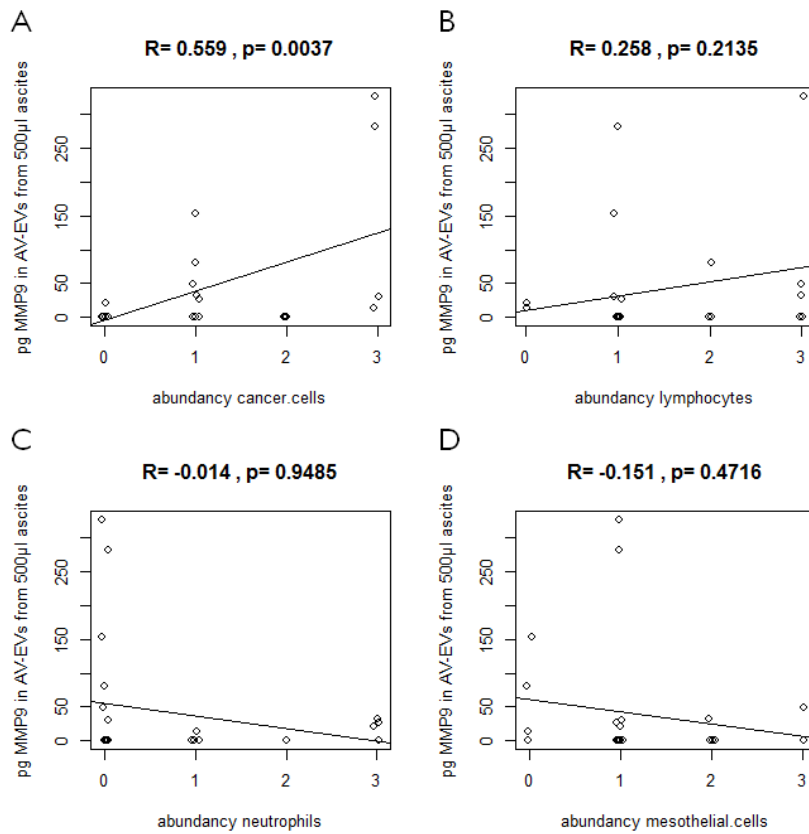


Figure 35 Correlation graphs of MMP9 levels in AV-EVs compared to the abundance of different cell types (A cancer cells, B lymphocytes, C neutrophils, D mesothelial cells) in ascites of all cancer and non cancer patients. MMP9 levels in AV-EVs were measured by ELISA. The correlations were calculated with the Spearman method; Spearman R values and p-values are indicated on top of each plot. For better illustration of the correlations a line of a linear regression model is displayed in each plot.

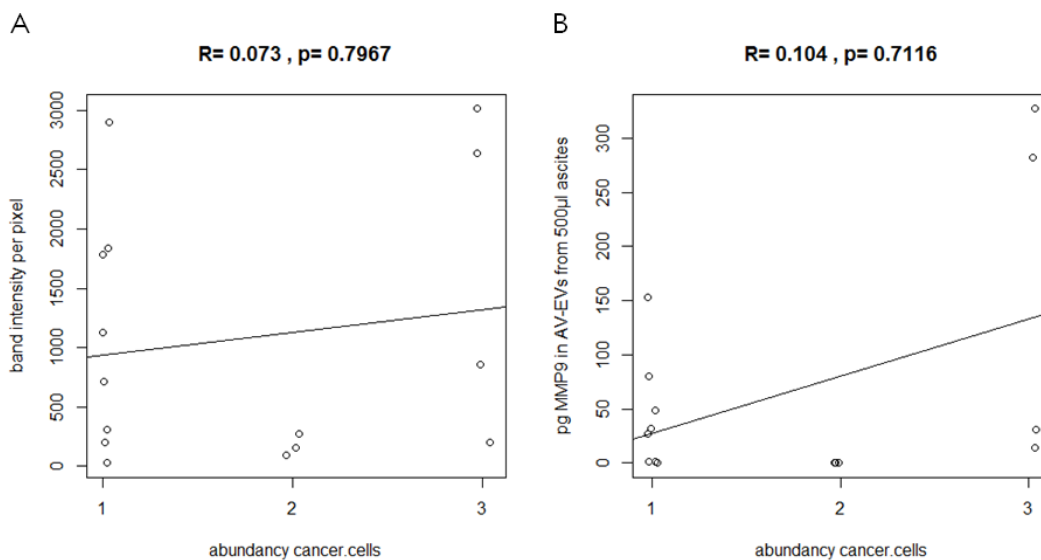


Figure 36 Correlation graphs of MMP9 levels in AV-EVs compared to the abundance of cancer cells in ascites of ovarian cancer patients. MMP9 levels in AV-EVs were measured by band intensity analysis of zymography (A) or ELISA (B). The correlations were calculated with the Spearman method; Spearman R values and p-values are indicated on top of each plot. For better illustration of the correlations a line of a linear regression model is displayed in each plot.

The cellular source of secreted MMP9 and thus also of MMP9 loaded to EVs in ovarian cancer was discussed already in plenty of studies. Different materials, including cell lines and ovarian tissues, ascites, serum and plasma from healthy volunteers or patients with benign or malignant ovarian lesions, were assessed and generally MMP9 levels were increased in malignant ovarian cancer samples compared to non-cancerous samples [196, 200-205]. Additionally each study reported differences in MMP9 expression depending on the course of disease [196, 203], the cell type (tumor cells vs stromal cells) [201], the histological type of the ovarian cancer [202], or the patient survival [204], to name just a few parameters that have been examined. However, even with this plethora of studies and results it is not clear yet where and when MMP9 is produced in the course of ovarian cancer, because many of the results are at least partially contradictory. Focusing on EVs carrying MMP9 in association with ovarian cancer only a few studies have been carried out that isolated EVs from ascites of ovarian cancer patients and identified MMP9 as their cargo [105, 106, 206]. All of these studies used ultracentrifugation based methods for isolation resulting in a bulk of different kinds of vesicles, thus the discrimination of different EV populations and conclusions about cellular sources were impossible. As ascites is a very complex body fluid containing components from different cellular sources (i.a. tumor cells, tumor associated stromal and immune cells [180]) we can also just speculate on the origin of the AV-binding EVs that carry MMP9. The finding of MMP9 in vesicles derived from an ovarian cancer cell line by Dolo et al. [104] suggests that such EVs could derive from the cancer cells. In contrast to this the already mentioned findings of Gasser et al. [199] showed the release of MMP9 carrying EVs by neutrophils, which are known to be present in the ovarian cancer environment and enhance metastatic potential through induction of epithelial to mesenchymal transition of cancer cells [207]. Even though it is not possible yet to discriminate EVs according to their origin and therefore get a clearer picture, the improvement of isolation techniques and the development of single vesicle analysis methods will enable researchers to address these open questions in the near future.

In order to exclude other clinical parameters that might influence EV presence in ascites, the MMP9 levels in AV-EVs were also compared to patient characteristics. No correlations between age, stage or grade of disease with the MMP9 content of isolated AV-binding EVs were observed (data not shown). Thus, only the diagnosis of ovarian cancer and in particular of HGSOc was decisive for the presence of PS-exposing EVs carrying MMP9 in ascitic fluid. Possible functions of these EVs could lead to an explanation why these MMP9 carrying EVs were found in HGSOc patients. Al Thawadi et al. [103] studied EVs from ovarian cancer cell lines and their effect on endothelial cells. They found that ovarian cancer cell derived EVs had a pro-angiogenic function and lead to the increase of endothelial cell proliferation, migration and tube formation

via the activation of β -catenin. This activation process required on the one hand the uptake of the EVs into the cells via the interaction of PS exposed on the vesicles and integrins on the cell surface. On the other hand the pro-angiogenic effect via β -catenin activation was dependent on MMPs carried by the EVs that cleaved E-cadherin on the surface of the endothelial cells and therefore triggered the intracellular release of β -catenin. Another possible function for ovarian cancer derived EVs was described by Graves et al. [105] who reported that EVs isolated from ascites of ovarian cancer patients promoted cell invasiveness in ovarian cancer cell lines via MMPs. Additionally MMP9 is generally known to have cancer-promoting effects in many different types of cancers [198, 208]. Based on these findings pro-angiogenic and pro-metastatic functions could be attributed to the AV-binding and MMP9 carrying EVs identified in this study. Since HGSOC is the deadliest and most aggressive type of ovarian cancer [209], the presence of EVs with cancer promoting effects in ascites of patients with HGSOC is logical. Furthermore the proposed pro-cancerous functions of these EVs could make them a potential target for the development of new therapies.

As mentioned above, one of the greatest obstacles for the usage of EVs as biomarker in clinical applications is the lack of isolation and analysis methods that reliably and reproducibly purify and identify distinct populations of EVs, because contaminants like protein aggregates or lipoproteins, that are abundantly present in body fluids, are often co-purified and cannot be discriminated from EVs. Specific isolation of EVs based on their surface proteins could overcome some problems due to contamination, but presently too little is known on vesicle composition and markers of specific vesicle populations to purify individual populations and determine their origin or function. Consequently, the identification of distinct and clearly defined vesicle populations that harbor potential biomarkers is required for a successful clinical application. The AV-binding and MMP9 carrying EVs that were detected in HGSOC patients are candidates for utilization as ovarian cancer marker, because this EV population is defined by a combination of lipid and protein markers, which enhances the ability of specific purification and detection from complex body fluids. Even though these EVs were identified in ascites, they have potential as circulating marker, because of the constant exchange of fluids and molecules between the peritoneal cavity, the lymphatic system and the blood stream [210, 211].

3.3 Conclusions

In summary, we demonstrated here a proof of concept that using membrane lipid-binding ligands to isolate different EV subpopulations from ascites fluid is an efficient method for biomarker discovery as it will enhance the signal-to-noise ratio. Specifically, by using ascites from small patient groups with HGSOC or cirrhosis, and a small set of cancer-associated proteins, we

observed that EV-associated MMP9 in HGSOC is predominantly localized in AV-binding EVs and that both CD59 and MMP9 in AV-binding EVs are candidate biomarkers for HGSOC. Without fractionating the EVs into subpopulations, MMP9 was unlikely to be identified as a candidate HGSOC biomarker as the high level of MMP9 in AV-EVs would have been obscured by the lack of MMP9 in the other EVs. The utility of CD59 and MM9 in AV-binding EVs as ovarian cancer biomarker will have to be further evaluated in large patient cohort studies for their specificity and sensitivity.

4 Magnetic Nanoparticle-enhanced Grating Coupled SPR for EV Detection

This chapter presents data that were published in [2] and uses text and figures from this publication.

The analysis of extracellular vesicles (EVs) gains increasing interest in life sciences and medical research due to their multiple functions in cell communication in healthy but also in pathological state. EVs hold great potential in many clinical applications spanning from diagnostics and disease monitoring to the use for therapeutics and even as vaccines. However, this potential is hampered by the lack of specific, sensitive and reliable methods for their analysis. Currently used methods typically stem from those used in micro- or molecular biology for the analysis of cells. Hence, one of the biggest challenges for these methods is the small size of the lipid vesicles. For instance, a well-established method for cell analysis - flow cytometry - is only able to detect lipid vesicles bigger than ~ 200 nm which translates to the fact that the majority of EVs is actually not detected [59, 61, 62]. Another method employed for the analysis of small particles is nanoparticle tracking analysis (NTA). Similar to flow cytometry, NTA also relies on the light scattering properties of particles but allows for the detection of smaller particles because of the addition of a microscopy unit. However, due to the EVs' refractive index being very close to that of surrounding medium and their small size, they scatter light very weakly, which results in low signal-to-noise ratios. Nevertheless, it should be noted that these methods are under constant development and dedicated flow cytometers with technical adjustments for EV analysis or the use of fluorescence detection have greatly improved their sensitivity for small EVs [62, 63, 212, 213].

Complementary to flow cytometry and NTA that can analyze EVs in a solution, optical biosensors have been pursued for detection and observation of EVs that are captured at surfaces. Among these, surface plasmon resonance (SPR) based techniques are suitable for the optical probing of affinity binding of EVs by the tightly confined field of surface plasmons (SPs) travelling along metallic surfaces [4]. One of the first SPR biosensors employed a SPR imaging platform for parallelized detection of EVs on antibody microarrays [164]. Spots of antibodies specific for a selected set of proteins carried by EVs were used for screening of EV samples as potential cancer biomarkers. Another high throughput platform was presented by Im et al., who used a plasmonic chip with arrays of plasmonic nanoholes [121]. Antibodies specific for the tetraspanin protein CD63 [which can be found on EVs [16]] were used for sensitive detection of EVs, and a limit of detection of 670 aM was reported for a sandwich assay amplified by metallic

nanoparticles. By incorporation of several microfluidic channels, the sensor could be used to analyze multiple markers or samples in parallel. The plasmonic biosensor was demonstrated to offer superior sensitivity compared to regular heterogeneous assays based on enzyme-linked immunoassays (ELISA) and western blot.

Höök's group focused on quantitative direct measurements of EVs by a SPR biosensor [167]. The sensor surface was functionalized with an antibody against CD63 and the analysis of diffusion-limited binding kinetics enabled determining the concentration of EVs in a sample in the pM range. The performance of such a SPR biosensor was improved by probing the bound EVs by SPs resonantly excited at two different wavelengths [168]. With this platform it was possible to determine the EV concentration with a relative error of only 10 % compared to the earlier 50 %.

In general, all currently pursued EV SPR biosensors rely on diffusion-limited binding kinetics on the sensor surface. As EVs are objects with a size around 100 nm, their diffusion is slow and limits the yield in the collection of analyte on the sensor surface. Grating-coupled SPR with magnetic nanoparticle (MNP)-driven collection of protein analytes on the sensor surface was demonstrated to overcome such limitation for small protein molecules [158], and in particular for detection of large, slowly diffusing bacterial pathogens [159]. Both these works relied on the measurements of angular reflectivity spectra, which complicates the multiplexing of the assay and requires rotating of the sample. This paper presents a sensor that utilizes wavelength interrogation of SPR which provides the advantage of simpler operation. It is applied for the analysis of EVs exhibiting a diameter of about 100 nm with an enhanced sensor response governed by a combination of an increased mass transfer rate and amplified refractive index changes associated with analyte affinity binding. EVs are extracted and delivered to the sensor surface by their binding to MNPs via lipid-binding proteins, Annexin V (AV) and Cholera toxin B chain (CTB), and they are affinity captured by antibodies against CD81 at the SPR grating sensor surface.

4.1 Material and Methods

4.1.1 Materials

Polydimethylsiloxane (PDMS) elastomer Sylgard 184 was obtained from Dow Corning and the UV-curable polymer Amonil MMS 10 was from AMO GmbH. Dithiolalkane aromatic PEG3 with hydroxyl endgroup (SPT-0013) and the dithiolalkane aromatic PEG6 with carboxyl endgroup (SPT0014A6) were purchased from SensoPath Technologies. N-(3-Dimethylaminopropyl)-N'-ethylcarbodiimide hydrochloride (EDC), N-Hydroxysuccinimide

(NHS), ethanolamine and ethylenglycol, as well as acetic acid and sodiumacetate for the preparation of acetate buffer were bought from Sigma-Aldrich. The mouse monoclonal antibody against human CD81 (1.3.3.22) and the HRP-conjugated goat anti-mouse secondary antibody (sc-2031) were purchased from Santacruz Biotechnology. Phosphate buffered saline (PBS) at a pH of 7.4 from Merck was used for the functionalization. PBS with addition of 0.05% Tween 20 (Sigma-Aldrich) only (PBST) or with 0.05% Tween 20 and 0.1% bovine serum albumine (Life Technologies) (PBSTB) were used as running buffers for the MNP-enhanced SPR measurements. The ligands CTB (SBL Vaccin AB) and AV (Biovision) for pre-incubation with EVs were biotinylated with Sulfo-NHS Biotin (Thermo Fisher Scientific). MNPs with a diameter of 200 nm and coated with streptavidin (fluidMAG-Streptavidin) were purchased from Chemicell. Prior to the use, streptavidin coated MNPs were washed twice with PBSTB by applying a magnetic field for separation of the MNPs from the solution. For the CD81-ELISA Dynabeads M280 Streptavidin and Amplex Red Substrate were purchased from Thermo Fisher Scientific.

4.1.2 Biological samples and EV characterization

We used EVs derived from mesenchymal stem cells (MSCs) that have been studied already in great detail [49, 214, 215]. EVs were obtained from the conditioned medium of MSCs. The cell cultivation and EV isolation were pursued as described earlier [49]. In short, conditioned medium was harvested after 3 days of cell growth and concentrated 100x for EVs by tangential flow filtration. Sample aliquots were stored at -80 °C. The total protein concentration was assessed by Coomassie Plus (Bradford) Assay (Thermo Fisher Scientific) and used as a surrogate for EV concentration. In addition the particle number in the EV samples was measured by NTA using the ZetaView instrument (ParticleMetrix) according to manufacturer's instructions. In brief, the EVs were diluted to a concentration of 0.5 µg/ml with 0.22µm filtered PBS and analyzed. The instrument setting were as follows: the sensitivity was set to 90, the shutter to 30, maximal size was set to 1000 and minimal size to 5, minimal brightness was set to 25, and measurement mode was size distribution at 1 cycle and 11 positions. After the measurement, the raw data was analyzed with the software ZetaView 8.03.08.

The EV samples were further characterized for their CD81 concentration in the CTB- and AV-binding subpopulation by an ELISA on MNPs, that was performed as described earlier [49]. Briefly 0.1 or 1 µg of MSC-derived EVs were incubated with 250 ng biotinylated CTB or AV, respectively. After 30 min incubation 30 µl of washed Dynabeads M280 Streptavidin were added and incubated for 30 min again. The MNPs with bound EVs were then washed twice and incubated with anti-CD81 antibodies, washed again and incubated with HRP-conjugated goat

anti-mouse secondary antibodies. The HRP activity was determined using Amplex Red Substrate as per manufacturer's instructions. A biotinylated-CD81 peptide was used as standard. The concentration is given as ng of CD81 per μg total protein of the MSC-EV sample used for the EV coupling to the MNPs.

4.1.3 Preparation of GC-SPR sensor chips

A linear relief sinusoidal grating was prepared by UV laser interference lithography and their multiple copies were made by soft lithography as described before [161]. Briefly, a structure with a period of $\Lambda=430$ nm and modulation depth of $d=60$ nm was casted to PDMS, which was cured for 3 days at room temperature before it was used as a working stamp. Cleaned BK7 glass substrates were coated with the UV-curable polymer Amonil MMS 10 by spin-coating at 3000 rpm for 120 s. Then, the PDMS working stamp was placed on the top of the Amonil surface and irradiated by UV light (UV lamp Bio-Link 365, Vilber Lourmat). Finally, the PDMS stamp was detached from the cured Amonil MMS 10 leaving a copy of the master structure on the glass substrate. The copied gratings were subsequently coated with 4 nm of chromium and 100 nm of gold by vacuum thermal evaporation (HHV AUTO 306 from HHV LTD) in vacuum better than 10^{-6} mBar.

4.1.4 Optical system

A flow-cell was clamped against the grating sensor chip and it consisted of a polished glass substrate with drilled input and output ports and a thin PDMS gasket. The volume of the flow-cell was of about $10 \mu\text{L}$ and analyzed liquid samples were flowed through by using the peristaltic pump REGLO Digital MS-4/8 (ISMATEC). The sensing spot in the flow-cell was illuminated with a polychromatic beam with a diameter of about 5 mm. The beam was emitted from a halogen bulb light-source (LSH102 from LOT-Oriel) and coupled to a multimode optical fiber (M25L02 from Thorlabs). The beam at the fiber output was collimated by using a lens ($f=30$ mm from Melles Griot) and subsequently passed through a polarizer and a cube beam-splitter (CM1-BS013 from Thorlabs). Then, the beam was made normally incident at the gold grating surface through the flow-cell and the reflected beam was separated at the beam splitter, coupled to a multimode optical fiber (M26L02 from Thorlabs) by using a collimator (F810SMA-635 from Thorlabs), and delivered to a spectrometer (HR4000 from Ocean Optics). The wavelength spectrum of the reflected light was measured for transversally magnetic polarization (TM) and normalized with that acquired for transversally electric polarization (TE). The normalized reflectivity TM/TE spectra with a SPR dip located at a wavelength of about 640 nm were processed by a dedicated software developed in-house by using LabView (National Instruments).

In order to track the SPR wavelength in time, the sequentially acquired spectra were fitted in a selected wavelength range with a polynomial function. The SPR wavelength λ_{SPR} was determined as the minimum of the fitted analytical function with a repetition time of about 5 sec. On the opposite side of the flow cell, a cylindrical permanent magnet (NdFeB with diameter of 10 mm and length of 35 mm from Neotexx) was approached to the grating sensor chip in order to attract MNPs at its surface. The optical system and assay setup including sample pre-incubation and details on the sensor surface architecture for affinity binding of the analyte are illustrated in Figure 37.

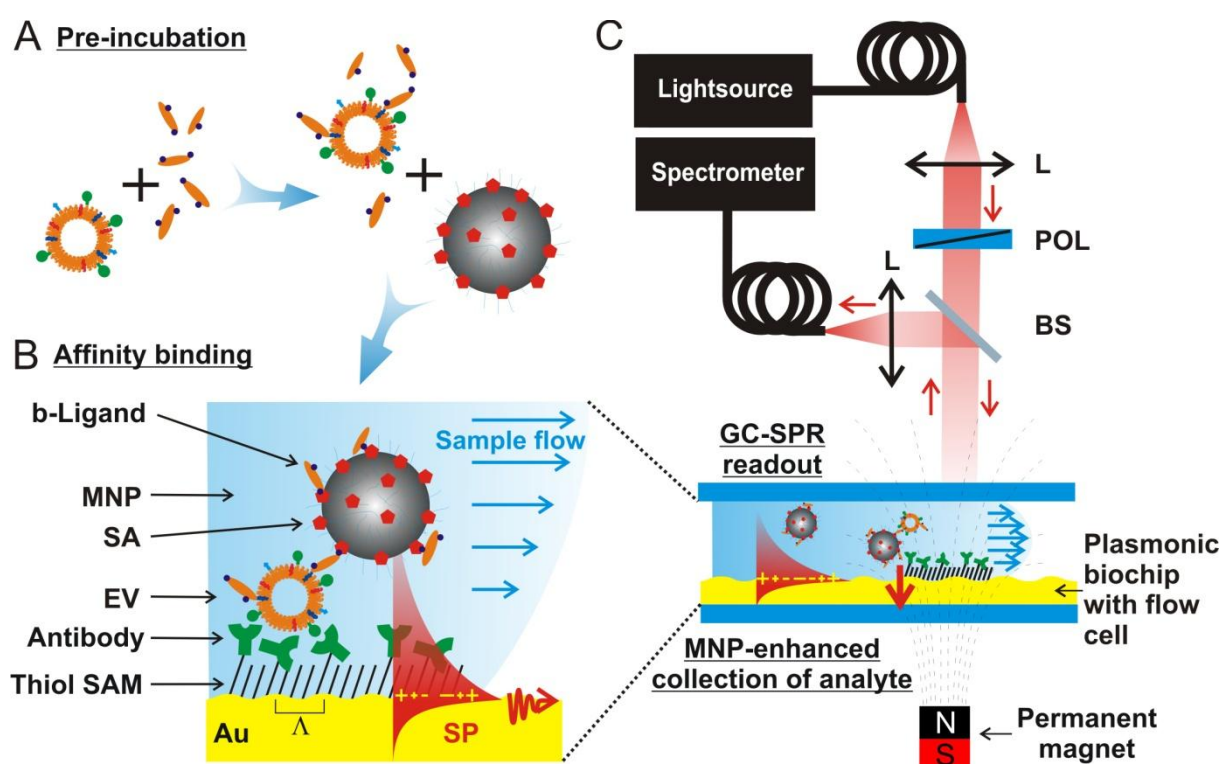


Figure 37 Schematics of the GC-SPR sensor system and developed assay. (A) shows the pre-incubation of extracellular vesicles (EVs) with the biotinylated lipid-binding ligand (b-ligand) and streptavidin (SA) coated magnetic nanoparticles (MNPs). (B) illustrates the surface chemistry used at the gold chip sensor surface for affinity binding of the target analyte. C depicts the optical setup of the MNP-enhanced GC-SPR assay and the system that allows the pulling of the target analyte to the sensor surface. SAM = thiol self assembled monolayer, Au = gold, SP = surface plasmon, L = lens, POL = polarizer, BS = beam splitter, GC-SPR = grating coupled surface plasmon resonance.

Figure reprinted from [2].

4.1.5 Functionalization of GC-SPR sensor chips

The gold-coated sensor chips were immersed in ethanol with thiols dissolved at 1 mM concentration in order to form a self-assembled monolayer (SAM). The solution contained a mixture of dithiol-PEG6 with carboxyl end group for later surface functionalization and dithiol-PEG3 with hydroxyl end group for passivation. The molar ratio of carboxyl to hydroxyl-

terminated thiols was 1:9. After the overnight incubation, the sensor chips were thoroughly rinsed with ethanol, dried immediately in a stream of air and stored under argon atmosphere. The functionalization with a specific antibody against CD81 was performed *in situ* by amine coupling according to standard protocols. All solutions were flowed over the sensor surface at a constant speed of 30 $\mu\text{l}/\text{min}$. As a first step PBS was rinsed through the flow cell to reach a stable baseline in the sensor response $\lambda_{\text{SPR}}(t)$. Then, PBS spiked with 2 % ethylenglycol was flowed through, producing a refractive index change of 2×10^{-3} refractive index units (2 mRIU) in order to calibrate the sensor. Afterwards, sodium acetate buffer with a pH-value of 5 was flowed and the carboxyl groups on the surface were subsequently activated by the incubation with EDC and NHS for 15 min at concentrations of 0.4 M and 0.2 M, respectively. Then, the surface was rinsed with sodium acetate buffer and the specific antibody against CD81, diluted in the same buffer at a concentration of 25 $\mu\text{g}/\text{ml}$, was flowed for 10 minutes. Finally, ethanolamine at 1 M and pH of 8.5 was used to inactivate all remaining carboxyl groups before the buffer was changed again to PBS.

4.1.6 Detection assay

EVs were diluted in a total of 100 μl PBS and each sample was spiked with 250 ng of biotinylated CTB or AV and incubated for 30 min at room temperature on a shaker. Calcium containing buffer was added to the incubation mix when incubated with AV at a final calcium concentration of 2 mM. Then, 10 μg of washed streptavidin coated MNPs were added to the EV-ligand-mix and incubated for 30 min at the same conditions as before to let EVs attach to the MNPs via the biotinylated lipid-binding proteins. Afterwards, the MNPs with bound EVs were collected from the sample and washed twice with PBSTB in order to remove any unbound EVs and other molecules. Finally, the MNPs were resuspended in 1 ml of PBSTB and analyzed with the GC-SPR biosensor. The amount of EVs is further quantified as amount of total protein in starting material of EVs diluted in 1 ml after the isolation procedure (ranging from 0.76 to 3.0 $\mu\text{g}/\text{ml}$).

Each sample was flowed across the sensor surface for 10 min with the magnetic field gradient applied by placing the permanent magnet in a distance of 5 mm from the sensor surface. The sensor surface was probed by resonantly excited SPs before and during collecting the MNPs and the SPR wavelength λ_{SPR} was tracked in time. Then the magnetic field was switched off by removing the magnet and the sensor surface was rinsed with PBSTB until a stable baseline in $\lambda_{\text{SPR}}(t)$ was reached again. Since the flow-cell was oriented in a vertical direction and the flow of liquid samples was directed upwards, the flow-cell had to be flushed shortly with PBSTB at high speed to remove all unspecifically attached MNPs and their aggregates.

The SPR signal $\lambda_{\text{SPR}}(t)$ was processed in the software Origin Pro. First the initial baseline was set to zero and it was normalized to the SPR response to a bulk refractive index change due to the spiking of PBS with 2 % ethylenglycol. SPR wavelength variations were converted to the unit of mRIU. The response to the affinity binding of MNP-bound EVs was determined as the sensor response difference between the baseline before the injection of a sample and after washing of the sensor surface with the magnetic field gradient switched off.

4.1.7 Observation of sensor chips

Atomic force microscopy (AFM) and scanning electron microscopy (SEM) were used to examine the biosensor surface before and after binding of MNP-bound EVs. For this purpose the functionalized sensor surface was exposed to either MNPs incubated only with the lipid-binding ligand as control or with MNPs incubated with ligand and EVs of different concentration. The assay was performed as described above, but in the end the flow cell was rinsed with water and the sensor surface was dried in a stream of air immediately after removal of the flow cell.

To get a detailed height information of the MNPs on the grating structure, the AFM system Molecular Imaging PicoPlus was employed, which is a multipurpose, high resolution scanning probe microscope and was operated in tapping mode [216]. The SEM SUPRA 40 microscope by Zeiss was employed to study the surface topography, which generates images of a sample by scanning it with a focused beam of electrons [217].

4.2 Results and Discussion

The resonant coupling to SPs on the gold diffraction grating is manifested as a narrow dip in the measured wavelength reflectivity spectrum. As can be seen in Figure 38A, this dip is centered at a wavelength of $\lambda_{\text{SPR}} \sim 637$ nm when PBS is flowed over the gold surface covered with a mixed thiol SAM. The excitation of SPs is due to the first order diffraction coupling by the normally incident beam, which occurs at a wavelength where the phase matching condition $\lambda_{\text{SPR}} = \Lambda \cdot N_{\text{SP}}$ is fulfilled. The N_{SP} stands for the effective refractive index of SPs travelling along the gold surface in contact with the aqueous sample. The resonant wavelength λ_{SPR} shifts to longer wavelengths when the refractive index on the gold sensor surface is increased, e.g. due to the binding of biomolecules or EVs. From the perturbation theory follows that such variations can be approximated by the following expression [218], which holds, if the thickness of the layer in which the biomolecules bind is much smaller than the wavelength λ_{SPR} :

$$\delta\lambda_{\text{SPR}} = S_b \frac{4\pi}{\lambda_{\text{SPR}}} \sqrt{N_{\text{SP}}^2 - n_b^2} \cdot \Gamma \frac{\partial n}{\partial c}, \quad (1)$$

where S_b is the signal sensitivity to variations of the bulk refractive index n_b , Γ is the surface mass density of bound biomolecules, and constant $\partial n/\partial c=0.2 \text{ mm}^3 \text{ mg}^{-1}$ for the majority of organic polymers [219]. The PBS bulk refractive index of $n_b=1.34$ was determined from the measured reflectivity spectrum which shows a sharp feature at the critical wavelength $\lambda_c=578 \text{ nm}$, see Figure 38A. This feature occurs at $\lambda_c=\Lambda \cdot n_b$ where the first diffraction order falls after the horizon. Similarly, the effective refractive index of SPs was determined as $N_{\text{SP}}=1.49$. The bulk refractive index sensitivity S_b was obtained from the time kinetics measurements presented in Figure 38B when the PBS spiked with 2% ethylenglycol was flown across the sensor surface. This composition induces a refractive index increase of $\delta n_b=2 \cdot 10^{-3}$ refractive index units (RIU). From the measured corresponding shift $\delta \lambda_{\text{SPR}}=0.85 \text{ nm}$ the sensitivity was obtained as $S_b=\delta \lambda_{\text{SPR}}/\delta n_b=425 \text{ nm RIU}^{-1}$. This value is similar to other GC-SPR sensors operated at a similar wavelength [218]. It is worth of noting that the developed sensor system allowed measuring the SPR wavelength with the standard deviation of $\sigma(\delta \lambda) \sim 9 \cdot 10^{-3} \text{ nm}$ which corresponds to the resolution of $2 \cdot 10^{-5} \text{ RIU}$.

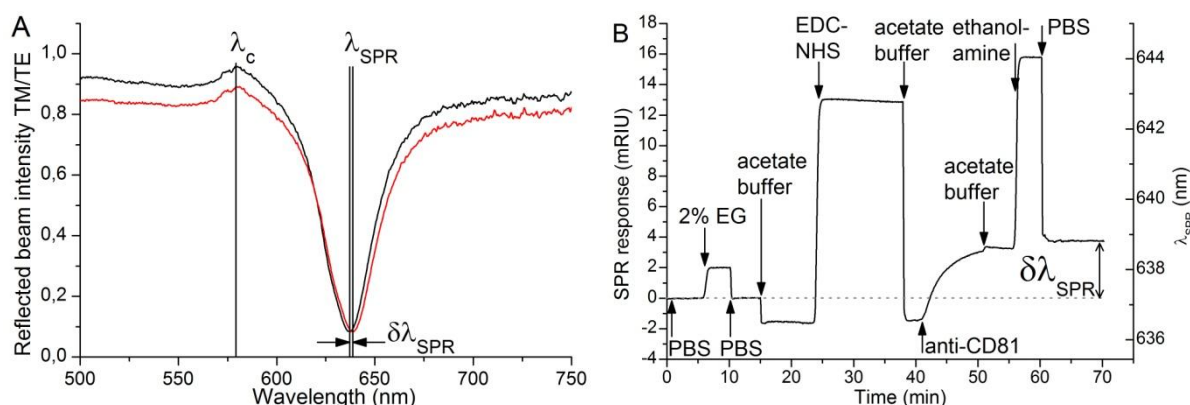


Figure 38 Wavelength reflectivity spectra (A) and SPR sensorgram (B) for a representative example of immobilizing antibodies against CD81 onto the grating-coupled SPR sensor chip. The black spectrum in (A) is taken at the PBS baseline at the beginning of the measurement and the red spectrum is acquired at the end of the measurement after the binding of the anti-CD81. $\delta \lambda_{\text{SPR}}$ refers to the SPR response change caused by antibody binding to the surface. mRIU = milli refractive index unit, PBS = phosphate buffered saline, EG = ethylenglycol. Figure reprinted from [2].

4.2.1 Modification of the sensor chip with ligands

The sensor surface was functionalized with antibodies specific to the transmembrane protein CD81, which is a known marker for EVs in general [16] and for the used MSC-derived EVs in particular [49]. In order to quantify the amount of antibody on the sensor surface, the immobilization was performed *in situ* and the attachment of molecules to the surface was monitored with GC-SPR. A typical sensorgram in Figure 38B shows a strong shift in $\delta \lambda_{\text{SPR}}$ after injecting EDC/NHS at time $t=23 \text{ min}$ due to the bulk refractive index change. After the rinsing

with acetate buffer at $t=38$ min, the SPR wavelength λ_{SPR} decreases to the original value. Then, anti-CD81 was flowed over the surface with activated carboxyl groups between $t=40$ and 50 min. The covalent binding of the antibody leads to a gradual shift in λ_{SPR} due to the increased surface mass density Γ . After the rinsing and passivating of unreacted carboxyl groups with ethanolamine at $t=60$ min, the difference in the SPR wavelength of $\delta\lambda_{\text{SPR}}=1.58$ nm was measured. By using equation (1), this shift can be translated to the surface mass density of immobilized antibody of $\Gamma\sim 1.5$ ng mm^{-2} which is close to a fully packed monolayer [220].

4.2.2 GC-SPR readout of MNP-enhanced EV assay

The herein used EVs are produced and isolated continuously from conditioned cell culture medium by tangential flow filtration and tested for total protein concentration and CD81 content in EV subpopulations by Bradford assay and ELISA, respectively. Since all cells secrete many different kinds of vesicles summarized as EVs, also in the MSC-EV sample several different vesicle populations could be isolated based on their binding to proteins with specific affinity to different lipids [49]. These EV populations are characterized by their distinct lipid and protein profile, which was used to test and develop the here presented EV analysis method.

Firstly, direct GC-SPR detection of all MSC-derived EVs without the isolation of subpopulations and binding to MNPs was tested. Samples with PBST used as running buffer and MSC-EVs diluted 100-, 1,000-, and 10,000-fold (resulting in a total protein concentration of 15, 1.5, and 0.15 $\mu\text{g}/\text{ml}$) were subsequently flowed over the sensor surface with anti-CD81 antibody. As seen in the inset of Figure 39A, the SPR signal was monitored in time and did not show a measurable direct response to the EV binding.

In order to enhance the GC-SPR sensor response, MNPs were employed for the more efficient collection of specific EV subpopulations at the sensor surface and to increase the binding-induced surface mass density Γ . In a pre-incubation step EVs were bound to MNPs and consecutively flowed across the sensor surface, while a magnetic field gradient was applied (see Figure 37). Due to the magnetic force experienced by the MNPs the bound EVs were accumulated on top of the functionalized surface. Afterwards, the magnetic field gradient was switched off by removing of the permanent magnet. Then, running buffer was rinsed and only affinity captured MNPs stayed on the surface that were bound via the CD81 present on the EVs' surface. It is worth of noting that without applying the magnetic field no measurable response was observed when flowing MNPs with or without bound EVs across the sensor surface.

A typical SPR sensorgram for the MNP-enhanced EV assay is presented in Figure 39A. Each measurement cycle consisted of a 10 min incubation step of MNPs with application of a

magnetic field, followed by 20 min rinsing with buffer after removal of the magnetic force, and flushing the flow cell with running buffer at maximum flow rate to remove all weakly bound particle aggregates. To ensure that the MNPs were not unspecifically bound to the antibodies or irreversibly sticking to the sensor surface, control MNPs, which were incubated only with the biotinylated lipid-binding ligands (b-ligand, i.e. CTB or AV) without EVs, were rinsed across the surface as the first measurement cycle in each experiment. Only if the SPR signal after the rinsing was equal to the baseline before the MNP incubation, indicating complete removal of MNPs from the sensor surface, the measurement was proceeded by incubation with MNPs pre-exposed to ligands and EVs.

As seen in Figure 39, the attraction of MNPs not incubated with EVs at the sensor surface is manifested by a decrease of the λ_{SPR} between t1 and t2 when the magnetic field gradient was applied. Interestingly, after the magnetic field is switched off at t2 the λ_{SPR} rapidly increases and then gradually shifts to the original baseline. Since the MNPs consist of a magnetite core, they strongly absorb light [221]. The associated decrease in reflected light intensity is more pronounced at shorter wavelengths compared to longer ones and lead to a flatter, broader and tilted SPR dip in the reflectivity spectrum (compare reflectivity spectra at t1 and t2 in Figure 39B). Particularly, the increasing absorption with decreasing wavelength can be ascribed to a decrease of the determined λ_{SPR} . After the magnetic field is switched off, the majority of accumulated MNPs is quickly expelled from the sensor chip which is accompanied by an increase in the overall reflectivity signal and λ_{SPR} . The afterwards gradual decrease of the λ_{SPR} can be ascribed to the slow release of unspecifically adsorbed MNPs from the surface. When the same detection cycle is performed for a sample where MNPs are incubated with EVs, the sensor response differs (see Figure 39A, time t3-t5). Firstly, a λ_{SPR} increase is observed for the phase when MNPs are accumulated at the surface with the magnetic field applied (t3-t4). After the release of the MNPs by switching off the magnetic field, a stronger increase in λ_{SPR} is measured and almost no desorption is apparent. The overall decrease in the intensity of the reflected beam after the incubation with MNP-bound EVs and rinsing with buffer (compare reflectivity spectra at t3 and t5 in Figure 39B) supports the finding that the SPR response change $\delta\lambda_{\text{SPR}}$ is caused by MNPs binding to the surface via the captured EVs rather than free vesicles or proteins. Only if the MNPs do not carry EVs, the intensity of the collected light goes back to its original level after removal of the magnetic field and rinsing (compare reflectivity curves measured at t1 and t3 in Figure 39B).

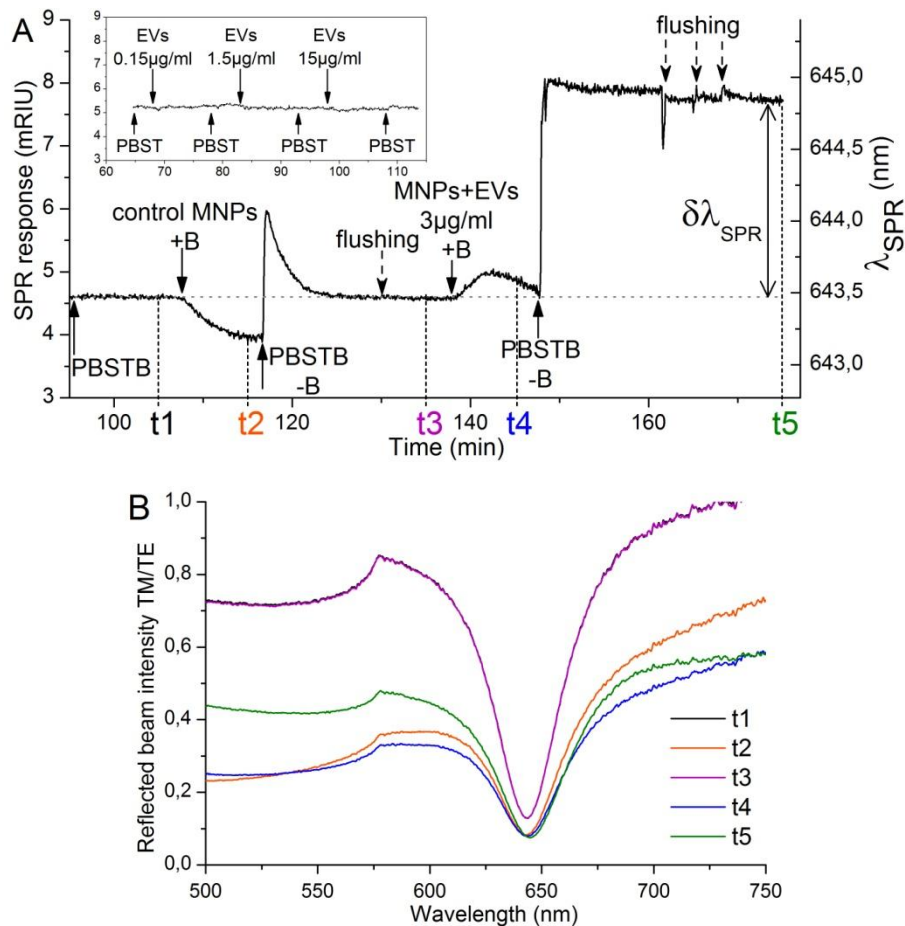


Figure 39 Magnetic nanoparticle (MNP)-enhanced assay measurement. (A) Representative example of a SPR sensorgram for negative control MNPs without extracellular vesicles (EVs) and affinity binding of MNP-captured EVs at the sensor surface functionalized with anti-CD81 antibodies. MNPs were collected on the sensor surface by a magnetic field gradient (indicated as “+B”), after incubation of 10 min the magnetic field was removed (“-B”) and unbound MNPs were washed away. $\delta\lambda_{\text{SPR}}$ refers to the SPR response change caused by MNP-bound EVs binding to the surface. The inset shows the SPR sensorgram for direct EV detection without MNP enhancement, when EVs were diluted to comparable concentrations and exposed to the same surface as in the MNP-enhanced assay. (B) Wavelength reflectivity spectra from different time-points during the MNP-enhanced assay (indicated as t1 to t5 in A). mRIU = milli refractive index units, PBST or PBSTB = phosphate buffered saline with Tween 20 or Tween 20 and bovine serum albumin. Figures reprinted from [2].

The experiment presented in Figure 39 shows that the employment of the MNP-based collection of EVs on the GC-SPR sensor surface allows enhancing the sensor response and observing the affinity binding of EVs at concentrations for which the direct detection assay is not sufficiently sensitive. Furthermore, it has to be taken into consideration that the indicated concentration of MNP-bound EVs is the total protein amount, used as input for the pre-incubation, divided by the volume of buffer used for resuspension of the MNPs after EV isolation. Hence this is the maximum concentration of EVs or protein that could be present on the MNPs. The actual concentration is most likely lower than this, because only a subpopulation of EVs, that is specifically binding to the ligands, is bound to the MNPs. Consequently, the MNP-enhanced

assay can detect EVs at even lower concentrations. In order to quantify the EV samples further, NTA was used and a particle count of $1.1\text{-}1.4 \cdot 10^8$ particles per μg of total protein in the EV sample was determined. From this the total protein concentration in the MNP-bound EV samples can be converted to molar concentrations. Using the MNP-enhanced GC-SPR assay CD81-carrying EVs were detectable down to a concentration of 0.76 ng/ml or 130 fM . Again it has to be emphasized that this is the maximum possible concentration of EVs in the MNP-bound sample, hence the actual concentration that is detectable by these means is most likely lower. Other plasmonic biosensors for EV analysis shows detectable EV concentrations ranging from 670 aM to 2 pM with the similar SPR signal resolution in the μRIU range [121, 164, 167]. As the used materials and methods, including EV source, isolation and characterization, detection assay, and optical setup and instruments, substantially differ, a direct comparison between these methods is rather complex task. In general, the combination of the earlier used methods with the herein presented MNP-capturing and collection of EVs by magnetic forces at the sensor surface could enhance the sensitivity of all of the different approaches.

In order to confirm that the SPR response change is related to the density of MNPs and captured EVs binding to the surface, we performed AFM and SEM of the sensor chips after the SPR assay. The high resolution AFM image of a sensor surface with captured MNPs clearly shows the accumulation of MNPs on top of the grating structure of the biosensor chip (see Figure 40A). As expected, the features bound to the surface exhibit a height of $\sim 200 \text{ nm}$ which agrees with the diameter of the used MNPs. Probably due to the partial aggregation of MNPs and EVs, actual counting of the particles and thus quantification of the density was not possible, but SEM images examining a wider area show clearly that many more particles are bound on the surface exposed to MNP-bound EVs (Figure 40B) compared to the surface exposed to control MNPs (Figure 40C). On the one hand, the aggregation of the MNPs can be due to the binding of several MNPs to multiple binding sites on one molecule, e.g. multiple biotins on the lipid-binding ligands CTB and AV and multiple ligands on each EV. On the other hand, the MNP aggregation can also occur when very strong magnetic forces are applied to the MNPs resulting in irreversible aggregation [222].

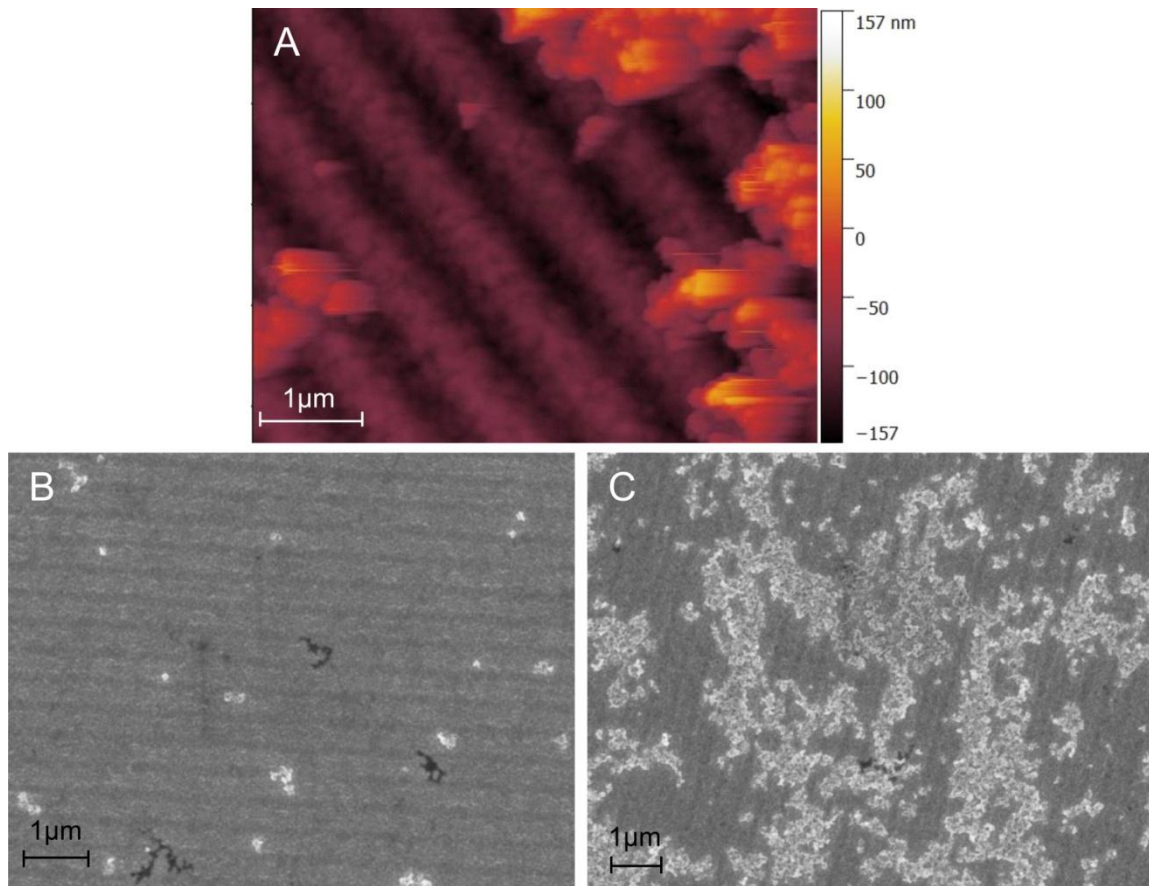


Figure 40 AFM and SEM observation of sensor chips after the magnetic nanoparticle (MNP)-enhanced assay. An AFM image of GC-SPR sensor chip incubated with MNP-bound EVs (EV concentration 3 $\mu\text{g}/\text{ml}$) is shown in A.

The grating structure of the surface with a modulation depth of about 60 nm and the bound MNPs with an approximate height of 200 nm can be seen. SEM images of the same chip as in A and of a sensor chip incubated with MNPs exposed to the lipid-binding ligand only are shown in B and C, respectively. Figures reprinted from [2].

4.2.3 Discrimination between AV- and CTB-binding EVs

To further examine the capabilities of this assay, the binding of different EV populations on the anti-CD81 functionalized sensor surface was investigated. For this purpose different amounts of MSC-derived EVs were incubated either with biotinylated AV or CTB, bound to MNPs, and consecutively analyzed with the MNP-enhanced SPR assay. As illustrated in Figure 41A the CTB-binding EVs were binding to the anti-CD81 antibodies on the sensor surface and the SPR response change increased in a concentration dependent manner (linear regression between 0.76 and 3.0 $\mu\text{g}/\text{ml}$ EVs with Pearson $R = 0.999$). However, for the AV-binding EVs no binding to the surface was observable even at higher concentrations, because they express CD81 only at a very low concentration compared to the CTB-binding EVs [49]. These results prove that the MNP-enhanced assay is capable of specifically detecting different EV populations based on their surface marker expression.

For further quantification and validation of these results, the CD81 concentration in CTB- and AV-binding EVs was determined by ELISA performed on MNPs. As displayed in Figure 41B the CTB-binding EVs carry ~ 8.0 ng of CD81 per μg of total protein of the EV sample used for the binding to the MNPs. The CD81 content of AV-binding EVs, in contrary, is barely detectable at ~ 0.2 ng per μg total protein of EVs. Hence we were able to detect CD81-carrying EVs with the MNP-enhanced assay down to a concentration of 6 ng CD81/ml in the CTB-binding EVs.

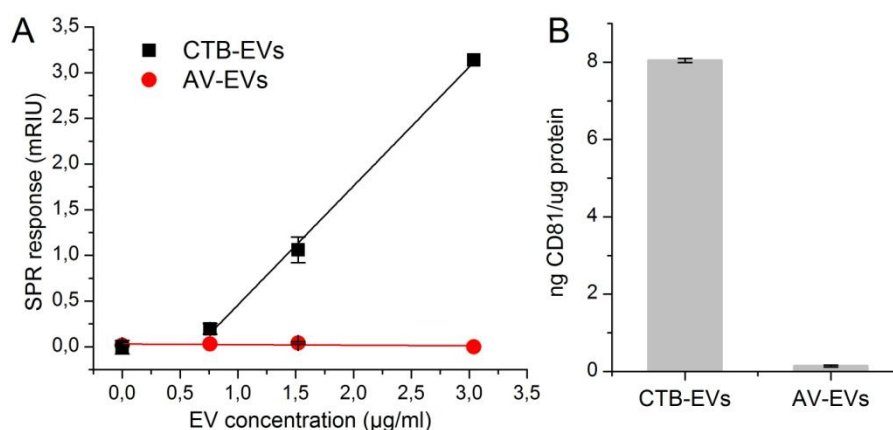


Figure 41 CD81 detection in CTB- and AV-binding EVs. A SPR response change for different concentrations of CTB-binding EVs and AV-binding EVs captured by anti-CD81 antibodies on the sensor surface of the magnetic nanoparticle (MNP)-enhanced GC-SPR assay. B CD81 concentration of CTB- and AV-binding EVs measured by MNP-coupled CD81-ELISA, concentration is given as ng CD81 per μg total protein of EVs used for binding to the MNPs. mRIU = milli refractive index units, EVs = extracellular vesicles, CTB-EVs = cholera toxin b chain-binding EVs, AV-EVs = annexin V-binding EVs. Figures reprinted from [2].

4.3 Conclusions

A new plasmonic biosensor for the analysis of EVs based on GC-SPR with wavelength interrogation is presented. The sensor makes use of the highly efficient accumulation of EVs on the sensor surface by their coupling with MNPs and applying a magnetic field gradient. This approach was demonstrated to enhance the SPR sensor response by a combined effect of increased speed of binding kinetics and enhanced surface mass density. The analysis of EVs secreted by mesenchymal stem cells at concentrations down to $0.76 \mu\text{g/ml}$ or 130 fM (quantified as total protein concentration or by nanoparticle tracking analysis, respectively) was achieved, which was not possible for direct SPR detection format or the sandwich MNP assay without active magnetic pulling. Through functionalization of the sensor with antibodies specific for CD81, specific detection of EV subpopulations isolated with lipid-binding ligands CTB and AV with the MNP enhanced GC-SPR assay was achieved. We believe that this detection platform may provide attractive means for rapid highly parallelized screening of EV-based biomarkers by e.g. grating-coupled SPR imaging [223]. In addition, by the use of grating-coupled surface

plasmon enhanced fluorescence [161], detection sensitivity can be further pushed forward and enable analysis of minute amounts of cancer-specific EVs in complex samples such as blood plasma.

5 Parallel Readout of Grating Coupled SPR and Plasmon-enhanced Epifluorescence

This chapter presents data that were published in [3] and uses text and figures from this publication.

Fluorescence is a widely used method in bioassays for sensitive detection of chemical and biological species. In order to advance their sensitivity, the fluorophores that are used as labels can be exposed to the confined field of surface plasmons [224, 225]. These optical waves are resonantly excited at surfaces of metallic films and metallic nanoparticles and they originate from coupled collective oscillations of the charge density and the associated electromagnetic field. The combination of a surface plasmon-enhanced excitation rate at the fluorophore absorption wavelength, directional surface plasmon-coupled emission at the fluorophore emission wavelength, and an improved quantum yield was demonstrated to enhance the detected fluorescence intensity by a factor up to 10^3 [226]. Such interaction with the intense and confined surface plasmon field was exploited for amplification of the fluorescence signal associated to the affinity binding of labeled analyte biomolecules in bioassays and biosensors in order to improve their performance characteristics [147, 160].

Besides plasmon-enhanced fluorescence (PEF) assays, the probing of molecular binding by surface plasmons allows for direct label-free detection of analytes. In surface plasmon resonance (SPR) biosensors, the affinity binding of analyte molecules increase the refractive index at a metallic sensor surface, which detunes the resonant coupling of light to surface plasmons and thus can be optically monitored as a shift of SPR. This method became an established tool in biomolecular interaction studies [227] and it is pursued for rapid and sensitive detection of chemical and biological analytes [228].

The possibility of parallel detection of SPR and PEF holds potential for more advanced detection schemes and molecular interaction studies. Up to now, the attenuated total reflection geometry (ATR) was dominantly used for the excitation of surface plasmons and it has been utilized for the combined SPR and PEF studies. It was reported for the SPR observation of functional biointerfaces combined with enhanced sensitivity of fluorescence-based detection of low molecular weight analytes [229] or biomolecules present at minute concentrations in complex samples [230, 231]. In addition, SPR and PEF was employed in the analysis of interaction between DNA polymerase, short oligonucleotide strands attached to a substrate, and labeled nucleotides that formed DNA duplexes [154]. Furthermore, the combination of fluorescence

detection of enzyme linked immunoassays and SPR in a single instrument was demonstrated to be suitable for the analysis of target analytes over a broad dynamic range [232].

According to the knowledge of the authors, the combined SPR and PEF readout was implemented up to now only by using ATR configuration. The metallic diffraction grating-coupled SPR on periodically corrugated metallic surfaces provides an alternative means for the excitation and interrogation of surface plasmons, which found its applications in SPR biosensors [223] as well as in PEF detection in epi-fluorescence geometry configurations [161, 233]. With respect to sensors utilizing ATR, diffraction gratings offer the advantage of simpler use that does not require optical matching of a sensor chip to a prism and it can be exploited in a format compatible with regular (fluorescence) microscopes. In addition, it enables the utilization of magnetic nanoparticle (MNP)-enhanced assays when a magnetic field gradient can be efficiently applied through a sensor chip in order to overcome diffusion-limited affinity binding kinetics and rapidly collect the pre-concentrated analyte at the sensor surface [2, 158].

This work reports on SPR and PEF signal detection based on diffraction grating-coupled SPR and the epifluorescence geometry, which was not yet reported. We demonstrate that such a system can in parallel directly detect binding of biomolecules to the surface via SPR monitoring as well as by PEF when fluorophore labels are used. The performance characteristics of PEF and SPR modalities are investigated for the direct detection of medium size protein molecules and for MNP-enhanced analysis of larger extracellular vesicles (EVs).

5.1 Material and Methods

5.1.1 Materials

Positive photoresist Microposit S1805 was purchased from Shipley and its developer AZ 303 was acquired from MicroChemicals. Polydimethylsiloxane elastomer (PDMS) Sylgard 184 was obtained from Dow Corning and the UV-curable polymer Amonil MMS 10 was from AMO GmbH. Dithiolalkane aromatic PEG3 with hydroxyl endgroup (SPT-0013) and the dithiolalkane aromatic PEG6 with carboxyl endgroup (SPT0014A6) were purchased from SensoPath Technologies. N-(3-dimethylaminopropyl)-N'-ethylcarbodiimide hydrochloride (EDC), N-hydroxysuccinimide (NHS), ethanolamine and ethylenglycol, as well as acetic acid and sodiumacetate for the preparation of acetate buffer were bought from Sigma-Aldrich. Phosphate buffered saline (PBS) at a pH of 7.4 from Merck was used for the functionalization steps. PBS with addition of 0.05 % Tween 20 (Sigma-Aldrich) and 0.1 % bovine serum albumine (Thermo Fisher Scientific) (PBSTB) were used as running buffers in all detection experiments. The biotinylated mouse antibody (MG2b-57) was obtained from BioLegend and the mouse

monoclonal antibody against human CD81 (1.3.3.22) from Santacruz Biotechnology. Streptavidin was from Thermo Fisher Scientific. Cholera toxin b-chain (CTB) from SBL Vaccin AB was biotinylated with EZ-link Sulfo-NHS-LC-Biotin (Thermo Fisher Scientific) and in parallel fluorescently labeled with Alexa Fluor 647 NHS ester (Thermo Fisher Scientific). MNPs with a diameter of 200 nm conjugated with streptavidin (fluidMAG-Streptavidin) were purchased from Chemicell. Prior to the use, streptavidin-coated MNPs were washed twice with PBSTB by applying a magnetic field for separation of the MNPs from the solution. EVs were generously provided from Sai Kiang Lim's group and their production and purification is described elsewhere [49].

5.1.2 Sensor chip preparation

A crossed relief grating was prepared by UV laser interference lithography and their multiple copies were made by soft lithography as described before [161]. Briefly, the used structure comprised of two superimposed crossed sinusoidal modulations with a period of $\Lambda=434$ nm. The structure was casted to PDMS, which was cured over night at 60 °C before it was used as a working stamp. Cleaned BK7 glass substrates were coated with the UV-curable polymer Amonil MMS 10 by spin-coating at 3000 rpm for 120 s. Then, the PDMS working stamp was placed on the top of the Amonil layer and the structure casted to this polymer was irradiated by UV light (UV lamp Bio-Link 365, Vilber Lourmat). Finally, the PDMS stamp was detached from the cured Amonil MMS 10 leaving a copy of the master structure on the glass substrate. The grating copies were subsequently coated with 4 nm of chromium and 100 nm of gold by vacuum thermal evaporation (HHV AUTO 306 from HHV LTD) in vacuum better than 10^{-6} mBar. Each sensor chip consisted of an area with grating structure and an area with plain gold that was used for control measurements.

5.1.3 Optical system

The used optical system for the *in situ* detection of diffraction grating-coupled SPR and PEF was adopted based on our previous work [161] and it can be seen in Figure 42. A beam emitted from a He-Ne laser (power of about 2 mW) at $\lambda_{\text{ex}}=633$ nm subsequently travelled through a chopper, polarizer and laser band-pass filter (LBP, FL632.8-10 from Thorlabs). Then it passed through a beam splitter and it was focused by a lens (AC-254-040) on a mirror of 2 mm diameter, consisting of a 100 nm thick gold layer deposited on a BK7 glass slide. The mirror was oriented at 45 deg with respect to the incident beam. A lens (AC-254-040) collimated the reflected beam towards the sensor surface with relief gold diffraction grating mounted in its focal distance. A flow-cell was clamped to the gold sensor chip surface in order to contain aqueous samples. The

flow-cell comprised of a flow chamber with a volume of $\sim 50 \mu\text{L}$ defined by a PDMS gasket and a transparent fused silica glass substrate with inlet and outlet ports. Upon its incidence at the gold grating surface, the laser beam at λ_{ex} was partially coupled to surface plasmons propagating along the gold surface and partially reflected. The reflected beam was focused back on the mirror by the objective lens and its intensity was detected by using a beam splitter and a photodiode connected to a lockin amplifier (7260 from EG&G). These means allowed the measurement of the detuning of SPR associated to the binding-induced refractive index variations. In addition, the enhanced field intensity at λ_{ex} was employed for the excitation of Alexa Fluor 647 (AF647) fluorophores that we used as labels in the fluorescence assays. The enhanced directional surface plasmon-coupled emission at $\lambda_{\text{em}}=670 \text{ nm}$ was collimated by the objective lens, passed around the small mirror and was focused by a lens (AC-254-080, Thorlabs) to a photomultiplier (H6240-01, Hamamatsu) that was connected to a counter (53131A from Agilent). In order to separate light at the excitation wavelength λ_{ex} and the fluorescence beam at λ_{em} , a set of filters was used consisting of a notch filter (XNF-632.8-25.0M from CVI Melles Griot) and two bandpass filters (FB670-10 from Thorlabs and 670FS10-25 from Andover Corporation Optical Filter). The output from the counter was recorded in counts per second (cps) by using software Wasplas developed at Max Planck Institute for Polymer Research in Mainz (Germany). It is worth of noting that the used implementation of SPR measurements allowed for measurements of refractive index changes as small as 3×10^{-4} RIU. This value was determined as the ratio $\Delta n / (\sigma(R) / \Delta R_B)$ where $\sigma(R) = 3.6 \cdot 10^{-3}$ a.u. is the standard deviation of the reflectivity signal $R(t)$.

In the MNP-enhanced assays, a gradient magnetic field ∇B was applied through the sensor chip. A cylindrical permanent magnet (NdFeB with diameter of 10 mm and length of 35 mm from Neotexx) was approached to the grating sensor chip in order to expose its surface to the field gradient of about $\nabla B = 0.10 \text{ T mm}^{-1}$ [158]. By removing the magnet, the magnetic field gradient was switched off to $\nabla B = 0$.

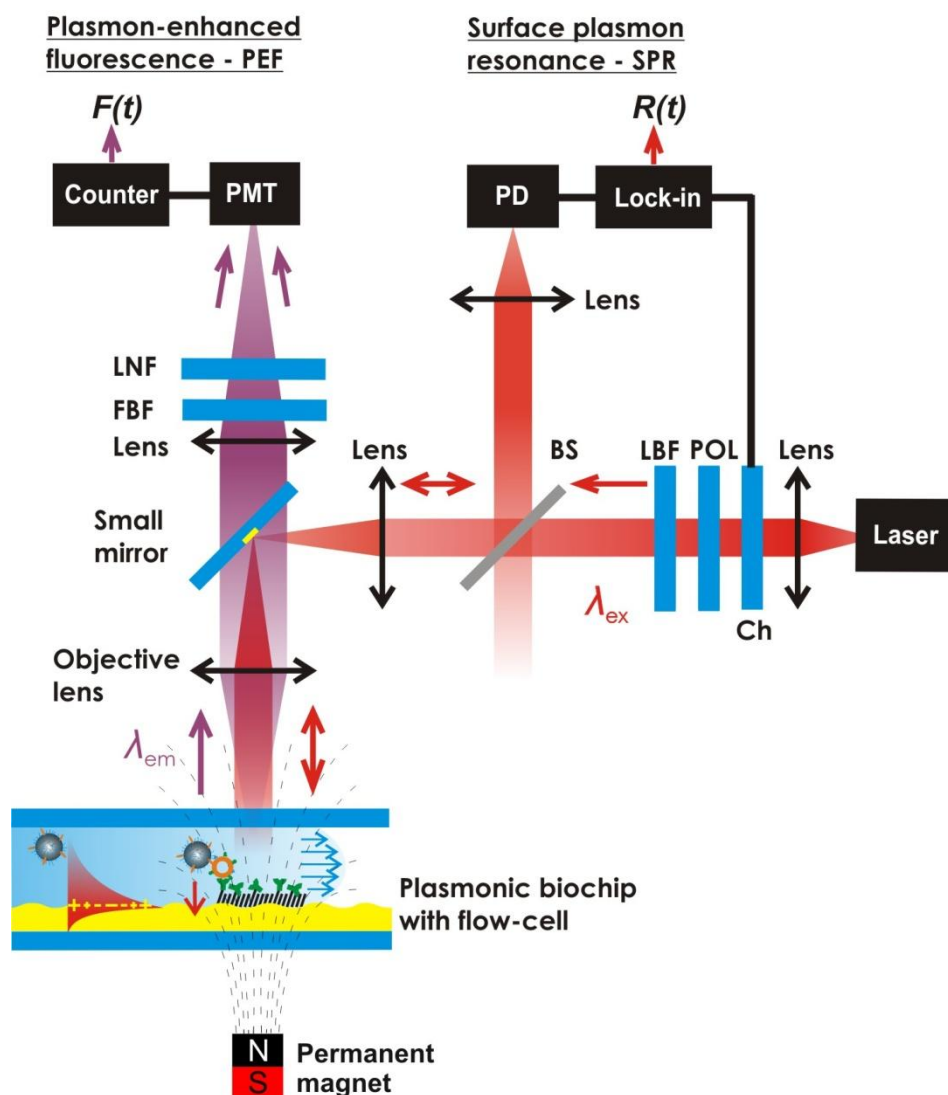


Figure 42 Schematics of the platform for parallel surface plasmon-enhanced fluorescence and surface plasmon resonance detection (Ch - chopper, POL - polarizer, LBF - laser band-pass filter, BS - beam splitter, FBF - fluorescence band-pass filter, LNF - laser notch filter, $F(t)$ - fluorescence readout, $R(t)$ - SPR readout, PD - photodiode, PMT - photomultiplier). Figure reprinted from [3].

5.1.4 Functionalization of sensor chips

The gold surface of the sensor chips was immersed in a 1 mM thiol solution in ethanol in order to form a mixed self-assembled monolayer (SAM). The solution comprised of a mixture of dithiol-PEG6 with carboxyl end group for later surface functionalization and dithiol-PEG3 with hydroxyl end group in order to form an antifouling background. The molar ratio of carboxyl to hydroxyl-terminated thiols was 1:9. After the overnight incubation, the sensor chips were thoroughly rinsed with ethanol, dried immediately in a stream of air and stored under argon gas.

The immobilization of either biotinylated unspecific antibodies or unconjugated specific antibodies against CD81 was performed *in situ* by amine coupling according to standard protocols. The sensor surface was exposed to the sample and buffer solutions at a constant flow

of 45 $\mu\text{L}/\text{min}$. As a first step PBS was rinsed through the flow cell to reach a stable baseline in SPR signal. In order to calibrate the sensor, PBS spiked with 2 % ethylenglycol was flowed through, triggering a refractive index change of 2×10^{-3} refractive index units (2 mRIU). Afterwards, sodium acetate buffer with a pH-value of 5 was rinsed to adjust the pH for the consecutive amine coupling. The carboxyl groups on the surface were activated by flowing a mixture of 0.4 M EDC and 0.2 M NHS in water for 15 min. After rinsing the surface with sodium acetate buffer, the antibody, diluted in the same buffer at a concentration of 25 $\mu\text{g}/\text{mL}$, was incubated for 10 minutes. Finally, ethanolamine at 1 M and pH of 8.5 was used to inactivate all remaining carboxyl groups before the buffer was changed again to PBS.

5.1.5 Direct detection bioassay

Unspecific biotinylated antibodies were immobilized on the sensor surface by amine coupling and followed by the affinity binding of streptavidin and a fluorescently labeled biotin-CTB conjugate (see Figure 43a). In these measurements PBSTB was used as running buffer. First streptavidin at a concentration of 5 $\mu\text{g}/\text{mL}$ in PBSTB was flown over the surface for 10 min. After washing with PBSTB, the biotinylated CTB that was also labeled with AF647 was pumped through the flow-cell at a concentration of 5 $\mu\text{g}/\text{mL}$.

5.1.6 Magnetic nanoparticle-enhanced bioassay

The MNP-enhanced bioassay for EV detection was performed as described in our previous work [2] with the addition of the AF647 labeling of the lipid-binding protein CTB. Briefly, 3 μg of mesenchymal stem cell-derived EVs were incubated with 250 ng of biotinylated and AF647-labeled CTB for 30 min at room temperature on a shaker. Then 10 μg of washed MNPs capped with streptavidin were added to the sample and incubated again at the same conditions (see pre-incubation in Figure 43b). Afterwards, the MNPs with bound EVs were washed twice with PBSTB and finally re-suspended in 1 mL buffer, resulting in an estimated concentration of 3 μg total protein amount of vesicles per mL PBSTB or 520 fM based on the particle count determined by nanoparticle tracking analysis of the input EV sample. As control sample the MNPs were incubated only with the biotinylated and fluorescently labeled CTB. Then the control MNPs or MNP-bound EVs were collected and captured on the sensor surface, which was first functionalized with antibodies specific for CD81, by flowing the samples across the surface while a magnetic field gradient $\nabla B = 0.10 \text{ T mm}^{-1}$ was applied (see Affinity binding in Figure 43b). After a 10 min incubation the magnetic field gradient was switched off $\nabla B = 0$ and the sensor surface was washed with PBSTB for 20 min. Due to the architecture of the setup and flow-cell, flushing

shortly with running buffer at high speed was necessary to remove any unspecifically attached MNPs and aggregates.

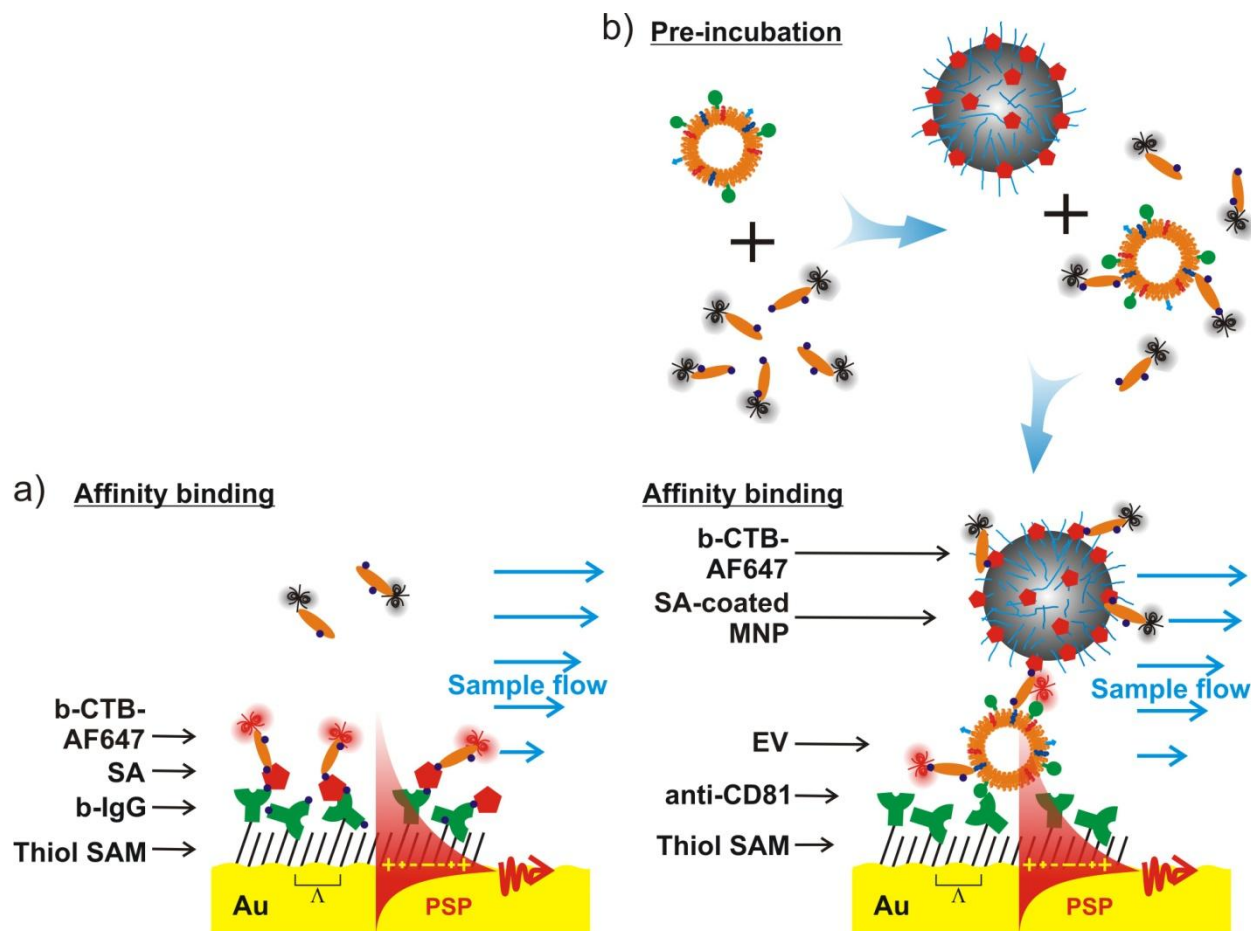


Figure 43 Schematics of the assays used for testing of the sensing platform. a) The detection assay of medium sized CTB protein based on biotin-streptavidin affinity binding and fluorescent labeling with AF647. b) Extracellular vesicle (EV) assay consisting of the pre-incubation step and collection of the EVs at the sensor surface. Fluorophores within the surface plasmon penetration depth are depicted in red, while those outside are shown in grey (MNPs - magnetic nanoparticles, b-CTB-AF647 - biotinylated cholera toxin b-chain conjugated with Alexa Fluor 647, SA - streptavidin, b-IgG - biotinylated unspecific antibody, anti-CD81 - specific antibody for CD81, SAM - self assembled monolayer, Au - gold, PSP - propagating surface plasmon, Λ - period). Figure adapted from [3].

5.2 Results and Discussion

5.2.1 Characterization of GC-SPR sensor chips

The prepared sensor chip with or without the crossed grating corrugation carried a conformal 100 nm thick gold film. Atomic force microscopy of these surfaces presented in Figure 44a and b reveal that the periodicity of the two overlaid crossed sinusoidal modulations on grating area was about the targeted $\Lambda=434$ nm, and the corrugation depth was 60 nm. This corrugation depth corresponds to the amplitude of the sinusoidal modulation in each perpendicular direction of about 15 nm. This value was showed before to be optimum for strong diffraction coupling to

propagating surface plasmons (PSP) in the red part of the spectrum at an interface between gold and water [223]. The wavelength reflectivity spectra of the grating structured sensor chip, which was clamped to a flow-cell and flooded with PBS buffer, was measured by using a system reported before [2]. As visible in Figure 45, a narrow dip in the reflectivity spectrum occurs at the wavelength $\lambda_{\text{SPR}}=638$ nm due to the first diffraction order excitation of PSPs on a periodically corrugated surface. The resonant wavelength λ_{SPR} can be controlled by varying the period A which was chosen in order to tune λ_{SPR} slightly above the excitation wavelength $\lambda_{\text{ex}}=633$ nm that is further used in fluorescence measurements. After forming a mixed thiol SAM at the gold surface, the SPR shifts to a longer wavelength of $\lambda_{\text{SPR}}=639$ nm due to the increase in the refractive index, as shown in Figure 45. The resonance wavelength shift of about 1 nm corresponds to the adlayer thickness of ~ 1 nm [218], which indicates that a compact mixed thiol SAM layer was formed on the gold surface. For the normally incident beam at λ_{ex} this shift is manifested as an increase in the reflectivity ΔR as its wavelength is coincident with the edge of the resonance dip.

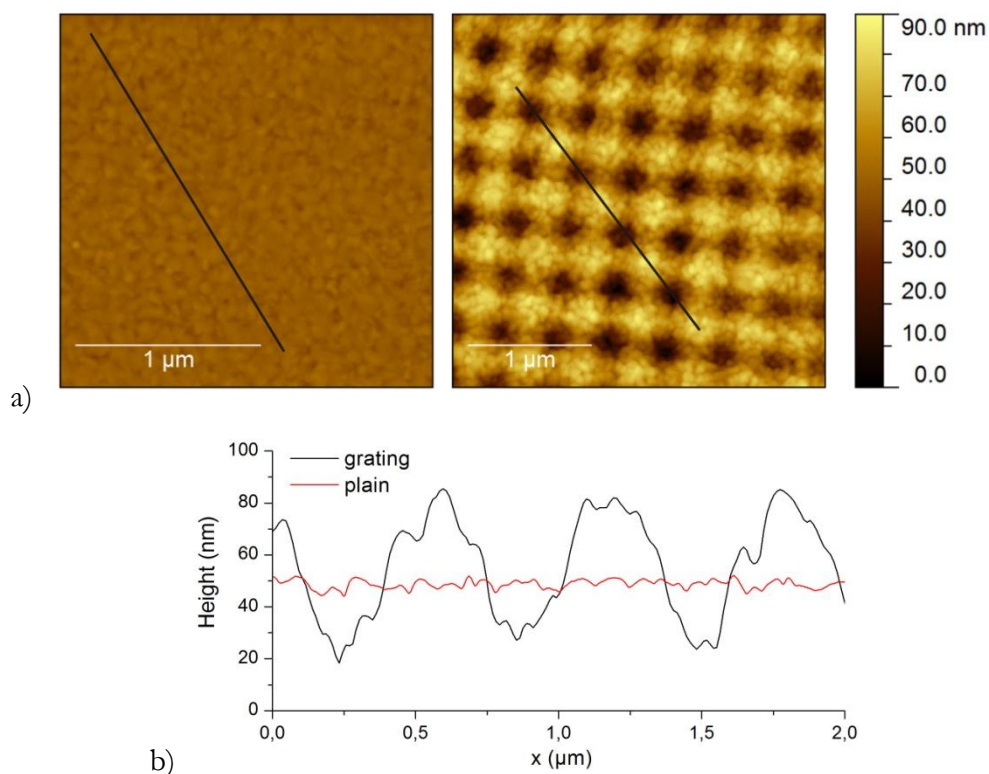


Figure 44 a) Atomic force microscopy image of the plain (left) and grating (right) sensor surface after the coating with gold (scale bar corresponds to 1 μm). b) Height profiles of the plain and grating sensor surface of the indicated black lines in a). Figures reprinted from [3].

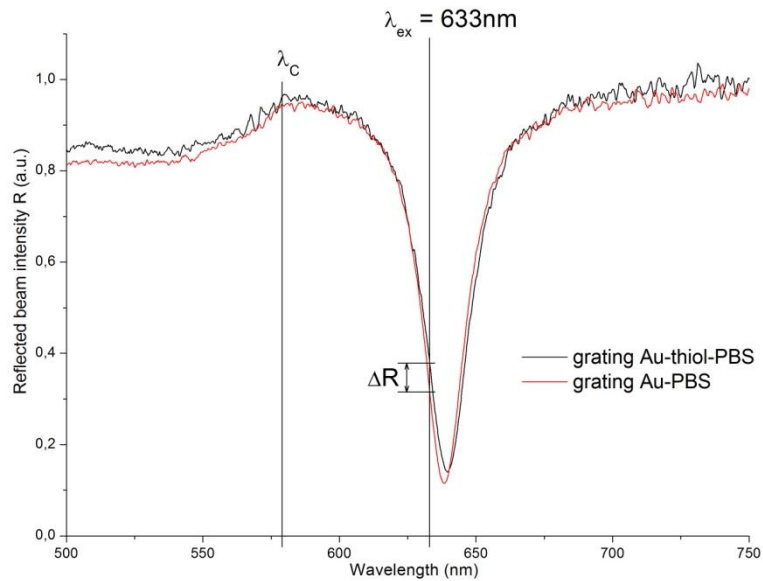


Figure 45 Wavelength reflectivity spectra for a normally incident beam at the sensor chip with a clamped flow-cell that was flooded with PBS before and after deposition of a mixed thiol SAM. The reflectivity change ΔR at a fixed wavelength of $\lambda_{ex}=633$ nm is indicated. Figure reprinted from [3].

In the further experiments, the gold grating structure was used to monitor affinity binding events in two modes in parallel by using the optical setup showed in Figure 42. First, the direct SPR observation of molecular binding was implemented by measuring the reflectivity ΔR changes. An increase in the refractive index is manifested as a red shift in the SPR wavelength λ_{SPR} which is accompanied with an increase in the reflectivity at the chosen wavelength λ_{ex} (tuned to the edge of the resonance peak). Second, the enhanced intensity of the electromagnetic field associated with the resonance excitation of PSPs at λ_{ex} increases the excitation rate of AF647-labeled molecules bound to the surface. In addition, the same structure allows to exploit directional surface plasmon-coupled emission at the AF647 emission wavelength $\lambda_{em}=670$ nm. The combination of these two effects offers means for the amplification of the fluorescence – PEF – signal $F(t)$ and *in situ* fluorescence monitoring of affinity binding events at the sensor surface [162].

Two assays are carried out in order to demonstrate the performance of dual SPR and PEF readout and compare the sensitivity of these two detection modalities. First, the combined SPR and PEF detection was used for the affinity binding of protein molecules in the close proximity to the gold sensor surface. Second, the implementation of SPR and PEF measurements for the detection of extracellular vesicles – EVs – is pursued with the aid of magnetic nanoparticles – MNPs – that allow for the efficient collection of such analytes at the sensor surface by application of a magnetic field gradient ∇B . For both experiments and readout modalities sensor chips with a plasmonic grating and a flat gold film for reference purposes were used.

5.2.2 Observation of affinity binding of protein analyte

Figure 46 and Figure 47 show the SPR and PEF sensorgrams measured upon the preparation of the sensor surface architecture as well as for the affinity binding of biotinylated cholera toxin b chain (b-CTB). As seen in Figure 43a, the surface of the sensor chip was functionalized with streptavidin (SA) and an additional layer of biotinylated antibody (b-IgG) was used between the gold surface and the SA layer in order to avoid the fluorescence quenching (that occurs at distances < 15 nm due to the Förster energy transfer [147, 234]). The acquired sensorgrams include the fluorescence signal $F(t)$ and SPR reflectivity changes $\Delta R(t)$. For comparison, the molecular binding experiments were performed at two areas on the sensor chip: Figure 46 shows the sensor response at the grating surface and Figure 47 at a reference flat area.

First, a baseline in the reflectivity $\Delta R(t)$ and fluorescence $F(t)$ signal was established upon a flow of PBS. Then, a PBS solution spiked with 2 % ethylene glycol was injected, followed by rinsing with PBS. This step was used to calibrate the SPR sensor channel by using the bulk refractive index change above the sensor surface which corresponds to about $\Delta n = 2 \times 10^{-3}$ refractive index units (RIU). As can be seen in Figure 46, this increase in the refractive index ($t=5-15$ min) caused a change in the SPR signal $\Delta R_b = 0.06$ a.u. on a grating surface and no response was observed on a reference flat gold film (as presented in Figure 47). Similarly, the fluorescence detection channel was tested by a flow of b-CTB carrying AF647 tags (dissolved at a concentration of $5 \mu\text{g/ml}$) over the gold grating (Figure 46, $t=20-25$ min) and on a flat gold surface (Figure 47, $t=80-85$ min) that did not carry SA moieties. A similar fluorescence signal increase in the range of $\Delta F_b = 0.75 - 1 \cdot 10^6$ cps was measured on both areas due to the excitation of fluorophores present in the bulk solution. The fluorescence signal F rapidly dropped back to the original baseline after the rinsing with PBS which indicates marginal unspecific adsorption to the surface.

Both grating and flat gold areas on the sensor chip were modified by b-IgG with the use of amine coupling followed by affinity binding SA. Figure 46 shows the obtained sensorgram on a grating surface for the activation of carboxyl groups by a mixture of EDC/NHS ($t=35-50$ min), covalent binding of b-IgG ($t=55-65$ min), passivation of unreacted carboxyl groups with ethanolamine ($t=70-75$ min), and binding of SA ($t=85-95$ min). The same sequence and incubation times were performed in the flat area on the sensor chip and respective sensorgrams are presented in Figure 47. On the grating surface, the binding of b-IgG and SA increased the reflectivity signal by $\Delta R_1 = 0.10$ a.u. and $\Delta R_2 = 0.06$ a.u., respectively, while no measurable change was observed on a flat gold surface ($t=20-105$ min). The observed reflectivity changes on the SPR grating area of the sensor chip correspond to the surface mass density of 1.2 ng/mm^2 for IgG and of 0.73 ng/mm^2 for SA which is comparable to values reported in literature [153, 220].

After the immobilization of b-IgG and SA, a solution with CTB conjugated with biotin and AF647 tags (b-CTB-AF647, concentration of 5 $\mu\text{g}/\text{mL}$) was flowed over the sensor surface for 10 min. On both grating area (Figure 46, $t=105\text{-}115$ min) and reference flat area (Figure 47, $t=110\text{-}120$ min) a weak drop in the reflectivity $R(t)$ occurs due to the absorption of the excitation light by fluorophores dissolved in the bulk solution. However, after the rinsing with buffer an increase in reflectivity of $\Delta R_3=0.02$ a.u. was measured on a grating while no measurable change occurred on a reference flat gold area. The SPR reflectivity response on the grating area due to b-CTB-AF647 binding showed a signal-to-noise ratio of $\Delta R_3/\sigma(R)\sim 5$. Contrary to the reflectivity measurement, the fluorescence detection channel $F(t)$ showed a much more pronounced signal. After the injection of b-CTB-AF647 a rapid increase in $F(t)$ is observed due to the dominant excitation of fluorophores in the bulk solution. After the 10 min incubation, the surface was rinsed with PBSTB and a strong change in fluorescence signal ΔF_s caused by the affinity binding becomes visible. The fluorescence change yields $\Delta F_s=1.22\times 10^5$ cps on the grating area and $\Delta F_s=1.2\times 10^3$ cps on the reference flat area. The associated signal-to-noise ratio of fluorescence response on the grating area was ~ 700 . Hence, the accuracy of PEF readout outperforms the SPR on the grating surface by more than two orders of magnitude. Besides allowing for dual fluorescence and SPR detection, the used plasmonic grating enhanced the fluorescence signal originating from the grating surface compared to the flat surface by a factor of ~ 100 , which agrees with earlier published simulations and measurements of PEF using epifluorescence geometry [161].

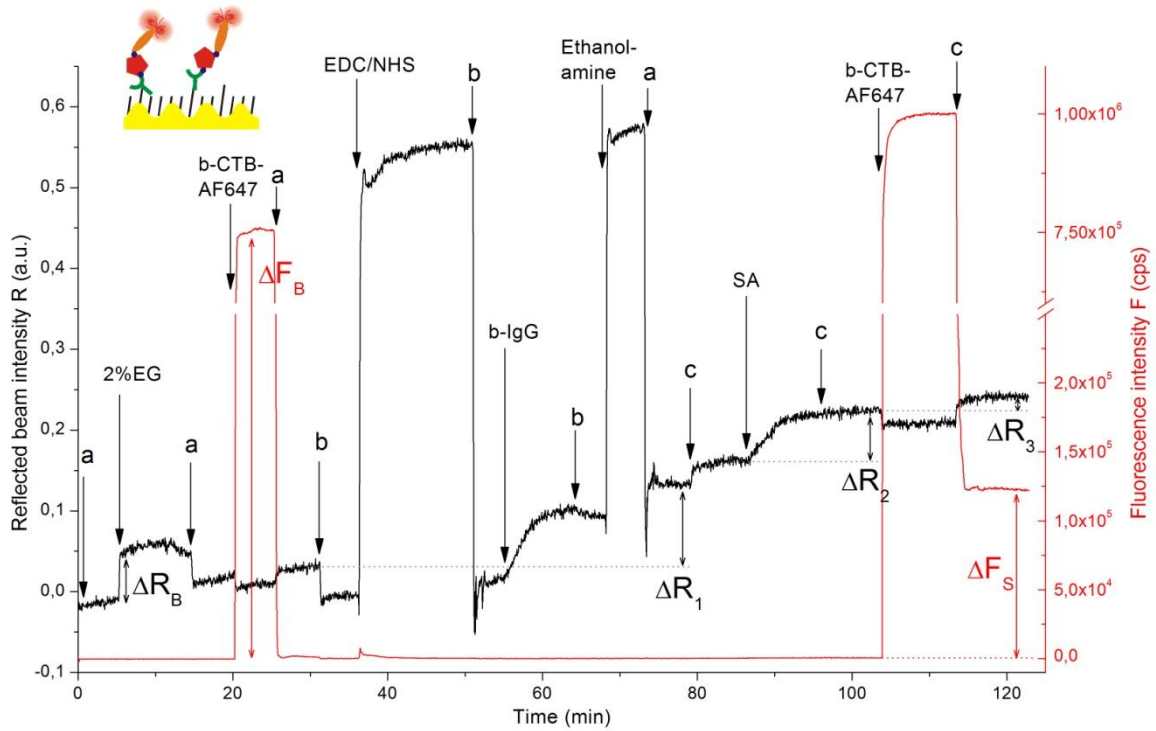


Figure 46 SPR signal $R(t)$ and fluorescence signal $F(t)$ during amine coupling of a biotinylated unspecific antibody (b-IgG) and affinity binding of fluorescently labeled and biotinylated cholera toxin b-chain (b-CTB-AF647) on a grating gold chip. Inset on the top left show a pictogram of the assay and the respective surface used. The signal responses to the affinity binding of molecules at the surface are indicated as ΔR or ΔF for SPR and fluorescence, respectively (a - PBS, b - acetate buffer pH=5, c - PBSTB, EG - ethylenglycol, b-IgG dissolved at 25 $\mu\text{g}/\text{ml}$, SA - streptavidin at 5 $\mu\text{g}/\text{ml}$). Figure reprinted from [3].

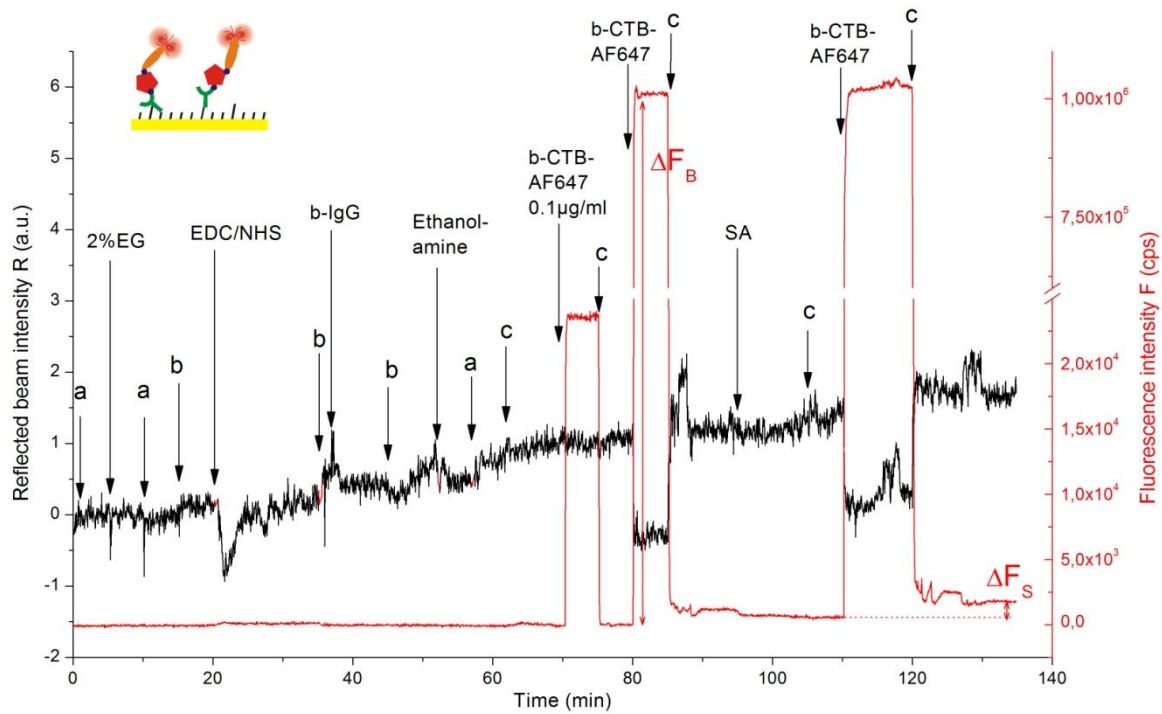


Figure 47 SPR signal $R(t)$ and fluorescence signal $F(t)$ for the same measurement as described in Figure 46 only performed on a reference plain gold chip as control. Inset on the top left show a pictogram of the assay and the respective surface used. The signal responses to the affinity binding of molecules at the surface are indicated as ΔR or ΔF for SPR and fluorescence, respectively (a - PBS, b - acetate buffer pH=5, c - PBSTB, EG - ethylenglycol, b-IgG dissolved at 25 $\mu\text{g}/\text{ml}$, SA - streptavidin at 5 $\mu\text{g}/\text{ml}$). Figure reprinted from [3].

5.2.3 Magnetic nanoparticle-enhanced observation of affinity binding of extracellular vesicles

Since the grating coupled SPR configuration and the epifluorescence geometry for PEF readout use only the front side of the sensor chip, there is free space at the back of the chip and flow-cell. This space was used for the integration of a magnetic field gradient ∇B for the improved collection of the target analyte, that is affinity bound to MNPs, at the sensor surface. As we reported before, this approach overcomes the slow diffusion-limited mass transfer of the analyte [158, 159]. Hence, we incorporated the MNP-enhanced detection assay for EVs [2] into our optical setup for combined detection of SPR and PEF. It is worth of noting that in this second assay the target analyte, EVs, exhibit a larger size of about 100 nm compared to the previous assay in which a protein with a size of about several nanometers was detected.

In a pre-incubation step, the target EV analyte was first bound to MNPs via the lipid binding protein CTB with biotin tags, as illustrated in Figure 43b. In order to achieve fluorescence detection of the EVs, CTB molecules were additionally labeled with AF647. For affinity binding of EVs at the sensor surface, the grating and reference flat areas were functionalized with antibodies specific for CD81 which is a protein present on the CTB-binding vesicles [49]. The

immobilization of the anti-CD81 at the surface was accompanied with an SPR shift of $\Delta R=0.13$ a.u. corresponding to the surface mass density of 1.6 ng/mm^2 (measured on the structured gold surface, sensorgram not shown), which is similar to the results discussed above.

First, PBSTB buffer was flowed over the gold grating (Figure 48) and reference flat (Figure 49) areas carrying anti-CD81 to establish a baseline ($t=0-5$ min). Then the sensor surface was exposed to control MNPs in order to test for unspecific binding to the sensor surface (Figure 48 and Figure 49, $t=5-15$ min). These sensorgrams show that the SPR signal R decreased and fluorescence intensity F increased upon the accumulation of MNPs reacted with CTB-AF647 conjugate at the sensor surface, to which the MNP-CTB-AF647 mixture without target EV analyte was pulled by the magnetic field gradient ∇B applied.

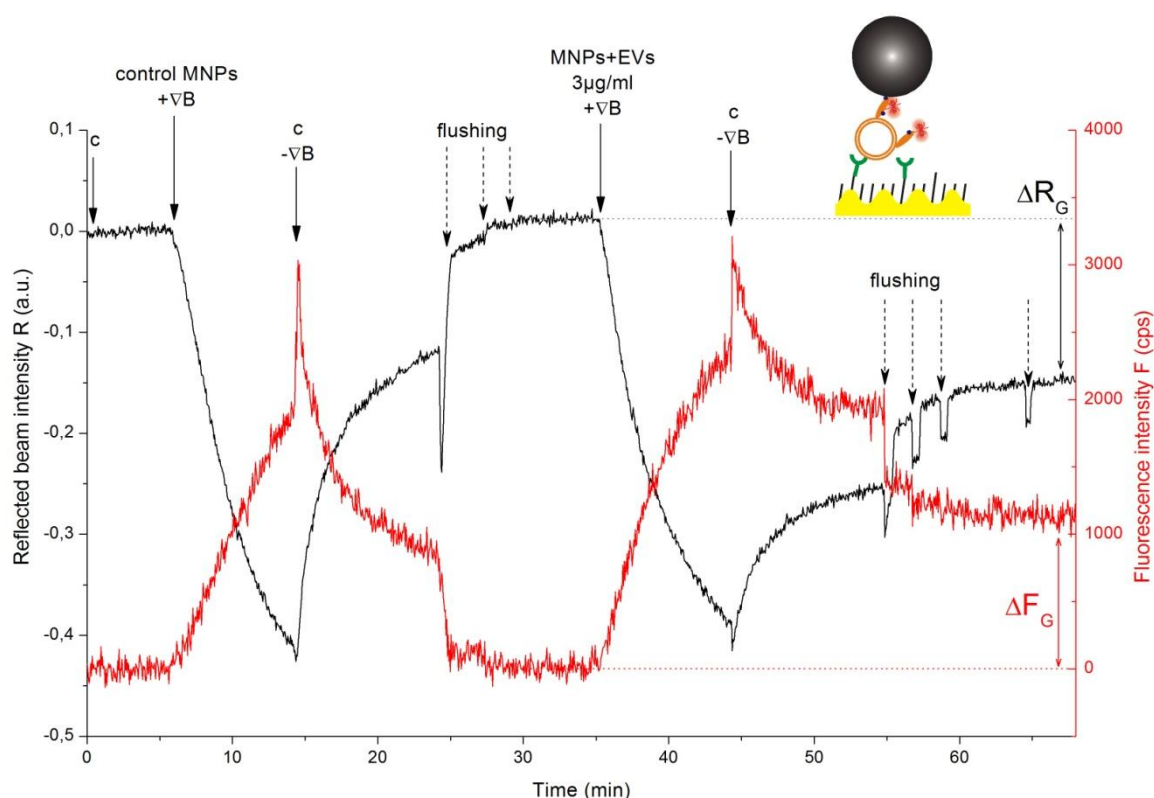


Figure 48 SPR signal $R(t)$ and fluorescence signal $F(t)$ of a magnetic nanoparticle (MNP)-enhanced assay measurement on a grating gold chip. Inset on the top right show a pictogram of the assay and the respective surface used. The application of the magnetic field for collection of MNPs and bound extracellular vesicles (EVs) is indicated as “ $+\nabla B$ ” and its removal as “ $-\nabla B$ ”. The signal responses to the affinity binding of molecules to the surface are indicated as ΔR or ΔF for SPR and fluorescence, respectively (c - PBSTB). Figure reprinted from [3].

Interestingly, the SPR signal decrease is more pronounced on the reference plain gold area of the sensor chip than on that with grating. The reason is that the accumulated MNPs (with the size of about 200 nm) form a layer on the sensor surface that is substantially thicker than the probing depth of PSPs (< 100 nm). Therefore, the decrease in the reflected intensity is mostly due to the scattering and absorption by MNPs. On the flat gold surface the beam passes twice through this

layer while on the grating surface only once as the majority of its intensity is transferred to the PSPs. Furthermore, MNPs in contact with the gold surface enhance the refractive index leading to an SPR signal increase R that counteracts the absorption of light intensity by the MNPs. The fluorescence signal change was observed at a similar level both on grating and plain gold as it mostly originates from a distance longer than the PSP probing depth and thus it is not plasmonically amplified.

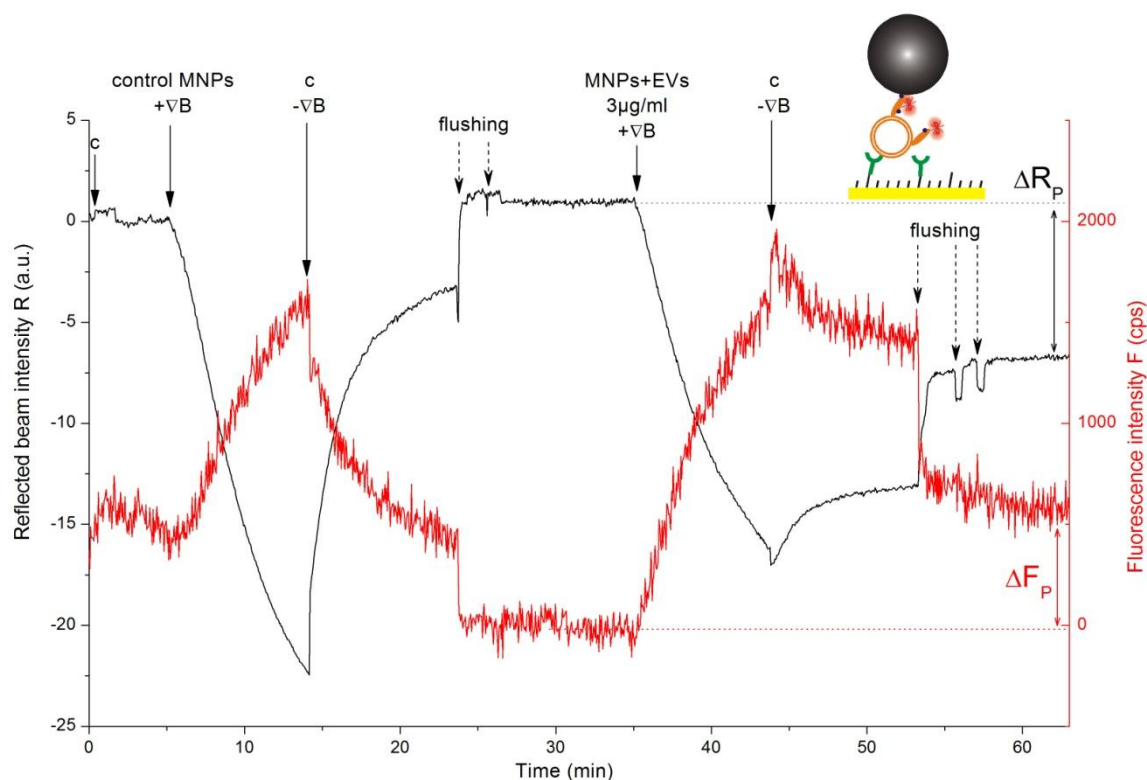


Figure 49 SPR signal $R(t)$ and fluorescence signal $F(t)$ of the same assay as described in Figure 48 performed on a reference plain gold chip as control. Inset on the top right show a pictogram of the assay and the respective surface used. The application of the magnetic field for collection of MNPs and bound extracellular vesicles (EVs) is indicated as “+ ∇B ” and its removal as “- ∇B ”. The signal responses to the affinity binding of molecules to the surface are indicated as ΔR or ΔF for SPR and fluorescence, respectively (c - PBSTB). Figure reprinted from [3].

After switching off the magnetic field gradient ∇B and rinsing the flow-cell with PBSTB (Figure 48 and Figure 49, $t=15-35$ min) the unbound MNPs were quickly washed away. Due to the architecture of the instrument, flushing of the flow cell with running buffer was required to remove all unbound MNPs. These flushing steps are indicated in the sensorgrams by a dashed arrow and present as sharp signal shifts. After flushing, SPR and PEF signals stabilized at the same level as before the MNP incubation, indicating that there was no unspecific binding to the functionalized surfaces.

Next the MNPs pre-incubated with the target EV analyte (at an estimated concentration of $3 \mu\text{g}$ total protein/mL or 520 fM) and CTB (conjugated with biotin and AF647) were collected at the

sensor surface in the same manner as before for the control MNPs (Figure 48 and Figure 49, $t=35-45$ min). Again a similar decrease in SPR was observable, but after switching off the magnetic field gradient and flushing with PBSTB (Figure 48 and Figure 49, $t=45-65$ min) a reflectivity change of $\Delta R_G=0.16$ a.u. on the grating gold area and $\Delta R_p=7.72$ a.u. on the plain gold area was measured due to the affinity binding of EVs carried by MNPs to immobilized anti-CD81 antibodies. Since a decrease in the reflectivity R is observed on both grating and plain gold surfaces, it can be concluded that mainly the effect of light absorption and scattering by the MNPs is responsible for the signal change. Therefore, on the grating exhibiting SPR the reflectivity increase due to the analyte capture is overrun by the reflectivity decrease due to the MNPs. This counteraction also translates in the signal-to-noise ratio that is 1.7-fold lower for the grating gold (~ 44) compared to the plain gold (~ 76), see overview in Table 2. Hence the measurement on plain gold, which detects only light absorption by MNPs, performed better. In order to make use of the SPR signal change in addition to the light absorption and thus reaching higher signal-to-noise ratios, the coupling resonance needs to be tuned (e.g. by varying the grating period Λ) in a way that the resonance wavelength λ_{SPR} is shorter than the excitation wavelength λ_{ex} , resulting in a signal decrease upon binding of the target analyte to the sensor surface. It is worth of noting that a similar approach was adopted for the angular modulation of GC-SPR [159].

Table 2 Comparison of the signal-to-noise ratio obtained for the tested assays in the reflectivity and fluorescence channel on grating and plain gold sensing areas. Table reprinted from [3].

Assay	Readout type	Grating gold	Plain gold
b-CTB-AF647 detection	SPR	5	-
	Fluorescence	700	18
MNP-enhanced detection of EVs	SPR	44	76
	Fluorescence	18	12

In the fluorescence channel a signal increase of $\Delta F_G=1100$ cps and $\Delta F_p=590$ cps for the grating and the plain gold chip, respectively, were observed due to binding of MNP-bound EVs to the sensor surface. Signal-to-noise ratios of ~ 18 on the grating gold and ~ 12 on the plain gold were reached with this assay, which implies a small signal improvement for the PSPs coupling with fluorophores. This also manifests in the relatively small fluorescence enhancement of only 2-fold by PSPs. There are several explanations for the weak performance of the fluorescence channel for this type of assay. First, the monitored reflected beam intensity indicates that the binding of MNPs to the surface is accompanied with strong light absorption. This absorption likely decreases the intensity of light at the excitation wavelength λ_{ex} as well as at the emission wavelength λ_{em} . The MNP-induced absorption at λ_{ex} leads to a less efficient excitation of PSPs, which again leads to lower levels of fluorescence signal amplification. Similarly for λ_{em} this effect

disrupts the surface plasmon-coupled emission. In addition, the fluorescence photons emitted from a volume between gold and MNPs (see Figure 43b) are partially blocked by these objects on both flat and grating surfaces.

Since the fluorescence enhancement in the grating coupled SPR and PEF sensor is inhibited by the presence of MNPs, a possible solution for signal improvement would be to remove the MNPs after the collection of the target analyte on the sensor surface. This could be achieved by dissociating the binding of the biotinylated CTB molecules and the SA coated MNPs and will be the subject of further studies. One solution could be to use desthiobiotin for the binding of EVs to the SA-MNPs. This type of biotin has a lower affinity to SA and therefore MNPs could be dissociated by replacement of desthiobiotin with biotin [153, 235]. As free biotin has a higher affinity to SA compared to surface bound biotin [236], another very similar approach is to replace the biotin that is bound to the MNPs by addition of a high concentration of free biotin in solution.

5.3 Conclusions

Plasmonic grating was implemented for the combined label-free surface plasmon resonance (SPR) and plasmonically enhanced fluorescence (PEF) measurement of the affinity binding at the sensor surface by using epifluorescence geometry. These measurements can be performed on the same spot in parallel and in real-time. The monitoring of the affinity binding of a medium sized protein that was labeled with Alexa Fluor 647 dyes showed a ~100-fold fluorescence enhancement on the gold grating surface compared to a reference flat gold surface. The PEF readout outperformed SPR for this assay when the molecular binding occurs at distances of 15-20 nm from the metallic sensor surface and the respective signal-to-noise ratio was ~140-fold higher. The reported geometry allows for the incorporation of magnetic nanoparticle (MNP)-enhanced assays for the detection of larger analytes, which exhibit slow diffusion that hinders their affinity binding to the sensor surface. The combined PEF and SPR readout was utilized for the detection of extracellular vesicles (EVs) with the size of about hundred nanometers. The MNPs offered means for efficient delivery and affinity binding of the target EV analyte at the sensor surface, but they substantially hindered the performance of the fluorescence-based assay. The SPR detection channel outperformed the PEF in the MNP-based assay and provided a 2.4-fold higher signal-to-noise ratio. For efficient PEF detection that takes advantage of MNPs, reversible coupling mechanism for the capture of the target analyte on MNPs should be adopted in order to detach them after the delivery and affinity binding of the target analyte at the sensor surface.

6 Concluding remarks

In this project the two new and emerging research fields of extracellular vesicles (EVs) and surface plasmon resonance (SPR)-based biosensors were combined in order to achieve an earlier diagnosis of ovarian cancer. A thorough study of EVs derived from ovarian cancer patients was performed to better understand and characterize the cancer associated vesicles. Furthermore plasmonic biosensing platforms have been studied intensely to achieve a highly specific and sensitive detection of EVs. Even though the ultimate goal of detecting ovarian cancer specific EVs in the plasma of ovarian cancer patients by utilization of plasmonic biosensors was not achieved yet, the findings presented herein show great potential for a future application in the clinics. Since the biggest hurdle for the translation of EV research to applications is the lack of reliable methods, this work helps finding the way towards the establishment of new detection methods for EVs and their use in clinical applications.

By isolation of EVs from ascites of ovarian cancer patients with the aid of lipid-binding proteins and their comparison with EVs from cirrhotic ascites, new biomarker candidates were identified that hold potential for the application in ovarian cancer diagnosis. Those EVs, that were binding to annexin V, carried the cancer associated proteins matrix metalloproteinase 9 (MMP9) and protectin (or CD59), which were not present in other subpopulations of EVs or in vesicles isolated from ascites of patients with cirrhosis. Furthermore, MMP9 in annexin V-binding vesicles was preferentially found in those ascites samples from patients with high grade serous ovarian cancer, which is the most common type of ovarian cancer, suggesting a potential of this marker for differential diagnosis. However, the presence of these annexin V-binding and MMP9-carrying EVs in blood has to be examined and validation studies on independent study cohorts need to be performed, before the real clinical value of these candidate biomarkers can be assessed.

In the second part of this project, a versatile plasmonic biosensor platform for the detection of EVs was developed that incorporates the lipid-binding ligand isolation procedure for improved specificity. Additionally, it makes use of the magnetic nanoparticles (MNPs) utilized for the EV isolation for sensitivity enhancement in two ways. First, a magnetic field is applied to efficiently collect all the vesicles coupled to MNPs at the sensor surface, to overcome the diffusion limited transfer, which can be very slow for analytes like vesicles, and enable them to interact with the capture molecules on the surface. Second, the MNPs, coupled to EVs that bind to the sensor surface, are enhancing the SPR signal through their big mass, thus allowing for highly sensitive detection of EVs. This method proved to be capable of detecting EVs derived from cell culture

medium of cultivated mesenchymal stem cells, which served as model system, down to fM concentrations of vesicles.

In order to further enhance sensitivity and allow for analysis of several different molecules carried by the captured EVs on the sensor surface, a biosensor combining SPR and plasmonically enhanced fluorescence (PEF) was developed. For this purpose, the already developed plasmonic biosensor for EV detection was adapted to allow for fluorescence readout. This advanced sensor platform was capable of parallel, real-time monitoring of SPR and PEF signals by using grating-coupled SPR and epifluorescence geometry and proved to be capable of enhancing the fluorescence signal detected from a simple protein binding assay. However, the combination of PEF with the MNP-enhanced EV assay was hampered by the fact that the MNPs absorbed the incident light and thus no significant fluorescence enhancement by surface plasmons was possible yet. Nevertheless, approaches for reversible attachment of EVs to the MNPs could enable the removal of the particles after binding of the EVs to the sensor surface and hence making fluorescence labeling and readout possible.

So far, the developed plasmonic biosensors were not applied to detect ovarian-cancer derived EVs – the initial aim of this study. However, since plasmonic biosensors are very versatile through the functionalization of their sensor surface, also the detection of the here identified ovarian cancer EVs, that bind to annexin V and carry MMP9 and CD59, should be rather straightforward and approachable in future studies.

7 References

1. Reiner, A.T., et al., *EV-Associated MMP9 in High-Grade Serous Ovarian Cancer Is Preferentially Localized to Annexin V-Binding EVs*. Disease Markers, 2017.
2. Reiner, A.T., et al., *Magnetic nanoparticle-enhanced surface plasmon resonance biosensor for extracellular vesicle analysis*. Analyst, 2017. **accepted with minor revisions**.
3. Reiner, A.T., S. Fossati, and J. Dostalek, *Biosensor platform for parallel surface plasmon-enhanced epifluorescence and surface plasmon resonance detection*. Sensors and Actuators B-Chemical, 2017. **in revision**.
4. Reiner, A.T., et al., *Plasmonic Exosome Biosensors for Medical Diagnostics*, in *Frontiers in Biophotonics for Translational Medicine, Progress in Optical Science and Photonics*, D.U.S. Olivo M., Editor 2016, Springer Science+Business Media Singapore: Singapore. p. 249-272.
5. Harding, C., J. Heuser, and P. Stahl, *Receptor-mediated endocytosis of transferrin and recycling of the transferrin receptor in rat reticulocytes*. J Cell Biol, 1983. **97**(2): p. 329-39.
6. Pan, B.T. and R.M. Johnstone, *Fate of the transferrin receptor during maturation of sheep reticulocytes in vitro: selective externalization of the receptor*. Cell, 1983. **33**(3): p. 967-78.
7. Raposo, G., et al., *B lymphocytes secrete antigen-presenting vesicles*. J Exp Med, 1996. **183**(3): p. 1161-72.
8. Witwer, K.W., et al., *Standardization of sample collection, isolation and analysis methods in extracellular vesicle research*. J Extracell Vesicles, 2013. **2**: p. 20360.
9. Lotvall, J., et al., *Minimal experimental requirements for definition of extracellular vesicles and their functions: a position statement from the International Society for Extracellular Vesicles*. J Extracell Vesicles, 2014. **3**: p. 26913.
10. Lener, T., et al., *Applying extracellular vesicles based therapeutics in clinical trials - an ISEV position paper*. J Extracell Vesicles, 2015. **4**: p. 30087.
11. Hill, A.F., et al., *ISEV position paper: extracellular vesicle RNA analysis and bioinformatics*. J Extracell Vesicles, 2013. **2**: p. 22859.
12. Mateescu, B., et al., *Obstacles and opportunities in the functional analysis of extracellular vesicle RNA - an ISEV position paper*. J Extracell Vesicles, 2017. **6**(1): p. 1286095.
13. Reiner, A.T., et al., *Concise Review: Developing Best-Practice Models for the Therapeutic Use of Extracellular Vesicles*. Stem Cells Translational Medicine, 2017. **in press**.
14. Akers, J.C., et al., *Biogenesis of extracellular vesicles (EV): exosomes, microvesicles, retrovirus-like vesicles, and apoptotic bodies*. J Neurooncol, 2013. **113**(1): p. 1-11.
15. van der Pol, E., et al., *Classification, functions, and clinical relevance of extracellular vesicles*. Pharmacol Rev, 2012. **64**(3): p. 676-705.
16. Colombo, M., G. Raposo, and C. Thery, *Biogenesis, secretion, and intercellular interactions of exosomes and other extracellular vesicles*. Annu Rev Cell Dev Biol, 2014. **30**: p. 255-89.
17. Skotland, T., K. Sandvig, and A. Llorente, *Lipids in exosomes: Current knowledge and the way forward*. Prog Lipid Res, 2017. **66**: p. 30-41.
18. Record, M., et al., *Exosomes as new vesicular lipid transporters involved in cell-cell communication and various pathophysiological processes*. Biochim Biophys Acta, 2014. **1841**(1): p. 108-20.
19. Schorey, J.S. and S. Bhatnagar, *Exosome function: from tumor immunology to pathogen biology*. Traffic, 2008. **9**(6): p. 871-81.
20. Andreu, Z. and M. Yanez-Mo, *Tetraspanins in extracellular vesicle formation and function*. Front Immunol, 2014. **5**: p. 442.
21. de Gassart, A., et al., *Lipid raft-associated protein sorting in exosomes*. Blood, 2003. **102**(13): p. 4336-44.
22. Phuyal, S., et al., *Regulation of exosome release by glycosphingolipids and flotillins*. FEBS J, 2014. **281**(9): p. 2214-27.
23. Chaput, N. and C. Thery, *Exosomes: immune properties and potential clinical implementations*. Semin Immunopathol, 2011. **33**(5): p. 419-40.

24. Yanez-Mo, M., et al., *Biological properties of extracellular vesicles and their physiological functions*. J Extracell Vesicles, 2015. **4**: p. 27066.
25. Gardiner, C., et al., *Extracellular vesicles, tissue factor, cancer and thrombosis - discussion themes of the ISEV 2014 Educational Day*. J Extracell Vesicles, 2015. **4**: p. 26901.
26. Mulcahy, L.A., R.C. Pink, and D.R. Carter, *Routes and mechanisms of extracellular vesicle uptake*. J Extracell Vesicles, 2014. **3**: p. 24641.
27. Crescitelli, R., et al., *Distinct RNA profiles in subpopulations of extracellular vesicles: apoptotic bodies, microvesicles and exosomes*. J Extracell Vesicles, 2013. **2**: p. 20677.
28. Valadi, H., et al., *Exosome-mediated transfer of mRNAs and microRNAs is a novel mechanism of genetic exchange between cells*. Nat Cell Biol, 2007. **9**(6): p. 654-9.
29. Patton, J.G., et al., *Biogenesis, delivery, and function of extracellular RNA*. J Extracell Vesicles, 2015. **4**: p. 27494.
30. Shelke, G.V., et al., *Importance of exosome depletion protocols to eliminate functional and RNA-containing extracellular vesicles from fetal bovine serum*. J Extracell Vesicles, 2014. **3**: p. 24783.
31. Wei, Z., et al., *Fetal Bovine Serum RNA Interferes with the Cell Culture derived Extracellular RNA*. Sci Rep, 2016. **6**: p. 31175.
32. Tosar, J.P., et al., *Ribonucleic artefacts: are some extracellular RNA discoveries driven by cell culture medium components?* J Extracell Vesicles, 2017. **6**(1): p. 1272832.
33. Aswad, H., A. Jalabert, and S. Rome, *Depleting extracellular vesicles from fetal bovine serum alters proliferation and differentiation of skeletal muscle cells in vitro*. BMC Biotechnol, 2016. **16**: p. 32.
34. Eitan, E., et al., *Extracellular vesicle-depleted fetal bovine and human sera have reduced capacity to support cell growth*. J Extracell Vesicles, 2015. **4**: p. 26373.
35. Yuana, Y., R.M. Bertina, and S. Osanto, *Pre-analytical and analytical issues in the analysis of blood microparticles*. Thromb Haemost, 2011. **105**(3): p. 396-408.
36. Yuana, Y., et al., *Handling and storage of human body fluids for analysis of extracellular vesicles*. J Extracell Vesicles, 2015. **4**: p. 29260.
37. Fendl, B., et al., *Characterization of extracellular vesicles in whole blood: Influence of pre-analytical parameters and visualization of vesicle-cell interactions using imaging flow cytometry*. Biochem Biophys Res Commun, 2016. **478**(1): p. 168-73.
38. Wisgrill, L., et al., *Peripheral blood microvesicles secretion is influenced by storage time, temperature, and anticoagulants*. Cytometry A, 2016. **89**(7): p. 663-72.
39. Gardiner, C., et al., *Techniques used for the isolation and characterization of extracellular vesicles: results of a worldwide survey*. J Extracell Vesicles, 2016. **5**: p. 32945.
40. Thery, C., et al., *Isolation and characterization of exosomes from cell culture supernatants and biological fluids*. Curr Protoc Cell Biol, 2006. **Chapter 3**: p. Unit 3 22.
41. Momen-Heravi, F., et al., *Current methods for the isolation of extracellular vesicles*. Biol Chem, 2013. **394**(10): p. 1253-62.
42. Cvjetkovic, A., J. Lotvall, and C. Lasser, *The influence of rotor type and centrifugation time on the yield and purity of extracellular vesicles*. J Extracell Vesicles, 2014. **3**: p. 23111.
43. Yuana, Y., et al., *Co-isolation of extracellular vesicles and high-density lipoproteins using density gradient ultracentrifugation*. J Extracell Vesicles, 2014. **3**: p. 23262.
44. Bobrie, A., et al., *Diverse subpopulations of vesicles secreted by different intracellular mechanisms are present in exosome preparations obtained by differential ultracentrifugation*. J Extracell Vesicles, 2012. **1**: p. 18397.
45. Linares, R., et al., *High-speed centrifugation induces aggregation of extracellular vesicles*. J Extracell Vesicles, 2015. **4**: p. 29509.
46. Boing, A.N., et al., *Single-step isolation of extracellular vesicles by size-exclusion chromatography*. J Extracell Vesicles, 2014. **3**: p. 23430.
47. Taylor, D.D. and S. Shah, *Methods of isolating extracellular vesicles impact down-stream analyses of their cargoes*. Methods, 2015. **87**: p. 3-10.

48. Tauro, B.J., et al., *Comparison of ultracentrifugation, density gradient separation, and immunoaffinity capture methods for isolating human colon cancer cell line LIM1863-derived exosomes*. *Methods*, 2012. **56**(2): p. 293-304.
49. Lai, R.C., et al., *MSC secretes at least 3 EV types each with a unique permutation of membrane lipid, protein and RNA*. *J Extracell Vesicles*, 2016. **5**: p. 29828.
50. Chen, C., et al., *Imaging and Intracellular Tracking of Cancer-Derived Exosomes Using Single-Molecule Localization-Based Super-Resolution Microscope*. *ACS Applied Materials & Interfaces*, 2016. **8**(39): p. 25825-25833.
51. Arraud, N., et al., *Extracellular vesicles from blood plasma: determination of their morphology, size, phenotype and concentration*. *J Thromb Haemost*, 2014. **12**(5): p. 614-27.
52. Rupert, D.L.M., et al., *Methods for the physical characterization and quantification of extracellular vesicles in biological samples*. *Biochimica Et Biophysica Acta-General Subjects*, 2017. **1861**(1): p. 3164-3179.
53. Rupp, A.K., et al., *Loss of EpCAM expression in breast cancer derived serum exosomes: role of proteolytic cleavage*. *Gynecol Oncol*, 2011. **122**(2): p. 437-46.
54. Yuana, Y., et al., *Atomic force microscopy: a novel approach to the detection of nanosized blood microparticles*. *J Thromb Haemost*, 2010. **8**(2): p. 315-23.
55. Pan, B.T., et al., *Electron microscopic evidence for externalization of the transferrin receptor in vesicular form in sheep reticulocytes*. *J Cell Biol*, 1985. **101**(3): p. 942-8.
56. Linares, R., et al., *Imaging and Quantification of Extracellular Vesicles by Transmission Electron Microscopy*. *Methods Mol Biol*, 2017. **1545**: p. 43-54.
57. Dragovic, R.A., et al., *Sizing and phenotyping of cellular vesicles using Nanoparticle Tracking Analysis*. *Nanomedicine*, 2011. **7**(6): p. 780-8.
58. Maas, S.L., et al., *Possibilities and limitations of current technologies for quantification of biological extracellular vesicles and synthetic mimics*. *J Control Release*, 2015. **200**: p. 87-96.
59. van der Pol, E., et al., *Particle size distribution of exosomes and microvesicles determined by transmission electron microscopy, flow cytometry, nanoparticle tracking analysis, and resistive pulse sensing*. *J Thromb Haemost*, 2014. **12**(7): p. 1182-92.
60. van der Pol, E., et al., *Optical and non-optical methods for detection and characterization of microparticles and exosomes*. *J Thromb Haemost*, 2010. **8**(12): p. 2596-607.
61. Arraud, N., et al., *A simple flow cytometry method improves the detection of phosphatidylserine-exposing extracellular vesicles*. *J Thromb Haemost*, 2015. **13**(2): p. 237-47.
62. Arraud, N., et al., *Fluorescence Triggering: A General Strategy for Enumerating and Phenotyping Extracellular Vesicles by Flow Cytometry*. *Cytometry Part A*, 2016. **89A**(2): p. 184-195.
63. van der Vlist, E.J., et al., *Fluorescent labeling of nano-sized vesicles released by cells and subsequent quantitative and qualitative analysis by high-resolution flow cytometry*. *Nat Protoc*, 2012. **7**(7): p. 1311-26.
64. van der Pol, E., et al., *Single vs. swarm detection of microparticles and exosomes by flow cytometry*. *J Thromb Haemost*, 2012. **10**(5): p. 919-30.
65. Maas, S.L., M.L. Broekman, and J. de Vrij, *Tunable Resistive Pulse Sensing for the Characterization of Extracellular Vesicles*. *Methods Mol Biol*, 2017. **1545**: p. 21-33.
66. Anderson, W., et al., *Observations of Tunable Resistive Pulse Sensing for Exosome Analysis: Improving System Sensitivity and Stability*. *Langmuir*, 2015. **31**(23): p. 6577-87.
67. Vogel, R., et al., *A standardized method to determine the concentration of extracellular vesicles using tunable resistive pulse sensing*. *J Extracell Vesicles*, 2016. **5**: p. 31242.
68. Sedmak, J.J. and S.E. Grossberg, *A rapid, sensitive, and versatile assay for protein using Coomassie brilliant blue G250*. *Anal Biochem*, 1977. **79**(1-2): p. 544-52.
69. Smith, P.K., et al., *Measurement of protein using bicinchoninic acid*. *Anal Biochem*, 1985. **150**(1): p. 76-85.
70. Sapan, C.V., R.L. Lundblad, and N.C. Price, *Colorimetric protein assay techniques*. *Biotechnol Appl Biochem*, 1999. **29 (Pt 2)**: p. 99-108.

71. Gyorgy, B., et al., *Detection and isolation of cell-derived microparticles are compromised by protein complexes resulting from shared biophysical parameters*. *Blood*, 2011. **117**(4): p. e39-48.
72. Coumans, F.A.W., E.L. Gool, and R. Nieuwland, *Bulk immunoassays for analysis of extracellular vesicles*. *Platelets*, 2017. **28**(3): p. 242-248.
73. Liang, B., et al., *Characterization and proteomic analysis of ovarian cancer-derived exosomes*. *J Proteomics*, 2013. **80**: p. 171-82.
74. Kanwar, S.S., et al., *Microfluidic device (ExoChip) for on-chip isolation, quantification and characterization of circulating exosomes*. *Lab Chip*, 2014. **14**(11): p. 1891-1900.
75. He, M., et al., *Integrated immunoisolation and protein analysis of circulating exosomes using microfluidic technology*. *Lab Chip*, 2014. **14**(19): p. 3773-3780.
76. Zhao, Z., et al., *A microfluidic ExoSearch chip for multiplexed exosome detection towards blood-based ovarian cancer diagnosis*. *Lab Chip*, 2016. **16**(3): p. 489-96.
77. Woo, H.K., et al., *Exodisc for Rapid, Size-Selective, and Efficient Isolation and Analysis of Nanoscale Extracellular Vesicles from Biological Samples*. *ACS Nano*, 2017. **11**(2): p. 1360-1370.
78. Lee, K., et al., *Acoustic Purification of Extracellular Microvesicles*. *ACS Nano*, 2015. **9**(3): p. 2321-2327.
79. Shao, H.L., et al., *Protein typing of circulating microvesicles allows real-time monitoring of glioblastoma therapy*. *Nature Medicine*, 2012. **18**(12): p. 1835-41.
80. Etayash, H., et al., *Nanomechanical sandwich assay for multiple cancer biomarkers in breast cancer cell-derived exosomes*. *Nanoscale*, 2016. **8**(33): p. 15137-15141.
81. Patko, D., et al., *Label-free optical monitoring of surface adhesion of extracellular vesicles by grating coupled interferometry*. *Sensors and Actuators B-Chemical*, 2013. **188**: p. 697-701.
82. Tatischeff, I., et al., *Fast characterisation of cell-derived extracellular vesicles by nanoparticles tracking analysis, cryo-electron microscopy, and Raman tweezers microspectroscopy*. *J Extracell Vesicles*, 2012. **1**: p. 19179.
83. Smith, Z.J., et al., *Single exosome study reveals subpopulations distributed among cell lines with variability related to membrane content*. *J Extracell Vesicles*, 2015. **4**: p. 28533.
84. Di Vizio, D., et al., *Large oncosomes in human prostate cancer tissues and in the circulation of mice with metastatic disease*. *Am J Pathol*, 2012. **181**(5): p. 1573-84.
85. Hanahan, D. and R.A. Weinberg, *Hallmarks of cancer: the next generation*. *Cell*, 2011. **144**(5): p. 646-74.
86. Siegel, R.L., K.D. Miller, and A. Jemal, *Cancer Statistics, 2017*. *CA Cancer J Clin*, 2017. **67**(1): p. 7-30.
87. Rojas, V., et al., *Molecular Characterization of Epithelial Ovarian Cancer: Implications for Diagnosis and Treatment*. *Int J Mol Sci*, 2016. **17**(12).
88. Cho, K.R. and M. Shih Ie, *Ovarian cancer*. *Annu Rev Pathol*, 2009. **4**: p. 287-313.
89. Prat, J., *Staging classification for cancer of the ovary, fallopian tube, and peritoneum*. *Int J Gynaecol Obstet*, 2014. **124**(1): p. 1-5.
90. Jelovac, D. and D.K. Armstrong, *Recent progress in the diagnosis and treatment of ovarian cancer*. *CA Cancer J Clin*, 2011. **61**(3): p. 183-203.
91. Soletormos, G., et al., *Clinical Use of Cancer Biomarkers in Epithelial Ovarian Cancer: Updated Guidelines From the European Group on Tumor Markers*. *Int J Gynecol Cancer*, 2016. **26**(1): p. 43-51.
92. Aust, S. and D. Pils, *Epithelial ovarian cancer - more data, more questions?* *Wien Med Wochenschr*, 2014. **164**(21-22): p. 479-86.
93. Meehan, K. and L.J. Vella, *The contribution of tumour-derived exosomes to the hallmarks of cancer*. *Crit Rev Clin Lab Sci*, 2016. **53**(2): p. 121-31.
94. Gercel-Taylor, C., et al., *Nanoparticle analysis of circulating cell-derived vesicles in ovarian cancer patients*. *Anal Biochem*, 2012. **428**(1): p. 44-53.
95. Al-Nedawi, K., et al., *Intercellular transfer of the oncogenic receptor EGFRvIII by microvesicles derived from tumour cells*. *Nat Cell Biol*, 2008. **10**(5): p. 619-24.

96. Cappellesso, R., et al., *Programmed cell death 4 and microRNA 21 inverse expression is maintained in cells and exosomes from ovarian serous carcinoma effusions*. *Cancer Cytopathol*, 2014. **122**(9): p. 685-93.
97. Safaei, R., et al., *Abnormal lysosomal trafficking and enhanced exosomal export of cisplatin in drug-resistant human ovarian carcinoma cells*. *Mol Cancer Ther*, 2005. **4**(10): p. 1595-604.
98. Zhang, F.F., et al., *Microvesicles mediate transfer of P-glycoprotein to paclitaxel-sensitive A2780 human ovarian cancer cells, conferring paclitaxel-resistance*. *Eur J Pharmacol*, 2014. **738**: p. 83-90.
99. Pink, R.C., et al., *The passenger strand, miR-21-3p, plays a role in mediating cisplatin resistance in ovarian cancer cells*. *Gynecol Oncol*, 2015. **137**(1): p. 143-51.
100. Weiner-Gorzal, K., et al., *Overexpression of the microRNA miR-433 promotes resistance to paclitaxel through the induction of cellular senescence in ovarian cancer cells*. *Cancer Med*, 2015. **4**(5): p. 745-58.
101. Taraboletti, G., et al., *Bioavailability of VEGF in tumor-shed vesicles depends on vesicle burst induced by acidic pH*. *Neoplasia*, 2006. **8**(2): p. 96-103.
102. Millimaggi, D., et al., *Tumor vesicle-associated CD147 modulates the angiogenic capability of endothelial cells*. *Neoplasia*, 2007. **9**(4): p. 349-57.
103. Al Thawadi, H., et al., *VE-cadherin cleavage by ovarian cancer microparticles induces beta-catenin phosphorylation in endothelial cells*. *Oncotarget*, 2016. **7**(5): p. 5289-305.
104. Dolo, V., et al., *Matrix-degrading proteinases are shed in membrane vesicles by ovarian cancer cells in vivo and in vitro*. *Clin Exp Metastasis*, 1999. **17**(2): p. 131-40.
105. Graves, L.E., et al., *Proinvasive properties of ovarian cancer ascites-derived membrane vesicles*. *Cancer Res*, 2004. **64**(19): p. 7045-9.
106. Runz, S., et al., *Malignant ascites-derived exosomes of ovarian carcinoma patients contain CD24 and EpCAM*. *Gynecol Oncol*, 2007. **107**(3): p. 563-71.
107. Yokoi, A., et al., *Malignant extracellular vesicles carrying MMP1 mRNA facilitate peritoneal dissemination in ovarian cancer*. *Nat Commun*, 2017. **8**: p. 14470.
108. Kobayashi, M., et al., *Ovarian cancer cell invasiveness is associated with discordant exosomal sequestration of Let-7 miRNA and miR-200*. *J Transl Med*, 2014. **12**: p. 4.
109. Enriquez, V.A., et al., *High LIN28A Expressing Ovarian Cancer Cells Secrete Exosomes That Induce Invasion and Migration in HEK293 Cells*. *Biomed Res Int*, 2015. **2015**: p. 701390.
110. Hoshino, A., et al., *Tumour exosome integrins determine organotropic metastasis*. *Nature*, 2015. **527**(7578): p. 329-35.
111. Abrahams, V.M., et al., *Epithelial ovarian cancer cells secrete functional Fas ligand*. *Cancer Res*, 2003. **63**(17): p. 5573-81.
112. Meng, Y., S. Kang, and D.A. Fishman, *Lysophosphatidic acid stimulates fas ligand microvesicle release from ovarian cancer cells*. *Cancer Immunol Immunother*, 2005. **54**(8): p. 807-14.
113. Kelleher, R.J., Jr., et al., *Extracellular Vesicles Present in Human Ovarian Tumor Microenvironments Induce a Phosphatidylserine-Dependent Arrest in the T-cell Signaling Cascade*. *Cancer Immunol Res*, 2015. **3**(11): p. 1269-78.
114. Labani-Motlagh, A., et al., *Differential expression of ligands for NKG2D and DNAM-1 receptors by epithelial ovarian cancer-derived exosomes and its influence on NK cell cytotoxicity*. *Tumour Biol*, 2016. **37**(4): p. 5455-66.
115. Szajnik, M., et al., *Tumor-derived microvesicles induce, expand and up-regulate biological activities of human regulatory T cells (Treg)*. *PLoS One*, 2010. **5**(7): p. e11469.
116. Ying, X., et al., *Epithelial ovarian cancer-secreted exosomal miR-222-3p induces polarization of tumor-associated macrophages*. *Oncotarget*, 2016. **7**(28): p. 43076-43087.
117. Rank, A., et al., *Circulating microparticles in patients with benign and malignant ovarian tumors*. *Anticancer Res*, 2012. **32**(5): p. 2009-14.
118. Whiteside, T.L., *Tumor-Derived Exosomes and Their Role in Cancer Progression*. *Advances in Clinical Chemistry*, 2016. **74**: p. 103-141.
119. Keller, S., et al., *Systemic presence and tumor-growth promoting effect of ovarian carcinoma released exosomes*. *Cancer Lett*, 2009. **278**(1): p. 73-81.

120. Taylor, D.D. and C. Gercel-Taylor, *MicroRNA signatures of tumor-derived exosomes as diagnostic biomarkers of ovarian cancer*. *Gynecol Oncol*, 2008. **110**(1): p. 13-21.
121. Im, H., et al., *Label-free detection and molecular profiling of exosomes with a nano-plasmonic sensor*. *Nat Biotechnol*, 2014. **32**(5): p. 490-5.
122. Press, J.Z., et al., *Microparticles from ovarian carcinomas are shed into ascites and promote cell migration*. *Int J Gynecol Cancer*, 2012. **22**(4): p. 546-52.
123. Zhang, P., M. He, and Y. Zeng, *Ultrasensitive microfluidic analysis of circulating exosomes using a nanostructured graphene oxide/polydopamine coating*. *Lab Chip*, 2016. **16**(16): p. 3033-3042.
124. Zhang, W., et al., *Characterization of exosomes derived from ovarian cancer cells and normal ovarian epithelial cells by nanoparticle tracking analysis*. *Tumour Biol*, 2016. **37**(3): p. 4213-21.
125. Li, J., et al., *Claudin-containing exosomes in the peripheral circulation of women with ovarian cancer*. *BMC Cancer*, 2009. **9**: p. 244.
126. Szajnik, M., et al., *Exosomes in Plasma of Patients with Ovarian Carcinoma: Potential Biomarkers of Tumor Progression and Response to Therapy*. *Gynecol Obstet (Sunnyvale)*, 2013. **Suppl 4**: p. 3.
127. Lea, J., et al., *Detection of phosphatidylserine-positive exosomes as a diagnostic marker for ovarian malignancies: a proof of concept study*. *Oncotarget*, 2017. **8**(9): p. 14395-14407.
128. Gomes, J., et al., *Extracellular Vesicles from Ovarian Carcinoma Cells Display Specific Glycosignatures*. *Biomolecules*, 2015. **5**(3): p. 1741-61.
129. Vaksman, O., et al., *Exosome-derived miRNAs and ovarian carcinoma progression*. *Carcinogenesis*, 2014. **35**(9): p. 2113-20.
130. Meng, X., et al., *Diagnostic and prognostic relevance of circulating exosomal miR-373, miR-200a, miR-200b and miR-200c in patients with epithelial ovarian cancer*. *Oncotarget*, 2016. **7**(13): p. 16923-35.
131. Zhang, J., et al., *Curcumin suppresses cisplatin resistance development partly via modulating extracellular vesicle-mediated transfer of MEG3 and miR-214 in ovarian cancer*. *Cancer Chemother Pharmacol*, 2017. **79**(3): p. 479-487.
132. Hu, Y., et al., *TWEAK-stimulated macrophages inhibit metastasis of epithelial ovarian cancer via exosomal shuttling of microRNA*. *Cancer Lett*, 2017. **393**: p. 60-67.
133. Li, Q.L., et al., *Ex vivo experiments of human ovarian cancer ascites-derived exosomes presented by dendritic cells derived from umbilical cord blood for immunotherapy treatment*. *Clin Med Oncol*, 2008. **2**: p. 461-7.
134. Reza, A.M., et al., *Human adipose mesenchymal stem cell-derived exosomal-miRNAs are critical factors for inducing anti-proliferation signalling to A2780 and SKOV-3 ovarian cancer cells*. *Sci Rep*, 2016. **6**: p. 38498.
135. de la Fuente, A., et al., *M-Trap: Exosome-Based Capture of Tumor Cells as a New Technology in Peritoneal Metastasis*. *J Natl Cancer Inst*, 2015. **107**(9): p. djv184.
136. Hadla, M., et al., *Exosomes increase the therapeutic index of doxorubicin in breast and ovarian cancer mouse models*. *Nanomedicine (Lond)*, 2016. **11**(18): p. 2431-41.
137. Wood, R.W., *On a remarkable case of uneven distribution of light in a diffraction grating spectrum*. *Philosophical Magazine*, 1902. **4**(19-24): p. 396-402.
138. Otto, A., *Excitation of nonradiative surface plasma waves in silver by method of frustrated total reflection*. *Zeitschrift Fur Physik*, 1968. **216**(4): p. 398.
139. Kretschmann, E. and H. Raether, *Plasma Resonance Emission in Solids*. *Zeitschrift Fur Naturforschung Part a-Astrophysik Physik Und Physikalische Chemie*, 1968. **A 23**(4): p. 615.
140. Liedberg, B., C. Nylander, and I. Lundstrom, *Surface-plasmon resonance for gas-detection and biosensing*. *Sensors and Actuators*, 1983. **4**(2): p. 299-304.
141. Zeng, S.W., et al., *Nanomaterials enhanced surface plasmon resonance for biological and chemical sensing applications*. *Chemical Society Reviews*, 2014. **43**(10): p. 3426-3452.
142. Homola, J., *Surface Plasmon Resonance Based Sensors*, J. Homola, Editor 2006, Springer-Verlag Berlin Heidelberg: Berlin Heidelberg. p. XII, 251.

143. Schasfoort, R.B.M. and A.J. Tudos, *Handbook of Surface Plasmon Resonance*, R.B.M. Schasfoort and A.J. Tudos, Editors. 2008, RSC Publishing.
144. Kooyman, R.P.H., *Chapter 2 Physics of Surface Plasmon Resonance*, in *Handbook of Surface Plasmon Resonance* 2008, The Royal Society of Chemistry. p. 15-34.
145. Rothenhausler, B. and W. Knoll, *Surface-Plasmon Microscopy*. Nature, 1988. **332**(6165): p. 615-617.
146. Dahlin, A.B., et al., *Promises and challenges of nanoplasmonic devices for refractometric biosensing*. Nanophotonics, 2013. **2**(2): p. 83-101.
147. Dostalek, J. and W. Knoll, *Biosensors based on surface plasmon-enhanced fluorescence spectroscopy*. Biointerphases, 2008. **3**(3): p. Fd12-Fd22.
148. Piliarik, M. and J. Homola, *SPR Sensor Instrumentation*, in *Surface Plasmon Resonance Based Sensors*, J. Homola, Editor 2006, Springer Berlin Heidelberg: Berlin, Heidelberg. p. 95-116.
149. Schasfoort, R.B.M. and A. McWhirter, *Chapter 3 SPR Instrumentation*, in *Handbook of Surface Plasmon Resonance* 2008, The Royal Society of Chemistry. p. 35-80.
150. Lindquist, N.C., et al., *Engineering metallic nanostructures for plasmonics and nanophotonics*. Reports on Progress in Physics, 2012. **75**(3): p. 61.
151. Vogel, N., J. Zieleniecki, and I. Koper, *As flat as it gets: ultrasmooth surfaces from template-stripping procedures*. Nanoscale, 2012. **4**(13): p. 3820-3832.
152. Gedig, E.T., *Chapter 6 Surface Chemistry in SPR Technology*, in *Handbook of Surface Plasmon Resonance* 2008, The Royal Society of Chemistry. p. 173-220.
153. Knoll, W., et al., *Streptavidin arrays as supramolecular architectures in surface-plasmon optical sensor formats*. Colloids and Surfaces a-Physicochemical and Engineering Aspects, 2000. **161**(1): p. 115-137.
154. Stengel, G. and W. Knoll, *Surface plasmon field-enhanced fluorescence spectroscopy studies of primer extension reactions*. Nucleic Acids Res, 2005. **33**(7): p. e69.
155. Hall, D., *Chapter 4 Kinetic Models Describing Biomolecular Interactions at Surfaces*, in *Handbook of Surface Plasmon Resonance* 2008, The Royal Society of Chemistry. p. 81-122.
156. *Selection guide Biacore systems*, 2016: GE Healthcare.
157. Nie, L.B., et al., *Applications of Gold Nanoparticles in Optical Biosensors*. Journal of Biomedical Nanotechnology, 2014. **10**(10): p. 2700-2721.
158. Wang, Y., J. Dostalek, and W. Knoll, *Magnetic nanoparticle-enhanced biosensor based on grating-coupled surface plasmon resonance*. Anal Chem, 2011. **83**(16): p. 6202-7.
159. Wang, Y., W. Knoll, and J. Dostalek, *Bacterial pathogen surface plasmon resonance biosensor advanced by long range surface plasmons and magnetic nanoparticle assays*. Anal Chem, 2012. **84**(19): p. 8345-50.
160. Bauch, M., et al., *Plasmon-Enhanced Fluorescence Biosensors: a Review*. Plasmonics, 2014. **9**(4): p. 781-799.
161. Bauch, M., S. Hageneder, and J. Dostalek, *Plasmonic amplification for bioassays with epifluorescence readout*. Opt Express, 2014. **22**(26): p. 32026-38.
162. Hageneder, S., M. Bauch, and J. Dostalek, *Plasmonically amplified bioassay - Total internal reflection fluorescence vs. epifluorescence geometry*. Talanta, 2016. **156-157**: p. 225-31.
163. Jung, L.S., et al., *Quantification of tight binding to surface-immobilized phospholipid vesicles using surface plasmon resonance: Binding constant of phospholipase A(2)*. Journal of the American Chemical Society, 2000. **122**(17): p. 4177-4184.
164. Zhu, L., et al., *Label-free quantitative detection of tumor-derived exosomes through surface plasmon resonance imaging*. Anal Chem, 2014. **86**(17): p. 8857-64.
165. Di Noto, G., et al., *Merging colloidal nanoplasmonics and surface plasmon resonance spectroscopy for enhanced profiling of multiple myeloma-derived exosomes*. Biosens Bioelectron, 2016. **77**: p. 518-24.
166. Thakur, A., et al., *Direct detection of two different tumor-derived extracellular vesicles by SAM-AuNIs LSPR biosensor*. Biosens Bioelectron, 2017. **94**: p. 400-407.
167. Rupert, D.L., et al., *Determination of exosome concentration in solution using surface plasmon resonance spectroscopy*. Anal Chem, 2014. **86**(12): p. 5929-36.

168. Rupert, D.L., et al., *Dual-Wavelength Surface Plasmon Resonance for Determining the Size and Concentration of Sub-Populations of Extracellular Vesicles*. *Anal Chem*, 2016. **88**(20): p. 9980-9988.
169. Pignataro, B., et al., *Specific adhesion of vesicles monitored by scanning force microscopy and quartz crystal microbalance*. *Biophysical Journal*, 2000. **78**(1): p. 487-498.
170. Jackman, J.A., V.P. Zhdanov, and N.J. Cho, *Nanoplasmonic biosensing for soft matter adsorption: kinetics of lipid vesicle attachment and shape deformation*. *Langmuir*, 2014. **30**(31): p. 9494-503.
171. Jackman, J.A., et al., *Quantitative Profiling of Nanoscale Liposome Deformation by a Localized Surface Plasmon Resonance Sensor*. *Analytical Chemistry*, 2017. **89**(2): p. 1102-1109.
172. Shpacovitch, V., et al., *Application of the PAMONO-Sensor for Quantification of Microvesicles and Determination of Nano-Particle Size Distribution*. *Sensors*, 2017. **17**(2): p. 244.
173. Tang, M.K. and A.S. Wong, *Exosomes: Emerging biomarkers and targets for ovarian cancer*. *Cancer Lett*, 2015. **367**(1): p. 26-33.
174. Dorayappan, K.D., et al., *The biological significance and clinical applications of exosomes in ovarian cancer*. *Gynecol Oncol*, 2016. **142**(1): p. 199-205.
175. Righetti, P.G., et al., *Proteome analysis in the clinical chemistry laboratory: myth or reality?* *Clin Chim Acta*, 2005. **357**(2): p. 123-39.
176. Sodar, B.W., et al., *Low-density lipoprotein mimics blood plasma-derived exosomes and microvesicles during isolation and detection*. *Sci Rep*, 2016. **6**: p. 24316.
177. Willms, E., et al., *Cells release subpopulations of exosomes with distinct molecular and biological properties*. *Sci Rep*, 2016. **6**: p. 22519.
178. Hian Tan, K., et al., *Plasma biomarker discovery in preeclampsia using a novel differential isolation technology for circulating extracellular vesicles*. *Am J Obstet Gynecol*, 2014. **211**(4): p. 380 e1-380 e13.
179. Kipps, E., D.S. Tan, and S.B. Kaye, *Meeting the challenge of ascites in ovarian cancer: new avenues for therapy and research*. *Nat Rev Cancer*, 2013. **13**(4): p. 273-82.
180. Ahmed, N. and K.L. Stenvers, *Getting to know ovarian cancer ascites: opportunities for targeted therapy-based translational research*. *Front Oncol*, 2013. **3**: p. 256.
181. Auer, K., et al., *Peritoneal tumor spread in serous ovarian cancer-epithelial mesenchymal status and outcome*. *Oncotarget*, 2015. **6**(19): p. 17261-75.
182. Bachmayr-Heyda, A., et al., *Small RNAs and the competing endogenous RNA network in high grade serous ovarian cancer tumor spread*. *Oncotarget*, 2016. **7**(26): p. 39640-39653.
183. Auer, K., et al., *Role of the immune system in the peritoneal tumor spread of high grade serous ovarian cancer*. *Oncotarget*, 2016. **7**(38): p. 61336-61354.
184. White, E.S. and A.F. Muro, *Fibronectin splice variants: understanding their multiple roles in health and disease using engineered mouse models*. *IUBMB Life*, 2011. **63**(7): p. 538-46.
185. Rybak, J.N., et al., *The extra-domain A of fibronectin is a vascular marker of solid tumors and metastases*. *Cancer Res*, 2007. **67**(22): p. 10948-57.
186. Jarnagin, W.R., et al., *Expression of variant fibronectins in wound healing: cellular source and biological activity of the EIIIA segment in rat hepatic fibrogenesis*. *J Cell Biol*, 1994. **127**(6 Pt 2): p. 2037-48.
187. Fishelson, Z., et al., *Obstacles to cancer immunotherapy: expression of membrane complement regulatory proteins (mCRPs) in tumors*. *Mol Immunol*, 2003. **40**(2-4): p. 109-23.
188. Clayton, A., et al., *Antigen-presenting cell exosomes are protected from complement-mediated lysis by expression of CD55 and CD59*. *Eur J Immunol*, 2003. **33**(2): p. 522-31.
189. Babiker, A.A., et al., *Transfer of functional prostatic CD59 of metastatic prostatic cancer cell origin protects cells against complement attack*. *Prostate*, 2005. **62**(2): p. 105-14.
190. Lai, R., et al., *Mesenchymal Stem Cell Exosomes: The future MSC-based therapy?*, in *Mesenchymal Stem Cell Therapy*, L.G. Chase and M.C. Vemuri, Editors. 2013, Springer Science and Business Media: New York. p. 39-62.
191. Bjorge, L., et al., *Ascitic complement system in ovarian cancer*. *Br J Cancer*, 2005. **92**(5): p. 895-905.

192. MacDonald, B.T., K. Tamai, and X. He, *Wnt/ beta-catenin signaling: components, mechanisms, and diseases*. Dev Cell, 2009. **17**(1): p. 9-26.
193. Dovrat, S., et al., *14-3-3 and beta-catenin are secreted on extracellular vesicles to activate the oncogenic Wnt pathway*. Mol Oncol, 2014. **8**(5): p. 894-911.
194. Young, T.N., et al., *Characterization of gelatinases linked to extracellular matrix invasion in ovarian adenocarcinoma: purification of matrix metalloproteinase 2*. Gynecol Oncol, 1996. **62**(1): p. 89-99.
195. Fishman, D.A., et al., *Production of extracellular matrix-degrading proteinases by primary cultures of human epithelial ovarian carcinoma cells*. Cancer, 1997. **80**(8): p. 1457-63.
196. Manenti, L., et al., *Expression levels of vascular endothelial growth factor, matrix metalloproteinases 2 and 9 and tissue inhibitor of metalloproteinases 1 and 2 in the plasma of patients with ovarian carcinoma*. Eur J Cancer, 2003. **39**(13): p. 1948-56.
197. Cathcart, J., A. Pulkoski-Gross, and J. Cao, *Targeting Matrix Metalloproteinases in Cancer: Bringing New Life to Old Ideas*. Genes Dis, 2015. **2**(1): p. 26-34.
198. Van den Steen, P.E., et al., *Biochemistry and molecular biology of gelatinase B or matrix metalloproteinase-9 (MMP-9)*. Crit Rev Biochem Mol Biol, 2002. **37**(6): p. 375-536.
199. Gasser, O., et al., *Characterisation and properties of ectosomes released by human polymorphonuclear neutrophils*. Exp Cell Res, 2003. **285**(2): p. 243-57.
200. Moser, T.L., et al., *Secretion of extracellular matrix-degrading proteinases is increased in epithelial ovarian carcinoma*. Int J Cancer, 1994. **56**(4): p. 552-9.
201. Kamat, A.A., et al., *The clinical relevance of stromal matrix metalloproteinase expression in ovarian cancer*. Clin Cancer Res, 2006. **12**(6): p. 1707-14.
202. Brun, J.L., et al., *Serous and mucinous ovarian tumors express different profiles of MMP-2, -7, -9, MT1-MMP, and TIMP-1 and -2*. Int J Oncol, 2008. **33**(6): p. 1239-46.
203. Hu, X., et al., *Matrix metalloproteinase-9 expression correlates with prognosis and involved in ovarian cancer cell invasion*. Arch Gynecol Obstet, 2012. **286**(6): p. 1537-43.
204. Li, L.N., et al., *Prognostic value of MMP-9 in ovarian cancer: a meta-analysis*. Asian Pac J Cancer Prev, 2013. **14**(7): p. 4107-13.
205. Yabushita, H., et al., *Vascular endothelial growth factor activating matrix metalloproteinase in ascitic fluid during peritoneal dissemination of ovarian cancer*. Oncol Rep, 2003. **10**(1): p. 89-95.
206. Peng, P., Y. Yan, and S. Keng, *Exosomes in the ascites of ovarian cancer patients: origin and effects on anti-tumor immunity*. Oncol Rep, 2011. **25**(3): p. 749-62.
207. Mayer, C., et al., *Neutrophil Granulocytes in Ovarian Cancer - Induction of Epithelial-To-Mesenchymal-Transition and Tumor Cell Migration*. J Cancer, 2016. **7**(5): p. 546-54.
208. Vandooren, J., P.E. Van den Steen, and G. Opdenakker, *Biochemistry and molecular biology of gelatinase B or matrix metalloproteinase-9 (MMP-9): the next decade*. Crit Rev Biochem Mol Biol, 2013. **48**(3): p. 222-72.
209. Vang, R., M. Shih Ie, and R.J. Kurman, *Ovarian low-grade and high-grade serous carcinoma: pathogenesis, clinicopathologic and molecular biologic features, and diagnostic problems*. Adv Anat Pathol, 2009. **16**(5): p. 267-82.
210. Mc, K.F., W.G. Wilt, Jr., and et al., *The circulation of ascitic fluid; interchange of plasma and ascitic fluid protein as studied by means of C14-labeled lysine in dogs with constriction of the vena cava*. J Exp Med, 1950. **91**(2): p. 115-22.
211. Tan, D.S., R. Agarwal, and S.B. Kaye, *Mechanisms of transcoelomic metastasis in ovarian cancer*. Lancet Oncol, 2006. **7**(11): p. 925-34.
212. Pospichalova, V., et al., *Simplified protocol for flow cytometry analysis of fluorescently labeled exosomes and microvesicles using dedicated flow cytometer*. J Extracell Vesicles, 2015. **4**: p. 25530.
213. Pasalic, L., et al., *Enumeration of extracellular vesicles by a new improved flow cytometric method is comparable to fluorescence mode nanoparticle tracking analysis*. Nanomedicine, 2016. **12**(4): p. 977-86.
214. Lai, R.C., et al., *Exosome secreted by MSC reduces myocardial ischemia/reperfusion injury*. Stem Cell Res, 2010. **4**(3): p. 214-22.

215. Tan, S.S., et al., *Therapeutic MSC exosomes are derived from lipid raft microdomains in the plasma membrane*. J Extracell Vesicles, 2013. **2**: p. 22614.
216. Hiesgen, R., Haiber, J., *Measurement Methods Structural Properties: Atomic Force Microscopy*, in *Encyclopedia of Electrochemical Power Sources*, J. Garche, Editor 2009, Elsevier: Amsterdam. p. 696-717.
217. Postek, M.T., Howard, K.S., Johnson, A.H., McMichael, K.L., *Scanning Electron Microscopy a student's handbook*1980.
218. Adam, P., J. Dostalek, and J. Homola, *Multiple surface plasmon spectroscopy for study of biomolecular systems*. Sensors and Actuators B-Chemical, 2006. **113**(2): p. 774-781.
219. Perlmann, G.L., L., *The specific refractive increment of some purified proteins*. J. Am. Chem. Soc., 1948. **70**(8): p. 2719-2724.
220. Voros, J., *The density and refractive index of adsorbing protein layers*. Biophysical Journal, 2004. **87**(1): p. 553-561.
221. Querry, M.R., *Optical Constants*, in *US Military Contractor Report CRDC-CR-850341985*, Defense Technical Information Center.
222. Faraudo, J., J.S. Andreu, and J. Camacho, *Understanding diluted dispersions of superparamagnetic particles under strong magnetic fields: a review of concepts, theory and simulations*. Soft Matter, 2013. **9**(29): p. 6654-6664.
223. Dostalek, J., J. Homola, and M. Miler, *Rich information format surface plasmon resonance biosensor based on array of diffraction gratings*. Sensors and Actuators B-Chemical, 2005. **107**(1): p. 154-161.
224. Li, M., S.K. Cushing, and N.Q. Wu, *Plasmon-enhanced optical sensors: a review*. Analyst, 2015. **140**(2): p. 386-406.
225. Lakowicz, J.R., et al., *Plasmon-controlled fluorescence: a new paradigm in fluorescence spectroscopy*. Analyst, 2008. **133**(10): p. 1308-1346.
226. Kinkhabwala, A., et al., *Large single-molecule fluorescence enhancements produced by a bowtie nanoantenna*. Nature Photonics, 2009. **3**(11): p. 654-657.
227. Gambari, R., et al., *Biospecific interaction analysis (BLA) of low-molecular weight DNA-binding drugs*. Journal of Pharmacology and Experimental Therapeutics, 2000. **294**(1): p. 370-377.
228. Homola, J., *Surface plasmon resonance sensors for detection of chemical and biological species*. Chemical Reviews, 2008. **108**(2): p. 462-493.
229. Liebermann, T., et al., *Complement hybridization from solution to surface-attached probe-oligonucleotides observed by surface-plasmon-field-enhanced fluorescence spectroscopy*. Colloids and Surfaces a-Physicochemical and Engineering Aspects, 2000. **169**(1-3): p. 337-350.
230. Wang, Y., et al., *Prostate Specific Antigen Biosensor Based on Long Range Surface Plasmon-Enhanced Fluorescence Spectroscopy and Dextran Hydrogel Binding Matrix*. Analytical Chemistry, 2009. **81**(23): p. 9625-9632.
231. Yu, F., et al., *Attomolar sensitivity in bioassays based on surface plasmon fluorescence spectroscopy*. Journal of the American Chemical Society, 2004. **126**(29): p. 8902-8903.
232. Breault-Turcot, J., et al., *Single chip SPR and fluorescent ELISA assay of prostate specific antigen*. Lab Chip, 2015. **15**(23): p. 4433-40.
233. Cui, X.Q., et al., *Enhanced Fluorescence Microscopic Imaging by Plasmonic Nanostructures: From a 1D Grating to a 2D Nanohole Array*. Advanced Functional Materials, 2010. **20**(6): p. 945-950.
234. Sergelen, K., et al., *Plasmon field-enhanced fluorescence energy transfer for loop aptamer assay readout*. ACS Sensors, 2017. **in press**.
235. Hirsch, J.D., et al., *Easily reversible desthiobiotin binding to streptavidin, avidin, and other biotin-binding proteins: uses for protein labeling, detection, and isolation*. Anal Biochem, 2002. **308**(2): p. 343-57.
236. Perez-Luna, V.H., et al., *Molecular recognition between genetically engineered streptavidin and surface-bound biotin*. Journal of the American Chemical Society, 1999. **121**(27): p. 6469-6478.

8 List of abbreviations

AF647	alexafluor 647
AFM	atomic force microscopy
ATR	attenuated total reflection
AV	annexin V
b-CTB	biotinylated cholera toxin b-chain
b-IgG	biotinylated antibody
CA-125	cancer antigen 125
CTB	cholera toxin b-chain
DLS	dynamic light scattering
DNA	deoxyribonucleic acid
EDC	N-(3-dimethylaminopropyl)-N'-ethylcarbodiimide hydrochloride
ELISA	enzyme linked immunosorbent assay
EpCAM	epithelial cell adhesion molecule
ESCRT	endosomal sorting complex required for transport
EV	extracellular vesicle
FC	flow cytometry
FN1-EDA	cellular fibronectin
GC-SPR	grating coupled surface plasmon resonance
HGSOC	high grade serous ovarian cancer
ISEV	international society of extracellular vesicles
LRSP	long-range surface plasmon
LSP	localized surface plasmon
MMP	matrix metalloproteinase
MNP	magnetic nanoparticle
MSC	mesenchymal stem cell
MV	microvesicle
MVB	multivesicular body
NHS	N-hydroxysuccinimide
NTA	nanoparticle tracking analysis
OC	ovarian cancer
PBS	phosphate buffered saline
PBST	phosphate buffered saline with tween 20
PBSTB	phosphate buffered saline with tween 20 and bovine serum albumin
PDMS	polydimethylsiloxane
PEF	plasmonically enhanced fluorescence
PEG	polyethylene glycol
PSP	propagating surface plasmon
RNA	ribonucleic acid
SA	streptavidin
SAM	self-assembled monolayer
SEM	scanning electron microscopy
SP	surface plasmon
SPR	surface plasmon resonance
STB	shiga toxin b-chain
TE	transversally electric polarization
TEM	transmission electron microscopy
TM	transversally magnetic polarization
TRPS	tunable resistive pulse sensing
VEGF	vascular endothelial growth factor

9 Curriculum Vitae

Name	Dipl.-Ing. Agnes Reiner, Bakk. techn.
Date of Birth	09/23/1987
Place of Birth	Vienna, Austria
Nationality	Austria
Education	
Since 4/2014	PhD program „International Graduate School (IGS) in Nanobiotechnology” at the University of Natural Resources and Life Sciences, Vienna, and the Nanyang Technological University, Singapore, in cooperation with Austrian Institute of Technology (AIT), Medical University of Vienna (Molecular Oncology Group), Centre for Biomimetic Surface Sensing (Singapore) and Agency for Science, Technology and Research (Institute of Medical Biology, Singapore) project „Cancer diagnosis based on plasmonic biosensors and exosome analysis”
10/2012-11/2013	Master thesis „Blood-based Biomarkers for the Detection of Breast Cancer”, at the Molecular Oncology Group, Department of Obstetrics and Gynaecology, Medical University of Vienna
7-12/2011	Exchange semester at Murdoch University, Perth, Western Australia
2011-2013	Master course in Biotechnology at the University of Natural Resources and Life Sciences, Vienna
1/2011	Bachelor’s degree with excellent effort, Bachelor thesis „Stability Enhancing Mutations in Immunoglobulin Domains on the example of Antigen-binding Fcabs” in the field of molecular biology and biochemistry
2007-2011	Bachelor course in Food- and Biotechnology at the University of Natural Resources and Life Sciences, Vienna
Science/Projects	
04/2017	1 st place for the oral presentation „Breaking the Wall of Ovarian Cancer Diagnosis” at the Falling Walls Lab Austria 2017
04/2017	Received funding from the program „International Communication” of the Austrian Research Association for the participation at the ISEV2017 conference
10/2015	Selected participant in the „1st Tropical School of Biophotonics” by A*STAR Singapore Bioimaging Consortium and International Union of Pure and Applied Biophysics in Singapore
12/2014	Received project funding by Anniversary Fund of the Oesterreichische Nationalbank for the project „Technical and clinical validation of an immune response signature for diagnosis of breast cancer”

